Mechanisms of Cell Polarity in Yeast

Morphogenesis in Microscopic Systems

Ben Klünder

München 2013

Mechanisms of Cell Polarity in Yeast

Morphogenesis in Microscopic Systems

Ben Klünder

Dissertation
an der Fakultät für Physik
der Ludwig–Maximilians–Universität
München

vorgelegt von
Ben Klünder
geboren in Elmshorn

München, 16. Januar 2013

Erstgutachter: Prof. Dr. Erwin Frey
Zweitgutachterin: Prof. Dr. Katharina Krischer
Tag der mündlichen Prüfung: 28. Februar 2013

Zusammenfassung

Der Schwerpunkt der Dissertation liegt auf der Erforschung von Mechanismen der Zellpolarisation in der Hefe *Saccharomyces cerevisiae*. Zellpolarisation ist ein fundamentaler zellulärer Prozess, bei dem eine räumliche Richtung innerhalb der Zelle definiert wird, und der Voraussetzung für zahlreiche Entwicklungsprozesse wie Zellproliferation oder -differenzierung ist.

Vorige Arbeiten schlugen zwei unabhängige Polarisationswege für die Akkumulation der GTPase Cdc42 zu einem Cluster auf der Plasmamembran von Hefe vor, wodurch dort die Entwicklung einer Tochterzelle in Form einer Knospe ausgelöst wird. Man nimmt an, dass einer der Polarisationswege abhängig ist von gerichtetem Transport des Cdc42 entlang von Aktinfilamenten. Währenddessen wird der andere vermutlich durch schnelles Recycling von Cdc42 durch das Zytosol mittels Bindung von Cdc42 an den GDP dissociation inhibitor (GDI) Rdi1 erzeugt. Allerdings sind die Details oder gar die Existenz dieser Polarisationswege umstritten. Außerdem wurde gezeigt, dass gewisse Mutationen das zeitgleiche Entstehen von mehreren stabilen Clustern und somit auch Knospen in Hefe hervorrufen.

Um ein tieferes Verständnis von Zellpolarisation in Hefe zu erlangen, entwickeln wir ein minimales stochastisches Modell beider Polarisationswege. In Übereinstimmung mit unseren Experimenten bildet der GDI-abhängige Polarisationsweg zuverlässig eine einzelne stabile Kappe, während auf Aktinfilamenten basierende Polarisation anfällig für das gelegentliche Entstehen von mehr als einem stabilen Cluster ist. Das Modell erlaubt uns, Vorhersagen für den Proteinaustausch zwischen Cluster und Zellinnerem sowie für das Entstehen von mehreren stabilen Clustern in mutierten Hefezellen zu treffen, die wir experimentell bestätigen. Beide Polarisationswege müssen erfolgreich koordiniert werden, um zuverlässig eine einzelne Polarisationsstelle für die anschließende Knospung zu erzeugen.

Eine frühere Arbeit schlug vor, dass während der Polarisation zunächst mehrere transiente Cluster entstehen, die dann in einen einzelnen Cluster übergehen. Beobachtet werden konnten mehrere transiente Cluster bisher allerdings nur in einer kleinen Teilpopulation von Wildtypzellen. Außerdem ist noch unverstanden, wie der Zellzyklus die Polarisation zeitlich reguliert.

Aufgrund der Koexistenz der beiden unabhängigen Polarisationswege sowie der unklaren Polarisationsdynamik untersuchen wir die grundlegenden Eigenschaften der GDI-abhängigen Polarisation und entwickeln ein detaillierteres mechanistisches Modell dieses Polarisationsweges. Mithilfe des Modells können wir neue Phänotypen für Dynamik und Endzustand der Polarisation voraussagen, die wir experimentell bestätigen.

Eine durch den Zellzyklus hervorgerufene Verstärkung von positiven Feedbackschleifen in der Membranbindung und Aktivierung von Cdc42 stellt den Schlüsselmechanismus für das Auslösen der GDI-abhängigen Polarisation dar. Diese Regulation beruht auf dem Erfolg oder Misserfolg der Feedbackschleifen, sich selbst zu verstärken, und hängt nicht von der Fähigkeit ab, der lateralen Diffusion auf der Membran entgegenzuwirken.

Die GDI-abhängige Polarisation wird begleitet von einem vielfachen Anstieg der Aktivität von Cdc42 und bildet direkt einen einzelnen sich beim Entstehen stets verengenden Cluster und nicht mehrere transiente Cluster, welche dann zu einem verschmelzen. Außerdem führen die vom Zellzyklus ausgelösten Veränderungen zuverlässig zur Entstehung eines sehr fokussierten Endzustandes der Polarisation. Unsere Ergebnisse deuten darauf hin, dass all diese Aspekte unter physiologischen Bedingungen gleichzeitig optimiert sind, um eine kontrollierte Signalwirkung von Cdc42 zu ermöglichen.

Um ein qualitatives Verständnis der Polarisationsdynamik unseres mechanistischen Modells im Vergleich zu früheren Modellen zu erlangen, entwickeln wir ein minimales konzeptionelles Modell für auf Diffusion basierende Zellpolarisation, das nur deren zentrale Eigenschaften berücksichtigt.

Unsere Analyse zeigt, dass es zwei qualitativ verschiedene Polarisationsdynamiken gibt. Zellen können entweder durch Verschmelzung mehrerer zu Beginn wachsender Cluster polarisieren oder durch direktes Entstehen eines einzelnen Clusters. Letzteres kann zuverlässig ermöglicht werden für im Vergleich zur Zelle große zytosolische Diffusionslängen und wird durch generisches Verengen des entstehenden Clusters begleitet. Zusätzlich zeigen wir, dass eine Variation der Proteinanzahl einen Wechsel zwischen beiden Polarisationsdynamiken auslösen kann. Dies steht in Einklang mit Experimenten in Hefezellen.

Unsere Ergebnisse liefern mit den Erkenntnissen über die gestörte Koordination der Polarisationswege eine mechanistische Erklärung für Zellteilungsdefekte und enthüllen die fundamentalen Designprinzipien, die es der GDI-abhängigen Polarisation erlauben, Entwicklungsprozesse zuverlässig zu einer bestimmten Zeit an einem bestimmten Ort auszulösen.

Contents

Zusammenfassung v

1 Introduction 1
- 1.1 Morphogenesis in microscopic systems . . . 1
- 1.2 Overview of this work and motivation . . . 3
- 1.3 Cell polarity in yeast . . . 3
  - 1.3.1 Polarity GTPase Cdc42 . . . 3
  - 1.3.2 Guanine nucleotide exchange factor Cdc24 . . . 4
  - 1.3.3 Cdc42 effector Bem1 . . . 5
  - 1.3.4 Proposed feedback loops in Cdc42 activation . . . 5
  - 1.3.5 GDP dissociation inhibitor Rdi1 . . . 6
  - 1.3.6 Bud-site selection . . . 6
  - 1.3.7 Actin-dependent polarization . . . 6
  - 1.3.8 Actin-independent polarization . . . 7
  - 1.3.9 Formation of multiple buds . . . 7
- 1.4 Turing mechanism of pattern formation . . . 7
- 1.5 Theoretical approaches to cell polarization in yeast . . . 9
  - 1.5.1 Turing-type model of yeast cell polarity . . . 9
  - 1.5.2 Stochastic model of yeast cell polarity . . . 10
  - 1.5.3 Phase separation model of yeast cell polarity . . . 10
  - 1.5.4 Models of actin-dependent polarization . . . 10

2 Establishment of a robust single axis of cell polarity by coupling of multiple positive feedback loops 13
- 2.1 Introduction . . . 13
- 2.2 Results . . . 14
  - 2.2.1 Parallel pathways for the establishment of cell polarity through Cdc42 recycling . . . 16
  - 2.2.2 A stochastic model for polarity establishment through Cdc42 recycling 18
  - 2.2.3 Determination of quantitative model parameters . . . 21
  - 2.2.4 Validating the model . . . 24
  - 2.2.5 The mechanism of formation of multiple polarization sites . . . 24
- 2.3 Discussion . . . 29
- 2.4 Materials and methods . . . 31
  - 2.4.1 Test of Turing-like model of Goryachev and Pokhilko . . . 31
  - 2.4.2 Stochastic model of cell polarity . . . 32
  - 2.4.3 Robustness of polarization dynamics . . . 37
  - 2.4.4 Experimental procedures . . . 38
  - 2.4.5 Genetic Interactions . . . 47

2.4.6 Physical Interactions . . . 53
2.4.7 FRAP values . . . 57
2.4.8 Double buds . . . 58

3 Cell polarization in yeast optimizes spatial and temporal control of Cdc42 signaling 59
3.1 Introduction . . . 59
3.2 Results . . . 60
3.2.1 Stable cell polarization with continuous exchange of proteins . . . 62
3.2.2 Polarization initially emerges as a single broad cap which narrows over time . . . 62
3.2.3 Cell cycle induced changes provide temporal control over GDI-mediated polarization . . . 66
3.2.4 Enhancing the positive feedback loops provides simultaneous switch-like regulation of polarization and Cdc42 activation . . . 67
3.2.5 Cell cycle regulated temporal control induces a direct and robust change into highly localized polarization . . . 69
3.3 Discussion . . . 71
3.4 Materials and methods . . . 73
3.4.1 Reaction-diffusion equations . . . 73
3.4.2 Determination of reaction rates . . . 74
3.4.3 Simulations . . . 74
3.4.4 Linear stability analysis . . . 75
3.4.5 Robustness of the polarization dynamics . . . 78
3.4.6 Experimental procedures . . . 79
3.4.7 Yeast strains . . . 81
3.4.8 Plasmids . . . 81
3.4.9 Primers . . . 81

4 Minimal mass-conserving model of cell polarity 83
4.1 Introduction . . . 83
4.2 Results . . . 83
4.3 Discussion . . . 89

5 Summary and Outlook 91

Bibliography 95

Danksagung 107

List of Figures

1.1 Mating of yeast. . . . 2
1.2 Budding of yeast. . . . 4

2.1 Effects of Cdc42 expression level on cell polarization. . . . 15
2.2 Polarity establishment through GDI- and actin-mediated recycling of Cdc42. 17
2.3 Building a mathematical model of the combined pathways. . . . 18
2.4 Extraction of Cdc42 from membranes. . . . 19
2.5 Competition between GEF and GDI for GTPase binding. . . . 20
2.6 Turnover of Cdc42 and Cdc24 in polarized caps. . . . 21
2.7 Fitting parameters - cap shape. . . . 22
2.8 Fitting parameters - Cdc42 turnover. . . . 23
2.9 Model predictions - effects of GTP hydrolysis on polarization efficiency and Cdc42 dynamics. . . . 25
2.10 Formation of multiple polarization sites. . . . 26
2.11 Delay of polarization causes formation of multiple polarization sites. . . . 27
2.12 Multiple polarization sites and DNA segregation. . . . 28
2.13 Results of parameter scan. . . . 38

3.1 Details of the mechanistic model for GDI-mediated cell polarization in yeast. 60
3.2 Steady state Cdc42 distribution. . . . 62
3.3 Predicted dynamics of GDI-mediated polarization. . . . 63
3.4 Unphysiological polarization dynamics. . . . 64
3.5 Experimental characterization of narrowing dynamics. . . . 65
3.6 Time evolution of polarizing yeast cells. . . . 66
3.7 Parameters affecting polarization efficiency. . . . 67
3.8 Cdc42 activation for changing parameters. . . . 68
3.9 Polarization efficiency for changing diffusion constants. . . . 69
3.10 Predicted cluster widths for changing parameters. . . . 70
3.11 Experimental verification of predicted cluster widths. . . . 71
3.12 Dispersion relation for control cells. . . . 78

4.1 Polarization dynamics for changing parameters and initial conditions. . . . 87
4.2 Polarization efficiency and dispersion relations. . . . 88

1 Introduction

1.1 Morphogenesis in microscopic systems

Life in all its forms shows an astonishing level of complexity. Only recent experimental advances such as the use of fluorescent proteins made it possible to gain mechanistic insight into many cellular processes. Of course, biology has to obey the fundamental laws of physics. However, they are of little help in describing biological systems as one usually has to cope with an insufficient knowledge about the system under consideration. Hence, one of the main tasks of scientists aiming to gain a mechanistic understanding of biology is the development of effective theories which can be tested experimentally and which hopefully lead to a more general understanding about the mechanisms of life.

The goal of this manuscript is to shed more light on the mechanisms of morphogenesis in microscopic cellular systems using the example of budding yeast. "Morphogenesis ... is the biological process that causes an organism to develop its shape." [1] Not only the final plan of an animal but also its accurate development and all temporary processes related to it are encoded in its DNA. For example, the fruit fly *Drosophila melanogaster* has been shown to evolve from a single fertilized egg which at later stages divides into many cells with distinct fates [2]. Even much simpler organisms such as bacteria need to orchestrate complex processes to control their cell division [3]. Animals constitute many body systems made of a huge collection of different proteins which just interact with their immediate environment. However, during the development of organisms higher order structures such as membranes, filaments, or whole cells need to be placed at the right position in space with respect to the remaining body. To this end processes evolved which allow to measure or determine positions in the animal or to define new symmetries which are used for construction. These mechanisms often provide their spatial information in terms of signaling molecules whose spatially varying concentrations are read out by cells or which directly interact with other proteins to initiate developmental processes. The establishment of pattern of these molecules can be broadly grouped into pattern formation in response to spatial cues or spontaneous pattern formation.

An example of the first class is the initial stripe patterning of the fruit fly *Drosophila melanogaster*. Here the mother already deposits messenger RNA (mRNA) at one tip of the egg which then continuously produces proteins of morphogen Bicoid [4, 5]. Bicoid diffuses and degrades and hence forms a gradient along the developing embryo [6, 7]. At later stages of development this gradient serves as regulator for downstream genes such as Hunchback which establishes the first anterior-posterior distinction [8, 9].

Another example of pattern formation in response to spatial cues is mating yeast. The single cell organism yeast *Saccharomyces cerevisiae* has three chromosomal sexes. It exists in an diploid a/α state with two copies of all chromosomes (as humans) or as a haploid state in an a

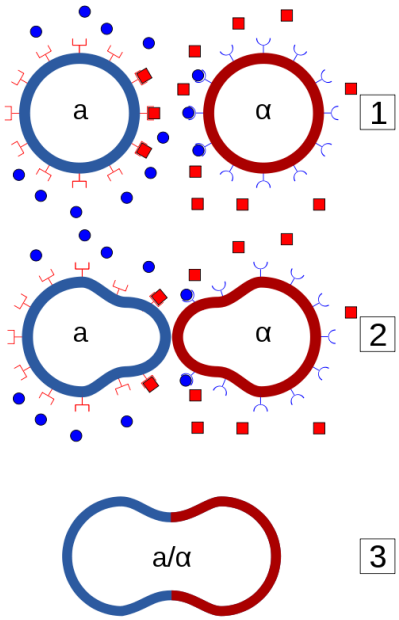

Figure 1.1: Mating of yeast. Two haploid yeast cells sense each other's pheromone gradient (1), grow towards each other (2), and unite to form a diploid (3) [13].

or α state with one copy of all chromosomes [10]. Two haploid cells, an a and an α cell, have the ability to unite and form a diploid a/α cell. One refers to this as mating. The process of mating is initiated by detection of appropriate mating partners in the direct vicinity as shown in Fig. 1.1. Both types of cells generate a gradient of pheromones which is sensed by cells of the opposite sex [11]. These signaling molecules trigger polarization of proteins at the inner site of the plasma membrane towards the mating partner and both cells then start to grow towards each other forming so-called mating projections [12].

Not in all cases it is possible or sufficient to have an external cue which determines the direction of growth. In the tube-like bacterium *Escherichia coli* the future division plane is determined by a spatially oscillating distribution of cell division regulators $MinC$, $MinD$, and $MinE$ along the main cell axis [3, 14]. $MinE$ is preferentially found at the center of the bacterium where it effectively allows the initiation of cell division [3]. However, no spatial cue is necessary to initiate the oscillation [14].

Another example of spontaneous pattern formation is cell polarization in budding yeast *Saccharomyces cerevisiae*. Prior to proliferation yeast cells need to determine the place on the plasma membrane where the daughter cell is constructed. This is facilitated by cell polarization where signaling protein Cdc42 accumulates within a restricted region of the membrane. In wild-type cells the direction of growth is not random but is controlled by bud site selection proteins [15]. However, these proteins are dispensable for polarization and cells with disturbed bud site selection spontaneously polarize Cdc42 in a random direction [16, 17].

Morphogenesis of microorganisms or similar sized cells of higher animals operates under adverse conditions. On the one hand it needs to function reliably in face of many kinds of noise. Pheromone gradients may consist only of a very small number of molecules rather than a

continuous concentration gradient or polarizing cells have to ensure that only one polarization site is established. On the other hand the complexity of its mechanisms is limited by the small size of the system.

1.2 Overview of this work and motivation

Yeast has been extensively used as model system. As an eukaryote it shares many features with higher animals such as humans. Yeast cells keep their DNA saved in chromosomes and can use some primitive version of sexual reproduction. However, yeast is a unicellular organism which is easy to breed and shows rapid proliferation making it an ideal target for genetic manipulation. Furthermore, many cellular processes in yeast are thought to be similar between yeast and other animals where genetic manipulations are more difficult or not desired due to ethical considerations. In this manuscript we focus on the question how cell polarization in budding yeast as part of the cell division machinery operates reliably in the inevitable presence of fluctuations. We expect that basic research of yeast cell polarity will lead to a mechanistic understanding of cell division defects which might apply to other animals as well.

In the remainder of this chapter we give an introduction to cell polarization in yeast. In chapter 2 we elucidate how singularity of polarization is facilitated in budding yeast and how malfunction of polarization mechanisms can result in the formation of multiple buds. Chapter 3 aims to reveal the fundamental properties of a diffusion-based polarization mechanism in yeast. In chapter 4 we develop a minimal model of cell polarity to gain a deeper understanding of the polarization dynamics. We conclude this work with a summary in chapter 5.

1.3 Cell polarity in yeast

The eukaryotic fungi yeast *Saccharomyces cerevisiae* is one of the best studied model systems of cell polarity. During proliferation yeast cells polarize to select a place on the plasma membrane for budding where the daughter is constructed [18].

The polarity machine consists of a complex network of interacting proteins which we call polarity regulators. To help readers understand the complex protein interactions we will give an individual description of the most relevant proteins involved in polarity establishment and how they relate to each other.

1.3.1 Polarity GTPase Cdc42

The central polarity regulator in yeast is GTPase Cdc42 (cell division cycle 42) which was first identified by a systematic screen of yeast budding defects [19] and later on found to be a GTP-binding protein [20]. Cdc42 shows a high DNA sequence similarity of 80% with its human version and expression of human Cdc42 can rescue a Cdc42 knockout in yeast arguing for an important evolutionary conserved role of Cdc42 [20].

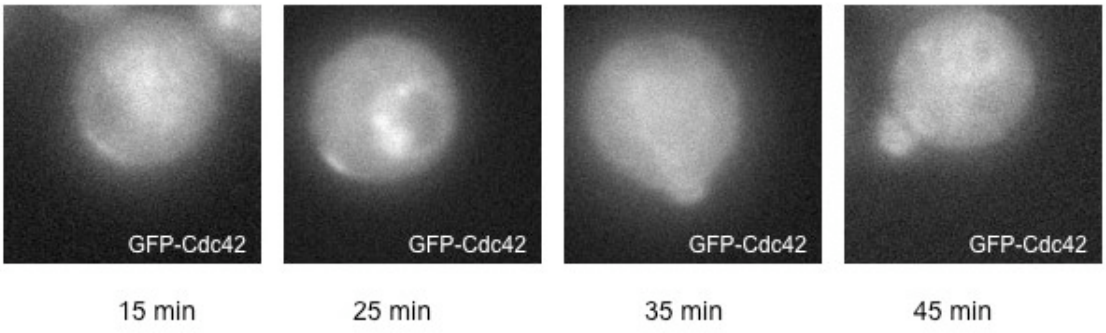

Figure 1.2: Budding of yeast. Shown is the distribution of GFP-Cdc42 in a budding yeast cell for different time points [21].

In yeast Cdc42 fulfills two functions. It orchestrates the establishment of cell polarity and also initiates downstream processes leading to bud formation. The distribution of Cdc42 in a budding yeast cell is shown in Fig. 1.2. At the beginning a cap of Cdc42 is established on the membrane (first two images) which determines the position where the future bud is constructed (third and fourth image).

As a GTPase Cdc42 exists in two states, an inactive GDP-bound state and an active GTP-bound state. In the latter state it interacts with various so-called effector proteins which participate in cell polarity, bud formation, and other developmental processes [18]. Proper regulation of Cdc42 activity is crucial for yeast proliferation as Cdc42 mutations causing continuous activation of Cdc42 irrespective of further regulation (hyperactive Cdc42) result in yeast cells with multiple buds and impaired viability [22]. Similarly, hyperactive Cdc42 has been shown to cause formation of giant multi-nucleated cells in mammalian cell lines indicating the ocurence of cell division defects [23]. Nucleotide exchange and hence activation of Cdc42 is facilitated by its sole guanine nucleotide exchange factor Cdc24 [24]. In contrast, down regulation of Cdc42 activity is facilitated by GTPase-activating proteins (GAPs) which catalyze the hydrolysis (deactivation) of Cdc42 [24, 25, 26, 27]. Cdc42 alone is not soluble and hence bound to membranes where it can slowly diffuse [18, 28]. To establish a cytosolic fraction Cdc42 needs to be extracted from membranes by its GDP dissociation inhibitor (GDI) Rdi1 [29, 30].

In summary, Cdc42 controls polarity establishment by interaction with various other polarity regulators.

1.3.2 Guanine nucleotide exchange factor Cdc24

Even before Cdc42 gene Cdc24 (cell division cycle 24) was identified as being crucial for bud formation [31] and it was shown to express a guanine nucleotide exchange factor (GEF) which catalyzes the activation of Cdc42 [24]. However, overexpression of Cdc24 also causes loss of polarization and hence budding defects [32].

During the cell cycle phosphorylation of GAPs and release of Cdc24 from the cell nucleus have been shown to contribute to polarization initiation [33, 34, 35] and localization of Cdc24 to

the nucleus depends on direct binding to protein Far1 [36, 34, 33]. The activity of the GEF is thought to be regulated as well. Phosphorylation of Cdc24 by PAK-like kinase Cla4 has been implicated in its regulation during polarity establishment. However, several studies arrived at contradicting results. One study argued for a negative role in Cdc24 regulation [37], two for a positive role [16, 38], and one work could not detect any impact of Cdc24 phosphorylation in polarity establishment at all [39]. In addition, Cdc24 is thought to exist in an auto-inhibited state which is resolved by binding to the proteins Bem1 or Bud1 [40]. These proteins have also been shown to recruit Cdc24 to the plasma membrane and polarity site [41, 42, 40].

Hence, Cdc24 likely plays a key role in polarization as it facilitates local activation of Cdc42.

1.3.3 Cdc42 effector Bem1

Another important protein is Bem1 (bud emergence protein 1) which was identified to be important for bud emergence as deletion of Bem1 causes the emergence of large multi-nucleated cells [43].

Bem1 was shown to bind to inactive bud-site selection GTPase Bud1 even though the importance of this interaction remains unclear [44]. More important are the findings that Bem1 localization to the polarity cluster depends on Cdc42-GTP and that Bem1 is necessary to maintain Cdc24 at the polarization site. These observations lead to the proposal of a positive feedback loop in Cdc42 activation [37, 42]. In addition, Bem1 needs to be able to bind to membranes as deletion of the binding domain is lethal [45, 16, 38]. Several studies also focused on the interaction of Bem1 with kinase Cla4 [37, 41, 38]. It was shown by a carefully designed experiment that Bem1 proteins need to be able to bind both Cdc24 and Cla4 [38]. Bem1 can also directly bind to Cdc42 even though this interaction does not seem to be essential for polarity establishment [46, 38]. In addition, Bem1 has been shown to activate Cdc24 and attach it to the membrane [40, 47].

The exact role of Bem1 in polarization still remains controversial as it is not clear whether it indeed facilitates a feedback loop or just functions to activate the GEF [48].

1.3.4 Proposed feedback loops in Cdc42 activation

Different feedback loops have been proposed to play an important role in polarity establishment. One study proposed that effector Bem1 creates a positive feedback loop of Cdc42 activation by binding to GEF Cdc24 and Cdc42-GTP [42]. Another study argued that such a feedback loop might be facilitated by Cla4 which binds to Cdc42-GTP and Bem1 (that in turns binds Cdc24) and in addition phosphorylates Cdc24 [38]. Recently, evidence for an additional negative feedback loop in Cdc42 activation was found which was proposed to improve the robustness of Cdc42 polarization even though the molecular mechanism remains unknown [49].

1.3.5 GDP dissociation inhibitor Rdi1

An additional Cdc42 regulator is given by a so called GDP dissociation inhibitor (GDI) of Cdc42 which was first identified in humans by its ability to inhibit the dissociation of GDP from Cdc42 [50]. It was also shown to catalyze the dissociation of Cdc42 from plasma membranes. Its yeast homolog Rdi1 was later on also identified and characterized [51, 52]. A further study questioned the importance of Rdi1 as deletion of Rdi1 causes no severe phenotype of yeast and only very strong overexpression is lethal [53]. However, the GDI Rdi1 was shown to provide a fast recycling pathway for Cdc42 polarization and deletion of Rdi1 makes polarization actin-dependent [29]. Recently, it was shown that extraction of Cdc42 by Rdi1 needs the action of a lipid flippase complex which reduces the binding affinity of Cdc42 to the membrane [54] but it still remains unclear in which state Cdc42 is extracted by its GDI. However, in vitro experiments suggest that Cdc42 is extracted in its GDP-bound form [30].

In summary, these findings indicate that GDI Rdi1 plays an important role in polarization by rapid redistribution of Cdc42 through the cytosol.

1.3.6 Bud-site selection

Yeast cells bud in characteristic orientation with respect to existing bud and birth scars from previous cell divisions [55, 56]. The spatial information is transmitted to the polarization machinery via GTPase Bud1 which is regulated by its GEF Bud5 and its GAP Bud2. Deletions of either of these proteins cause budding in a random direction [15, 57, 58]. Interaction of Bud1-GTP with Cdc24 is crucial for proper bud-site selection as deletion of the Bud1 interaction domain in Cdc24 induces budding in a random direction [44, 40]. In addition, Bud1 has been shown to bind to Bem1 in its inactive form and to Cdc42 [44, 59]. However, the relevance of these interactions remains unclear.

In summary, these findings show that bud-site selection is not necessary for polarization and its removal allows to study the pattern formation mechanism itself. Therefore, bud-site selection is disabled in this study if not stated otherwise.

1.3.7 Actin-dependent polarization

Given that proteins diffuse on the plasma membrane it is necessary to continuously redistribute them in order to maintain polarity clusters. One polarization pathway has been proposed that relies on directed transport of Cdc42 in vesicles along actin filaments [60]. Cells expressing permanently active Cdc42 have been shown to polarize via actin structures as depolymerization of actin abolished polarization [17]. This polarization pathway is thought to be facilitated by a Cdc42-GTP-controlled positive feedback loop of Cdc42 transport via formin Bni1 which links Cdc42-GTP and actin nucleation [61]. Recently, the existence of actin-dependent polarization was questioned by a theoretical work [62] even though cells without GDI Rdi1 still polarize via actin [29]. A negative contribution of actin-dependent structures in polarization has also been identified arguing for an additional negative feedback [63, 64].

Hence, actin structures seem to be involved in polarity establishment but their exact role remains controversial.

1.3.8 Actin-independent polarization

A second actin-independent polarization pathway has been identified which shows rapid membrane-cytosol exchange of Cdc42 [60, 16, 65]. Without Cdc42 effector Bem1 polarization becomes actin-dependent and additional deletion of bud-site selection GTPase Bud1 is lethal [16, 65]. Moreover, it was shown that cells expressing permanently active or inactive Cdc42 need actin to polarize suggesting that Cdc42 needs to cycle between its states for this polarization mechanism to work [65]. In a subsequent study extraction of Cdc42 by GDI Rdi1 was found to be necessary as cells without Rdi1 do not polarize in the absence of actin structures [29].

These findings suggest that a GDI-dependent polarization mechanism exists which needs the interaction between several polarity regulators.

1.3.9 Formation of multiple buds

Wildtype yeast cells always form a single polarization site and bud. However, certain mutations instead cause the formation of multiple buds. Hyperactive Cdc42 was shown to induce the formation of multiple buds in a subpopulation of cells [22]. In addition, some cells expressing constitutively active Cdc42 polarize and bud into multiple directions [17]. Similarly, more than one bud was detected in a subpopulation of cells without Bem1 or GAP Bem2 [65, 35] or in some cells overexpressing Bem1 [66].

Most of the aforementioned mutations affect the activity of Cdc42. Hence, these findings suggest that the formation of multiple buds depends on a disturbed regulation of Cdc42.

1.4 Turing mechanism of pattern formation

After having discussed the molecular details of yeast polarization we will provide an introduction into the theory of pattern formation.

Presumably the first important theoretical approach to describe pattern formation in biology came from Alan Turing. He proposed that a system of reacting and diffusing chemicals can produce pattern out of an homogeneous state [67]. This idea was further developed by Gierer and Meinhardt proposing short range autocatalytic activation and long range inhibition as a mechanism for biological pattern formation [68, 69]. Many modeling approaches to cell polarity rely on reaction-diffusion mechanisms [70]. Therefore, it is important to understand the similarities and differences between them and Turing models. In the following we will summarize a convenient analysis of a conceptual Turing model given by Cross and Greenside which highlights the fundamental aspects of Turing mechanisms [71].

We start by introducing a system of two chemicals u and v in a homogeneous infinite system whose time evolution obeys

$$\begin{aligned} \partial_t u &= f_1(u,v) + D_1 \partial_x^2 u \,, \\ \partial_t v &= f_2(u,v) + D_2 \partial_x^2 v \,. \end{aligned} \tag{1.1}$$

Aim of the following calculation is to derive the conditions which allow pattern formation from a homogeneous state. To this end we apply a linear stability analysis to a spatially homogeneous fix point u_0, v_0 which is obtained from $f_1(u_0, v_0)$=$f_2(u_0, v_0)$=0. We calculate the linearized time evolution of a small perturbation δu, δv of the homogeneous fix point and ask whether the perturbation grows or decays. Growth would imply that an arbitrarily small deviation from a perfect homogeneous state induces pattern formation. The linearized time evolution of the perturbations reads

$$\begin{aligned} \partial_t \delta u &= \alpha_{u1}\delta u + \alpha_{v1}\delta v + D_1 \partial_x^2 \delta u \,, \\ \partial_t \delta v &= \alpha_{u2}\delta u + \alpha_{v2}\delta v + D_2 \partial_x^2 \delta v \end{aligned} \tag{1.2}$$

with the Jacobi coefficients $\alpha_{ui} = \partial_u f_i(u, v_0)|_{u=u_0}$, $\alpha_{vi} = \partial_v f_i(u_0, v)|_{v=v_0}$. Eq. (1.2) can be solved using the ansatz

$$\begin{pmatrix} \delta u \\ \delta v \end{pmatrix} = \begin{pmatrix} \delta u_q \\ \delta v_q \end{pmatrix} e^{\omega_q t} e^{iqx} \tag{1.3}$$

where ω_q and q denote growth rate and wave number, respectively. Perturbations can then be constructed by a superposition of (1.3) with different q.

Decay of the perturbation and hence no pattern formation occurs if $\mathrm{Re}(\omega_\mathrm{q}) < 0$ and these rates can be obtained by combining (1.2) and (1.3). The real part of the growth rate remains negative if

$$\alpha_{u1} + \alpha_{v2} - (D_1 + D_2)q^2 < 0 \,, \tag{1.4}$$

$$(\alpha_{u1} - D_1 q^2)(\alpha_{v2} - D_2 q^2) - \alpha_{v1}\alpha_{u2} > 0 \,. \tag{1.5}$$

Turing's main finding was that diffusion causes the instability of an otherwise stable homogenous state [67]. By setting the diffusion constants in (1.4) and (1.5) equal to zero one obtains the necessary conditions

$$\alpha_{u1} + \alpha_{v2} < 0 \,, \tag{1.6}$$

$$\alpha_{u1}\alpha_{v2} - \alpha_{v1}\alpha_{u2} > 0 \tag{1.7}$$

for the stability of the homogeneous state without diffusion. Eq, (1.4) is always satisfied if condition (1.6) holds. However, Eq. (1.5) can be violated even if condition (1.7) is satisfied. Hence, given that the homogeneous state is stable without diffusion one can destabilize it by allowing the chemicals to diffuse.

The Turing condition for the onset of pattern formation at finite diffusion can be calculated as follows. For pattern formation to occur one needs to violate Eq. (1.5). To this end one determines the minimum of the left-hand site of Eq. (1.5) and with respect to q^2 and determines its value at this minimum.

For the violation of Eq. (1.5) we obtain the necessary condition

$$\alpha_{u1} D_2 + \alpha_{v2} D_1 > 0\,. \tag{1.8}$$

Eqs. (1.6) and (1.8) together imply that α_{u1} and α_{v2} need to have opposite signs and one usually chooses $\alpha_{u1} > 0$ and $\alpha_{v2} < 0$. Accordingly, u is then called an activator as it enhances its own production and v an inhibitor as it suppresses its own production. By introducing the diffusion lengths $l_u = \sqrt{D_1/\alpha_{u1}}$ and $l_v = \sqrt{D_2/(-\alpha_{v2})}$ one can rewrite Eq. (1.8) and arrives at the famous Turing condition

$$l_u^2 < l_v^2\,. \tag{1.9}$$

The diffusion length of the activator needs to be shorter than the diffusion length of the inhibitor as a necessary condition for pattern formation.

Turing mechanisms provide a simple possibility for pattern formation but many other have also been proposed. In the following we present models related to yeast cell polarization.

1.5 Theoretical approaches to cell polarization in yeast

The mechanisms of cell polarity remain incompletely understood even in the best-studied model system yeast. In this section we will give a summary of proposed models of yeast cell polarization.

1.5.1 Turing-type model of yeast cell polarity

A Turing-type mechanism was proposed by Goryachev and Pokhilko for yeast cell polarity in 2008 [72]. A complex reaction network incorporating Cdc42, Rdi1 and Bem1-Cdc24 complexes was proposed and subsequently simplified to a two species activator substrate model. The model robustly provides cell polarization and predicts the transient emergence of multiple polarity clusters which coalesce into a single one due to competition for limited amounts of proteins. Indeed, emergence of multiple clusters which then merge into a single one was observed in an small subpopulation of wild-type cells [66].

The necessary nonlinearity is generated by a nonlinear positive feedback loop of Cdc42 activation. The mechanism relies on the formation of Cdc42-GTP-Bem1-Cdc24 complexes (denoted by M) on the membrane. These complexes are formed by always membrane-bound Cdc42-GTP and Bem1-Cdc24 complexes (denoted by E) from the membrane or from the cytosol. M can then decay to membrane-bound E and Cdc42-GTP. In addition, membrane-bound E is allowed to detach from the membrane. The authors showed that complex formation of Cdc42-GTP both with cytosolic and with membrane-bound E is crucial for generating the nonlinear positive feedback in Cdc42 activation. Disruption of either of these processes results in a M distribution on the membrane proportional to Cdc42-GTP generating only a linear positive feedback in Cdc42 activation. Hence, the nonlinear positive feedback is generated by rebinding of E complexes to Cdc42-GTP. First, cytosolic E directly binds to Cdc42-GTP forming complex M. This complex decays producing E on the membrane proportional to the Cdc42-GTP distribution. E then rebinds to Cdc42-GTP effectively forming a distribution of M proportional to the square of Cdc42-GTP.

1.5.2 Stochastic model of yeast cell polarity

Altschuler et al. proposed a simple conceptual model for yeast cell polarity where a single protein species enhances its own membrane attachment with a linear positive feedback loop [73]. The model provides stochastic clustering of proteins at low protein number in the cell. However, the clusters are not stable due to their stochastic nature and can transiently split up. Recently, this model was questioned as overexpression of Cdc42 does not abolish polarization [49].

1.5.3 Phase separation model of yeast cell polarity

A conceptual phase separation model was developed by Semplice et al. and proposed to account for yeast cell polarity [74]. The model consists of a membrane-bound signaling molecule ϕ, which exists in the two states ϕ_+ and ϕ_-, and two kinds of enzymes, X and Y, which can exchange between cytosol and membrane. X catalyzes the exchange of ϕ_- to ϕ_+ whereas Y catalyzes the exchange of ϕ_+ to ϕ_-. Two opposing positive feedback loops are established as ϕ_+ and ϕ_- activate X and Y, respectively. The self-enhancement of both phases of ϕ allows a spatial separation and hence polarization. A finite perturbation is needed to induce polarization from a homogeneous monophasic state. These perturbations produce small germs which then expand on the membrane via coarsening dynamics till only two opposing domains remain.

1.5.4 Models of actin-dependent polarization

The models presented so far were based on reaction and diffusion of proteins. However, it has been shown that yeast cells can polarize using directed transport along actin filaments [17]. A simple model was introduced where signaling protein Cdc42 induces the local nucleation of actin filaments on the membrane which then cause transport of Cdc42 to these sites effectively describing a process called exocytosis. This model was further developed explicitly

including diffusion and removal of Cdc42 through endocytosis [28]. Recently, this approach was questioned by a more detailed model which explicitly described the processes of exo- and endocytosis [75]. The model included not only the delivery of Cdc42 via actin to the polarization site but also took into account that transport of Cdc42 is facilitated by vesicles. These carriers are made of membrane lipids and are inserted into the plasma membrane upon arrival on the plasma membrane. Hence, the surrounding plasma membrane was assumed to shift away and special conditions needed to be satisfied to concentrate Cdc42 at all. However, the model could not maintain polarization using measured diffusion constants even though actin-dependent polarization has been shown to occur [17, 29].

2 Establishment of a robust single axis of cell polarity by coupling of multiple positive feedback loops

This chapter is based on a manuscript originating from a cooperation with the experimental group of Roland Wedlich-Söldner for which I contributed all theoretical results [76].

2.1 Introduction

The small Rho-type GTPase Cdc42 is a central regulator of cell polarity in animal and fungal cells [77, 78]. At the G1-S transition in the cell cycle of *Saccharomyces cerevisiae*, Cdc42 becomes concentrated in a cortical cap that defines the future bud site [79, 80]. Cdc42 binds to various effectors that control essential morphogenetic processes, such as polarized transport of membrane vesicles along actin cables [81], assembly of a septin diffusion barrier [82] and fusion of exocytic vesicles with the plasma membrane [18, 83]. To fulfill its various functions, Cdc42 must constantly cycle between GTP-bound/active and GDP-bound/inactive states. In budding yeast activation of Cdc42 is controlled by a single guanine nucleotide exchange factor (GEF), Cdc24, and its intrinsic hydrolytic activity is promoted by four GTPase-activating proteins (GAPs), Bem2, Bem3, Rga1 and Rga2 [18]. Finally, Cdc42 is extracted from membranes by the only Rho-GDI in *S. cerevisiae*, Rdi1 [52, 53].

Concentration of Cdc42 at the polarization site in yeast cells can occur via several feedback mechanisms that produce patterns by amplifying stochastic fluctuations [84, 85]. Localized accumulation requires either focused, actin-mediated transport of vesicle-bound Cdc42 [17, 65] or Bem1-mediated recruitment of soluble, Rdi1-bound Cdc42 from the cytoplasm [16, 38, 29, 65]. Both pathways are highly dynamic and drive polarization through constant recycling of Cdc42 [29, 65].

Fusion of Cdc42-bearing vesicles with the plasma membrane, to which they are transported along actin cables by type V myosin, has been shown to be sufficient for spontaneous polarization of constitutively active and membrane-restricted Cdc42 via a simple positive feedback mechanism [17]. In addition, polarization of wild-type Cdc42 partially depends on actin-based recycling of membrane material, and Cdc42 caps are less robust in the absence of actin [65]. Importantly, in the absence of Bem1, actin-based focused delivery to the plasma membrane becomes essential for Cdc42 polarization [65]. Also, if membrane-bound Cdc42 is stabilized by removing Rdi1, polarized caps cannot be maintained without actin [29]. While a role for membrane transport in polarity establishment has been widely established [86, 87], the relevance of actin-mediated transport for polarization of wild-type yeast cells is still controversial

[63, 84, 38, 62, 88]. Moreover, a negative role for actin in cell polarization has been proposed based on endocytosis of polarity regulators [63, 64] or dilution of Cdc42 through membrane addition to the cap region [49, 75]. Such mechanisms provide attractive explanations for phenomena such as travelling waves [64] or oscillating polarization patches [49]. However, they cannot account for the positive role of actin during the actual process of symmetry breaking - both in the presence and absence of Bem1-driven feedback [17, 65].

In addition to actin-mediated recycling of Cdc42, a second polarization mechanism has been proposed to rely on self-enhanced activation of Cdc42 through a Bem1-Cdc24-Cla4 complex [41, 42, 16, 38, 74]. There is also experimental evidence which suggests that extraction of Cdc42 from membranes by Rdi1 is itself essential for maintenance of polarity in the absence of actin [29]. Motivated by these observations an elaborate Turing-type model incorporating GDI-mediated extraction of Cdc42 and a Bem1- mediated positive feedback loop of Cdc42 activation has been advanced to explain this putative second polarization mechanism [72]. However, many details of the reaction scheme proposed for GDI-mediated polarization are incompletely understood and remain under debate [70, 62, 85]. Moreover, the precise relationship between the actin- and GDI-dependent mechanisms in the establishment of polarization in wild-type cells is unclear.

In the present study, we combined experimental and theoretical approaches to build a particle-based stochastic and mechanistic model for yeast polarity establishment through combined actin- and GDI-mediated recycling of Cdc42. We established assumptions and parameter values for this model through a combination of genetic analyses, in vitro reconstitution and quantitative live cell imaging. Several predictions regarding polarization efficiency, Cdc42 recycling rates and appearance of multiple polarization sites derived from the model were tested and validated experimentally. In summary, we demonstrate that the establishment of a stable and unique polarization axis requires the coordination of two pathways for Cdc42 recycling. Actin-mediated polarization is regulated by active Cdc42, and is very stable but does not reliably result in formation of a single polarization site. In contrast, GDI-dependent polarization is sensitive to changes in the kinetics of the GTPase cycle of Cdc42 but faithfully generates a unique polarization site. Moreover, we show that formation of multiple buds directly correlates with mis-segregation of nuclei. Our results thus suggest that correct polarity establishment is achieved through coupling of multiple feedback loops.

2.2 Results

In order to build a mathematical model that can explain general mechanisms of yeast cell polarity establishment we first sought to establish firm mechanistic connections between all the regulators and pathways involved. Spontaneous cell polarization has been proposed to occur via amplification of stochastic concentration fluctuations through simple positive feedback in the presence of low concentrations of reacting molecules [73, 70]. However, a recent report indicated that yeast cell polarization was not sensitive to moderate variations in Cdc42 expression level [49]. In an attempt to resolve this issue we varied expression levels of GFP-Cdc42 in control and LatB-treated cells with the aid of an inducible GAL promoter [73]. Using the same criteria described previously [73], we indeed found that Cdc42 expression level had no effect on polarization efficiency (Fig. 2.1A). We also generated strains that constitutively

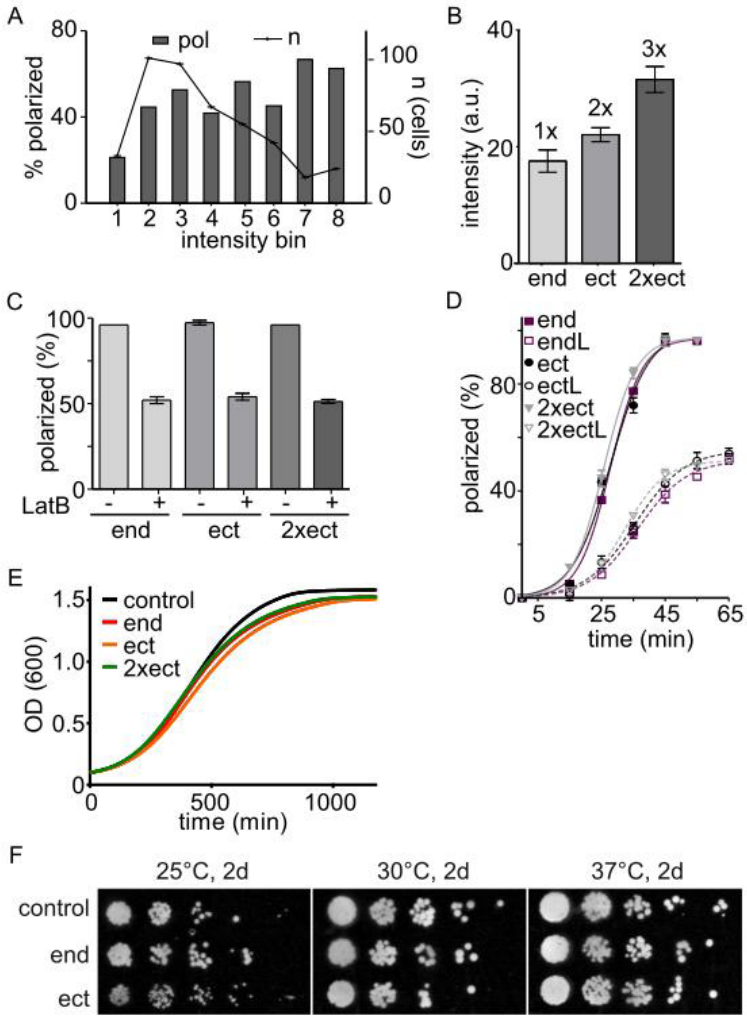

Figure 2.1: Effects of Cdc42 expression level on cell polarization. **A** No correlation is seen between GFP-Cdc42 expression levels (intensity bins represent ranges of relative GFP fluorescence intensity) and polarization efficiency. The number of cells analyzed for each bin is indicated (axis on the right). Levels of GFP-Cde42 were varied by inducing expression of a GFP-CDC42 construct driven by the GAL1 promoter for 0.5-3 h as in [73]. **B** Fluorescence intensities of cells expressing GFP-Cdc42 inserted at the endogenous locus (end, 1 copy), at a single ectopic site (ect; two CDC42 copies but only one with GFP) or at two ectopic sites (2xect, three copies but only two with GFP). **C** Efficiency of polarization in strains used in (B) after release from G1 arrest in the absence or presence of LatB. Bars indicate means ± SEM of three experiments with > 50 cells each. **D** Kinetics of polarization kinetics in the strains used in (B) after release from G1 arrest in the absence or presence of LatB. Data (mean ± SD) are from three experiments with > 50 cells each. **E** Growth curves (average curves from three experiments shown) for control cells and cells expressing GFP-Cdc42 as indicated in (B). **F** Comparison of untagged control cells with cells expressing GFP-Cdc42 from the endogenous locus (end) or ectopic sites (ect, total of two copies of Cdc42). Serial dilutions are shown for colonies grown for 2 days (2d) at the indicated temperatures.

express 1-3 copies of Cdc42 (Fig. 2.1B) and again observed no differences in polarization efficiency (Fig. 2.1C) or kinetics (Fig. 2.1D). Note that, in contrast to the case in the strain used by Howell et al. [49], GFP-labelled Cdc42 was fully functional in our strain background (Fig. 2.1A-D). Cells expressing GFP-Cdc42 fusions either as the sole copy at the endogenous locus or as additional ectopic copies exhibited no growth defects or temperature sensitivity compared to untagged control cells (Fig. 2.1E,F). These results confirm that polarization in yeast is insensitive to the exact level of Cdc42 present in cells.

2.2.1 Parallel pathways for the establishment of cell polarity through Cdc42 recycling

We reasoned that the lack of impact of Cdc42 overexpression might be attributable to the buffering effect of its GDI, which is generally found in a 1:1 complex with its substrates in the cytosol [89]. Actin and Rdi1, the yeast GDI for Cdc42, have been proposed to act in parallel pathways during polarity maintenance [29]. To investigate the connection between Rdi1-mediated recycling of Cdc42 via the cytosol and actin-dependent recycling of membrane-bound Cdc42 via endocytosis during polarity establishment, we first systematically investigated genetic interactions of Cdc42 and its regulators with synthetic genetic arrays [90]. Genetic lesions in all the components examined had a negative impact on processes that were linked to actin functions (Fig. 2.2A, section 2.4.5). In contrast, relatively few physical interactions of Cdc42 regulators with actin-associated proteins have been reported (Fig. 2.2A, section 2.4.6). These results indicate that, in addition to the established role of Cdc42 in the formation and polarization of actin structures, Cdc42 signalling and actin-mediated transport processes also act in parallel pathways during essential cellular processes - including polarity establishment.

In our genetic interaction screen, Rdi1 exhibited interactions with several components involved in endocytic recycling (Fig. 2.2A, section 2.4.5), which would be consistent with a role for Rdi1 in actin-independent recycling of Cdc42 during polarity establishment. To test this, we studied synchronized yeast cells expressing GFP-Cdc42 fusions (Fig. 2.1B-D), and monitored Cdc42 cap formation [65]. As expected from the role of the GDI in extraction of membrane-bound Cdc42, in Δrdi1 cells Cdc42 accumulated on membranes (Fig. 2.2B). Nevertheless, polarization kinetics were unaffected both in Δrdi1 cells and in cells expressing $Cdc42^{R66E}$, a mutant that is unable to interact with the GDI [91] (Fig. 2.2B). However, depolymerization of actin with latrunculin B (LatB), which only has a moderate effect on control cells [65] (Fig. 2.2C), completely blocked polarization in Δrdi1 and in $Cdc42^{R66E}$-expressing cells (Fig. 2.2C). A similar synergistic effect was observed when exocytosis was blocked using a temperature-sensitive allele for the secretory myosin motor MYO2 (myo2-16, Fig. 2.2D). In addition, reduction of endocytic recycling by deletion of the ESCRTIII component VPS27 [92] resulted in less efficient polarization of Δrdi1 cells (Fig. 2.2E). Colocalization of GFP-Cdc42 and FM4-64-stained endocytic membranes in Δvps27 cells revealed Cdc42 accumulation in aberrant endocytic compartments, confirming passage of Cdc42 through the endocytic system (Fig. 2.2E).

Our results confirm that Rdi1- and actin-based cycling of Cdc42 contribute to polarity establishment via distinct and parallel mechanisms. We therefore proceeded to design a particle-

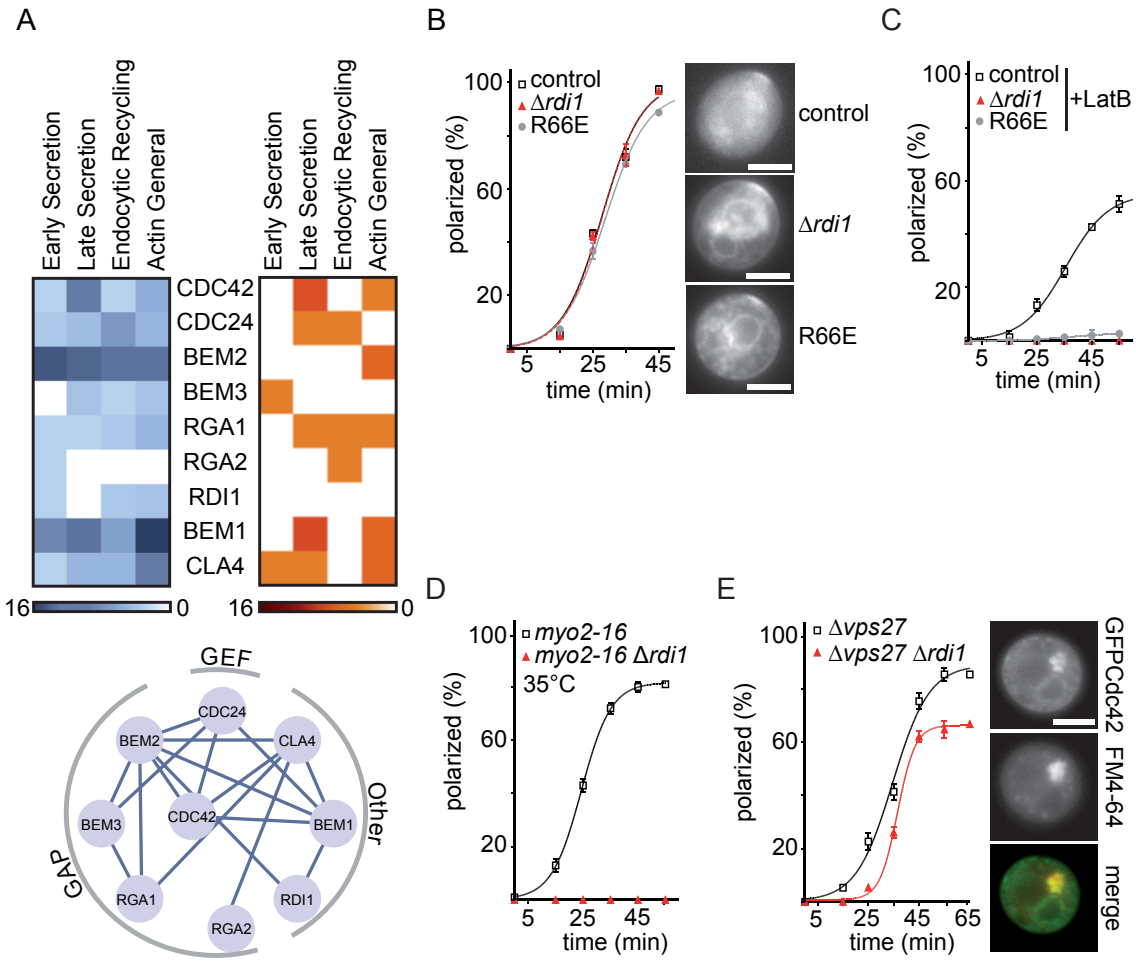

Figure 2.2: Polarity establishment through GDI- and actin-mediated recycling of Cdc42. **A** Heat plots of genetic (blue) and physical (red) interactions between Cdc42 regulators and proteins involved in actin-related processes. Genetic interactions among Cdc42 regulators are indicated in the lower panel. **A-E** Effects of genetic and pharmacological perturbations on polarization kinetics of Cdc42. Data points represent means of three experiments with >50 cells each. Error bars indicate SDs of the means. Continuous lines are sigmoidal fits. Individual plots depict the effects of: **B** inhibiting extraction of Cdc42 from the plasma membrane in Δrdi1 and cdc42^{R66E} cells; **C** disruption of actin polymerization (by LatB) in control, Δrdi1 and cdc42^{R66E} cells; **D** inactivation of the temperature-sensitive myo2-16 allele in control and Δrdi1 cells, and **E** deletion of VPS27 in control and Δrdi1 cells. Colocalization of Cdc42 and the membrane dye FM4-64 in aberrant endosomal compartments of Δvps27 cells is demonstrated in panel (E). Scale bars: 4 μm.

based mathematical model of Cdc42 polarization in yeast cells which allows to study the interplay between the two pathways.

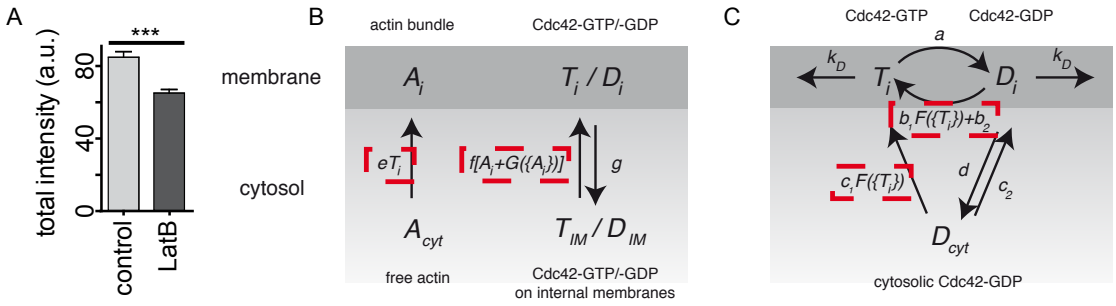

Figure 2.3: Building a mathematical model of the combined pathways. A Comparison of total intensities of GFP-Cdc42 caps in controls and LatB-treated cells. Bars indicate means ±SEM. N>80. ***: t-test, p<0.0001. **B,C** Schematic depiction of model reactions for actin- (B) and GDI-mediated (C) recycling pathways. See section 2.4.2 and Tables 2.1 and 2.2 for details. Nonlinear feedback reactions are indicated by dashed boxes.

2.2.2 A stochastic model for polarity establishment through Cdc42 recycling

In order to build an experimentally tractable model we considered the two recycling pathways for Cdc42 separately. Recent studies on actin-mediated transport of membrane-bound Cdc42 have stressed the importance of considering individual vesicle carriers instead of simple protein flux [75, 62] to represent actual concentrations of proteins in recycling intermediates. However, many mechanistic details of actin-based membrane recycling are unknown or difficult to estimate, rendering detailed molecular models highly speculative. Importantly, the proposed dilution effect of vesicle delivery on Cdc42 concentration in the cap [62] is not supported by our experiments, as Cdc42 cap intensities are significantly higher in control cells compared to LatB-treated cells, in which actin-mediated transport processes are disrupted (Fig. 2.3A). We therefore opted to simulate actin-mediated recycling of Cdc42 using a coarse-grained approach that builds on an earlier model for spontaneous polarization of constitutively active Cdc42 [17] (Fig. 2.3B, see section 2.4.2 and Tables 2.1 and 2.2 for a detailed description of parameters and reactions). Briefly, we assumed that membrane-bound Cdc42 molecules are delivered to the plasma membrane from internal membranes via transport along actin cables. Sites of enhanced cable nucleation are effectively generated (or recruited) at a rate that depends on the amount of active Cdc42 present at the respective nucleation site (see section 2.4.2). Endocytosis was modelled with a constant extraction rate.

For the Rdi1-mediated recycling pathway we assumed that a well-mixed pool of Cdc42 is present in the cytosol and that Cdc42 diffuses laterally in the plasma membrane with a diffusion constant $D = 0.036 \mu m^2 s^{-1}$ [28]. Nucleotide exchange can occur spontaneously or be catalyzed by the GEF Cdc24 via a bounded positive feedback loop involving the Cdc42 effector Bem1 [16, 65]. Such bounded feedback is essential to achieve realistic protein accumulation (see Figure 2.7) and corresponds to depletion of limiting components involved in Cdc42 recruitment (either Bem1, Cdc24 or another essential activator). GTP hydrolysis is modelled with a constant rate depending on GAP activity.

It is commonly assumed that GDIs preferentially extract the inactive form of Rho GTPases, and this has been confirmed recently using purified components and model membranes [30, 93].

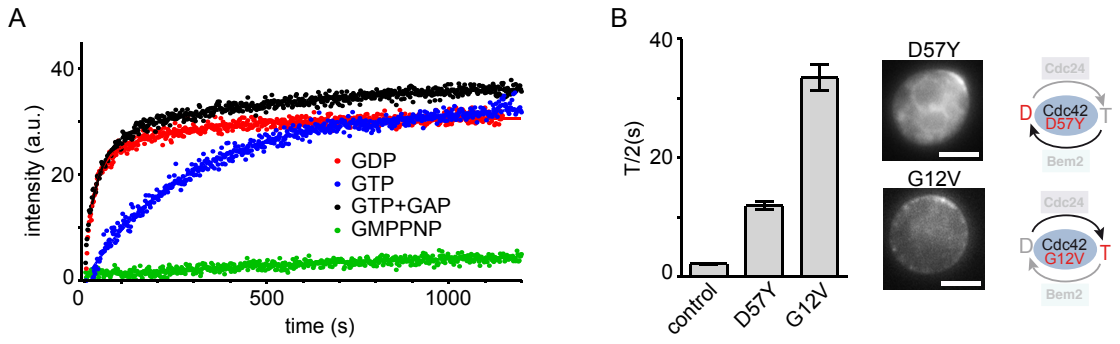

Figure 2.4: Extraction of Cdc42 from membranes. A Extractability of Cdc42 from hexadecanoylaminofluorescein (HAF)-labeled liposomes loaded with the indicated methylanthraniloyl-modified (Mant-) nucleotides. **B** Halftimes (FRAP T/2) for localization of inactive $Cdc42^{D57Y}$ and constitutively active $Cdc42^{G12V}$. Bars indicate means ± SEM. N > 10. The schematics illustrate changes in the Cdc42 GTPase cycle. Scale bars: 4μm. See section 2.4.4 for details.

To firmly establish this important aspect in our model, we performed in-vitro extraction experiments with purified Cdc42 and RhoGDI [30]. We found that the GDI indeed extracted GDP-bound Cdc42 around 10 times faster than GTP-Cdc42 (Fig. 2.4A). Importantly, in the presence of catalytic amounts of a GTPase-activating protein (GAP) domain, GTP-Cdc42 was effectively extracted at nearly the same rate as GDP-Cdc42, indicating that GTP hydrolysis is the rate-limiting factor for GDI-mediated Cdc42 extraction. This was further supported by the extremely slow extraction of Cdc42 bound to a non-hydrolyzable GTP analogue (GMPPNP, see Fig. 2.4A). In living yeast cells, we confirmed a previous report [29, 65] that a non-cycling, constitutively active Cdc42 ($Cdc42^{G12V}$) is restricted to membranes and is recycled exclusively via the slow actin-mediated recycling pathway (Fig. 2.4B, section 2.4.7). We therefore incorporated into our model the selective extraction of GDP-Cdc42 from the plasma membrane directly into the cytosol by Rdi1.

Recruitment from the cytosolic Rdi1-GDP-Cdc42 pool to the membrane was assumed to occur at a spontaneous background rate, and via a second positive feedback loop that leads to enhanced attachment of cytosolic Cdc42 to sites of already high Cdc42 activity on the plasma membrane. This feedback represents the previously proposed competition between Rab and Rho GEFs and the respective GDIs [94, 95, 96]. We wanted to directly observe, whether such competition could also occur for Rho GTPases. To this end we used purified components to investigate the effect of GDP exchange activity on the interaction between GDI and mammalian Rac1, which is very similar in mechanism and rate to GDI-Cdc42 interaction [30]. Exposure to the GEF domain of Dock180 (DHR2C) and a non-hydrolyzable GTP analog was sufficient to dissociate soluble GDI-Rac1 complexes, allowing free GMPPNP-bound Rac1 to bind to liposomes (Fig. 2.5A). Conversely, nucleotide exchange by the GEF was strongly reduced in the presence of GDI (Fig. 2.5B), consistent with competition between the two regulators for binding to the switch II region of the GTPase [95]. Our results show that competition between GEF and GDI can occur in principle for Rho GTPases, but can of course not be directly transferred to living yeast cells. However, we found that the dominant-negative mutant $Cdc42^{D57Y}$, which strongly binds and sequesters its GEF [97, 98], could no

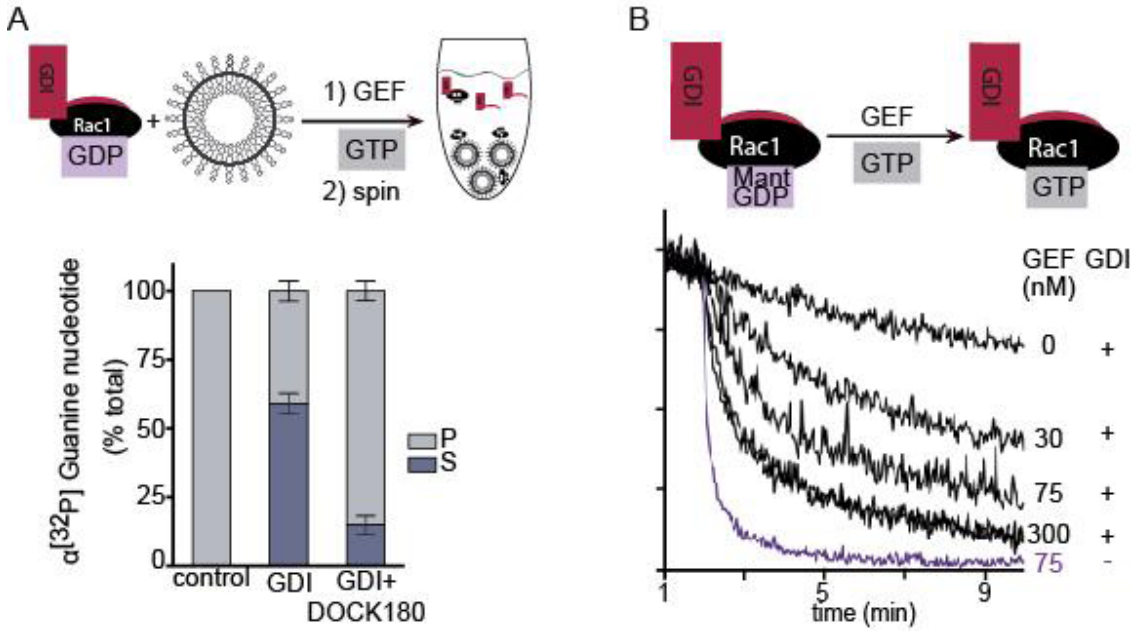

Figure 2.5: Competition between GEF and GDI for GTPase binding. A Schematic depiction (top) and result (bottom) of liposome pelleting assay. Addition of the Rac1-GEF DOCK180 blocks GDI-mediated extraction of Rac1 from liposomes. Amounts of radioactively labeled Rac1 were measured in pellet (P) and soluble (S) fractions after addition of GDI with or without the GEF domain of Dock180 (DHR2C). **B** Schematic depiction (top) and result (bottom) of the GDP exchange assay. The GDI inhibits nucleotide exchange. Rac1 was preloaded with Mant-GDP in the presence of liposomes, unlabelled GTP and GDI. Loss of Mant fluorescence due to nucleotide exchange was monitored after addition of the DHR2C GEF domain at 2 min. The exchange curve without added GDI is shown in purple. See section 2.4.4 for details.

longer be extracted by the GDI and was instead slowly recycled via actin-mediated transport [29, 65] (Fig. 2.4B). This result is consistent with competition between GEF and GDI for binding of Cdc42-GDP in vivo. In our model we therefore implemented interference of GEF activity with Cdc42-GDI interaction by increasing the rate of Cdc42 membrane association in regions of high Cdc42 activity (equivalent to high GEF concentrations).

GDI-mediated polarization is of considerable theoretical interest [73, 72, 99]. Our results indicate that GDI-mediated recycling of Cdc42 depends on the latters catalytic cycle, and both GAP and GEF need to be regulated to allow rapid shuttling between membrane and cytosol. In a previous model, activation of Cdc42 was assumed to be enhanced by a positive feedback based on nonlinear recruitment of the GEF Cdc24 to Cdc42-GTP [72, 66]. The model predicts slower turnover of Cdc24 if Cdc42 activity is increased (cf. derivation of the prediction in section 2.4.1). However, we found that the level of GEF expression or actin or Cdc42 activity had no influence on Cdc24 turnover at the polarized site (Fig. 2.6B), indicating that feedback must be implemented in a fashion that differs from the previously proposed mechanism [72]. Our model relies on a linear rate of recruitment of the GEF to Cdc42-GTP, and incorporates two GEF-mediated, and experimentally supported, positive feedback loops

for activation and physical recruitment of Cdc42 (red dashed boxes in Fig. 2.3C), respectively.

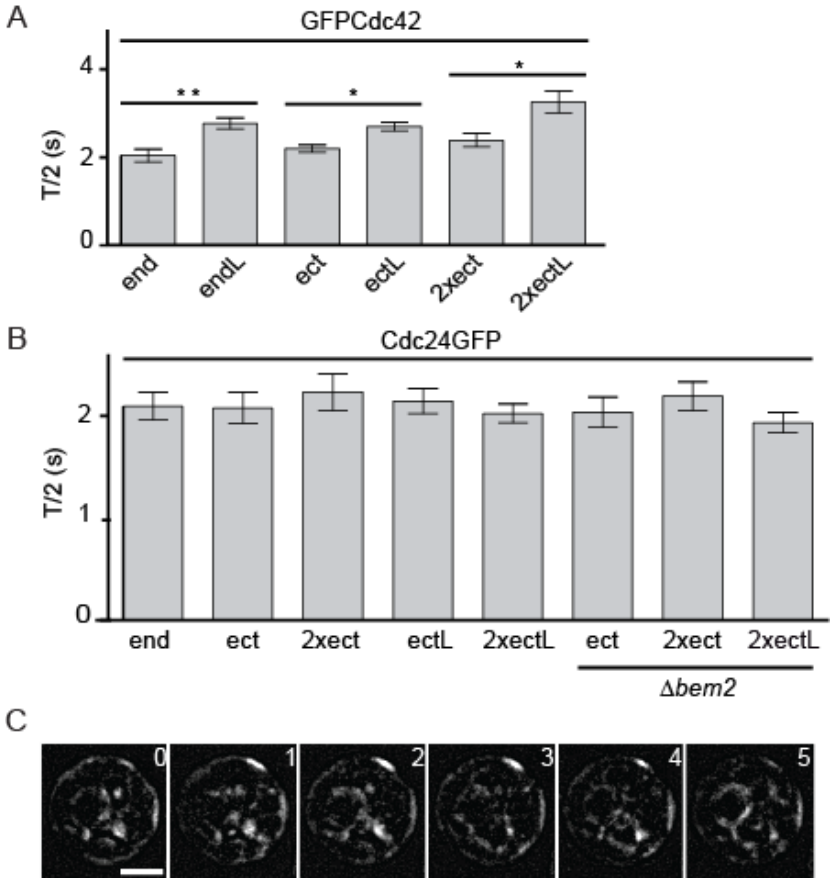

Figure 2.6: Turnover of Cdc42 and Cdc24 in polarized caps. A T/2 of GFP-Cdc42 recovery after photobleaching of polar caps in cells expressing 1-3 copies of Cdc42 (see Fig. 2.1B) with (endL, ectL, 2xectL) and without (end, ect, 2xect) LatB treatment. Bars represent means ± SEM, N>10 (see also section 2.4.7). Significant ($p<0.05$, *) and highly significant ($p<0.01$, **) differences are indicated (unpaired t-test with Welsh correction). **B** T/2 of Cdc24-GFP in polar caps in cells expressing 1-3 copies of Cdc24 (endogenously tagged or ectopically integrated copies). Recovery values (means ± SEM, N>10, section 2.4.7) are shown for control cells, cells treated with LatB, and Δbem2 cells. **C** An unstable GFP-Cdc42 cap in a cell exposed to LatB. Time is indicated in min. Scale bar: 4 μm. Images were subjected to background subtraction and Gaussian smoothing in ImageJ.

2.2.3 Determination of quantitative model parameters

Having established a general structure for the two Cdc42 recycling pathways we set out to determine realistic values for the parameters involved in their operation. Our aim was to base all model reactions (Table 2.1) and parameters (Table 2.2) on experimental evidence. Several parameter values and data concerning the distribution of Cdc42 between cell compartments were taken from the literature (section 2.4.2). The remaining values were fitted to quantitatively reproduce characteristics of control cells (Figs. 2.7A,D; 2.8C) and of the individual

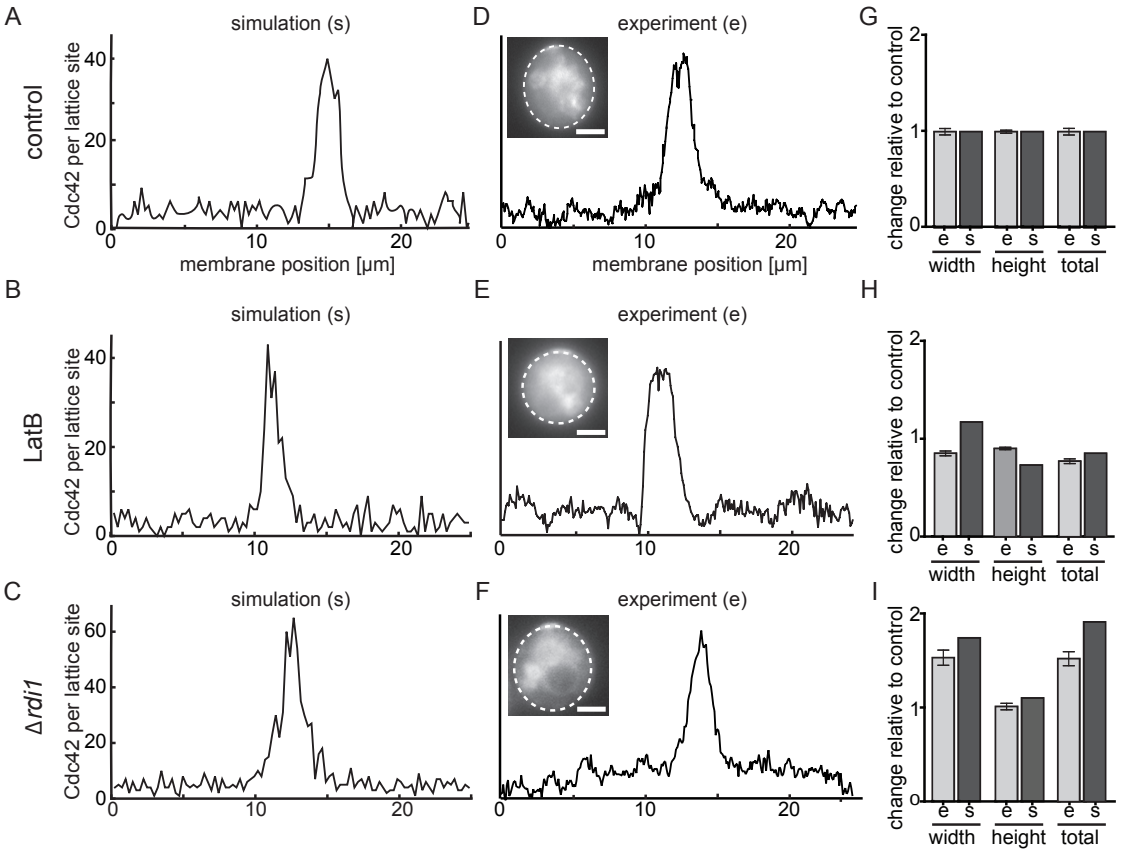

Figure 2.7: Fitting parameters - cap shape. A-F Examples of simulated (A-C) and experimentally determined (D-F) cap profiles in control cells (A, D), LatB-treated cells (B, E) and Δrdi1 cells (C, F). Dashed lines in images indicate fields of view used for line scans. Scale bars: 4 μm. **G-I** Comparisons of cap size (width), average cap intensity (height) and total cap intensity (total = width * height) in experiments (e) and simulations (s) for control (G), LatB-treated (H) and Δrdi1 cells (I). Bars represent means ± SEM of measurements normalized to values for control cells (N=80 for control and LatB cells, and 35 for Δrdi1 cells). Note that total intensity values for control and LatB cells correspond to the values used in Figure 2.3A.

recycling pathways as seen in LatB-treated (Figs. 2.7B, E, 2.8D) or Δrdi1 (Figs. 2.7C, F; 2.8E) cells. In all three conditions our model was able to recapitulate polarization profiles of Cdc42 with realistic background levels (Fig. 2.7A, B, C) and values for cap width and cap height (Fig. 2.7G, H, I).

The mobility of Cdc42 itself is a major element in any dynamic polarization model. We therefore performed fluorescence recovery after photobleaching (FRAP) experiments to monitor the kinetics of Cdc42 recycling mediated by actin or Rdi1. In agreement with previous measurements [29, 65], recovery of Cdc42 fluorescence in control cells occurred rapidly, with an average T/2 of 2.2 s, and was independent of Cdc42 expression level (Figs. 2.8A,B, 2.6A, section 2.4.7). Disruption of actin structures with LatB led to a slight increase of T/2 to 2.5 s (Figs. 2.8A,B, 2.6A, section 2.4.7). This slower recovery was proposed to result from

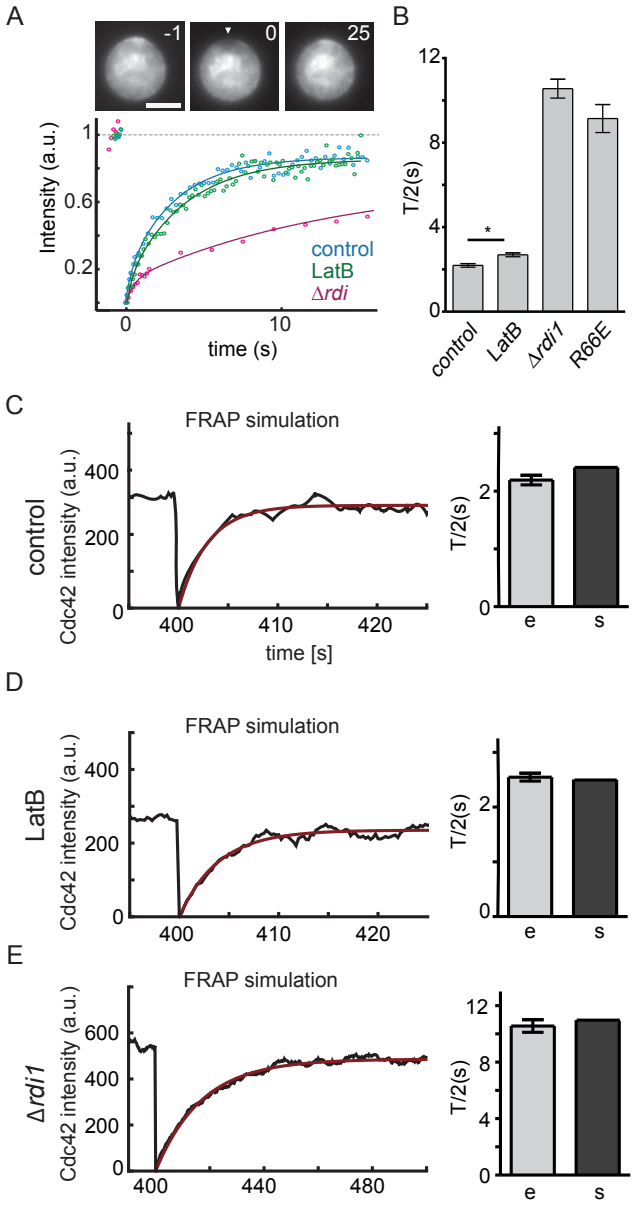

Figure 2.8: Fitting parameters - Cdc42 turnover. **A,B** Representative FRAP curves (A) and FRAP T/2 values (B) for GFP-Cdc42 in controls, Δrdi1 cells, cells expressing GFPCdc42^{R66E} and cells treated with LatB. The arrowhead in (A) indicates the position targeted for FRAP. Bars in (B) represent means ± SEM. N>10. *: t-test, p<0.05. Time is indicated in s. Scale bar: 4 μm. **C-E** Simulated FRAP curves (black) and exponential fits (red), and comparison of T/2 values for simulated (s) and experimental (e, identical to bars in (B)) recovery. Actual and simulated FRAP data are shown for control (C), LatB-treated (D) and Δrdi1 (E) cells.

greater accumulation of Cdc42 in caps in the absence of dilution by the delivery of Cdc42-poor membrane [62]. However, as discussed above, Cdc42 cap intensities in LatB-treated cells were significantly reduced (Fig. 2.3A), supporting a positive role for actin in Cdc42 polarization. Perturbation of Cdc42-Rdi1 interactions by deletion of RDI1 or the use of the $Cdc42^{R66E}$ mutant drastically slowed recovery to a T/2 of 10 s (Fig. 2.8B, section 2.4.7), which is consistent with previous work on polarity maintenance [29]. These results again confirm that Rdi1- and actin-dependent Cdc42 recycling act in parallel during polarity establishment, and show that the pathways act on different time scales – with GDI-mediated cytosolic cycling being 4-5 times faster than actin-mediated transport. Importantly, all values for Cdc42 mobility could be accurately reproduced with the fitted parameters in our model (Fig. 2.8C-E).

2.2.4 Validating the model

Our model was able to reproduce quantitative characteristics of Cdc42 mobility and distribution under various experimental conditions. We next wanted to test whether it could also make predictions regarding features of the polarization process that we could test experimentally. One critical aspect of the model is the fact that GDI-mediated extraction is restricted to GDP-Cdc42. This is predicted to result in a loss of polarization at very low rates of hydrolysis specifically in LatB-treated cells (Fig. 2.9A). The hydrolysis rate in control cells, estimated by fitting values for cap height/width and FRAP times, was 2.74/s (gray dashed line Fig. 2.9A). To check the model-based prediction in vivo we reduced the rate of hydrolysis of Cdc42-bound GTP by deleting BEM2, the Cdc42 GAP with the largest number of genetic interactions with actin (Fig. 2.2A). Δbem2 cells were still able to polarize efficiently, albeit with slightly reduced speed (Fig. 2.9B). However, when actin polymerization was prevented with LatB, most Δdem2 cells were no longer able to polarize (Fig. 2.9B). In our simulations we observed that polarization occurred over a wide range of hydrolysis values, with the wild-type rate being close to the maximum permissible before polarization breaks down (Fig. 2.9A). To study the impact of changes in hydrolysis rates on a more precisely quantifiable parameter than the polarization efficiency, we next tested the effect of deletion of BEM2 on Cdc42 mobility as measured by FRAP. The model predicted a gradual increase in FRAP T/2 upon progressive reduction of the rate of GTP hydrolysis (Fig. 2.9C), and this slowdown should be even more pronounced in LatB-treated cells. In agreement with these expectations, in Δbem2 cells and with the slow-acting mutant $Cdc42^{G60A}$ [22], FRAP halftimes increased from 2.2 s to 6.7 s and 6.8 s, respectively (Fig. 2.9D, section 2.4.7). In our model this recovery rate corresponds to a roughly 16-fold decrease in the rate of GTP hydrolysis to a value of around 0.17/s (gray dashed lines in Fig. 2.9C). At this hydrolysis rate, Cdc42 in LatB-treated cells is predicted to recycle with a T/2 of 8.7 s - a value close to the measured 9.6 s for LatB-treated Δbem2 cells (section 2.4.7). Hence, our results indicate that the relative contribution of actin to Cdc42 recycling is increased in Δbem2, likely due to the reduction in the rate of extraction of active Cdc42 by its GDI.

2.2.5 The mechanism of formation of multiple polarization sites

In all our simulations and experimental conditions, the GDI pathway alone was never able to generate more than one stable polarization site (see section 2.4.3). However, yeast cells are

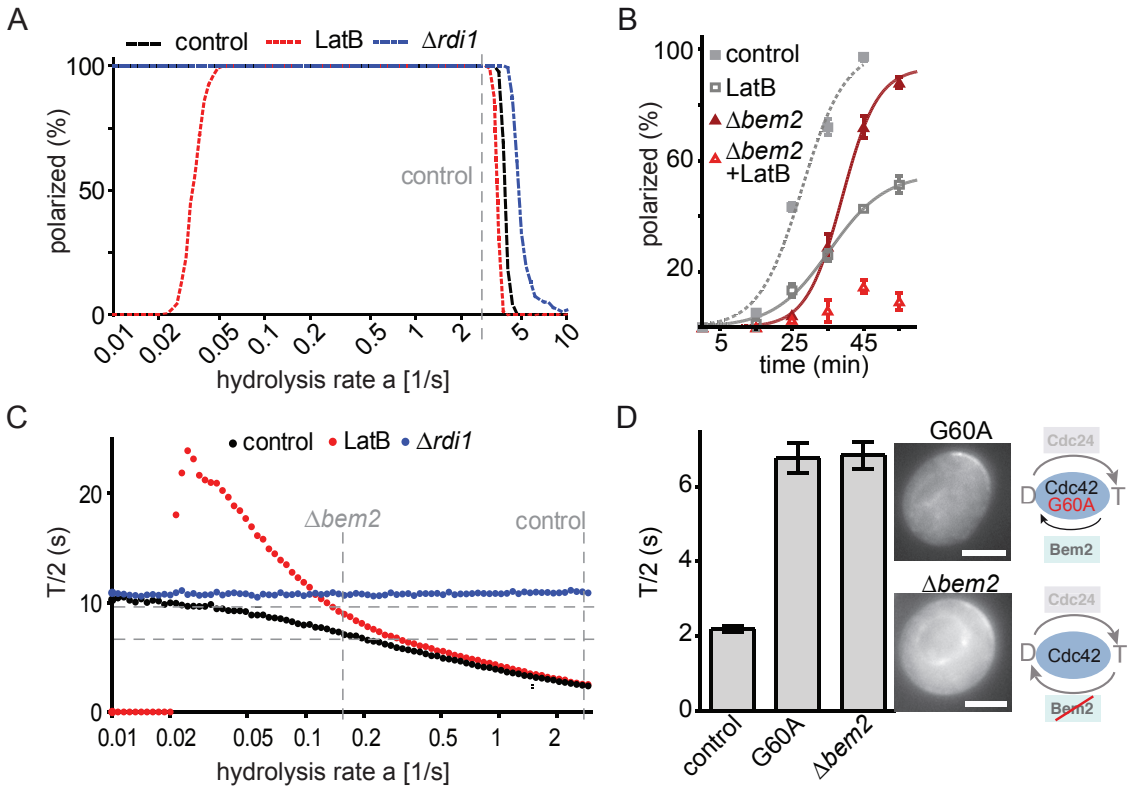

Figure 2.9: Model predictions - effects of GTP hydrolysis on polarization efficiency and Cdc42 dynamics. A Predicted dependence of polarization efficiencies in control, LatB-treated and Δrdi1 cells on the rate of GTP hydrolysis. The hydrolysis rate for control cells (a = 2.74/s) was estimated by fitting model parameters (Figs. 2.7, 2.8), and is indicated by the vertical dashed gray line. **B** Polarization efficiency of Cdc42 in control and Δbem2 cells in the presence or absence of LatB. Data points represent means of three experiments with 50 cells each. Error bars indicate SD. The lines are sigmoidal fits. **C** Plot of simulated Cdc42 FRAP T/2 (mean values from 400 runs/data point) against rate of GTP hydrolysis. Fitted and estimated hydrolysis rates in control and Δbem2 cells are indicated as vertical dashed gray lines. T/2 values measured in Δbem2 cells without (6.8 s) and with LatB (9.6 s) are indicated as horizontal dashed gray lines. **D** FRAP T/2 and localization of Cdc42 in Δbem2 cells and in cells expressing $Cdc42^{G60A}$, a mutant with a lower GTPase activity. Bars represent means ±SEM. N>10. Schematics illustrate changes in the Cdc42 GTPase cycle. Scale bars: 4 μm.

capable of simultaneously polarizing at two or more sites, for example after deletion of BEM2 [35], deletion or overexpression of BEM1 [38, 65] or overexpression of constitutively active Cdc42 [17]. Interestingly, we noticed that 2.3 ± 0.5% (n= 4x100 cells) of Δrdi1 cells formed two stable polarization sites (Fig. 2.10A, section 2.4.8). A comparable frequency of multiple polarization sites could be robustly reproduced in our model after fitting the actin-mediated pathway (Fig. 2.10C, gray dashed line at a = 2.74/s, section 2.4.3). Varying the parameters in the model then generated two testable predictions. First, increased Cdc42 activation should strongly increase the percentage of Δrdi1 cells that form multiple polarization sites (Fig. 2.10C, blue curve). Second, even cells with a functional GDI should form multiple caps

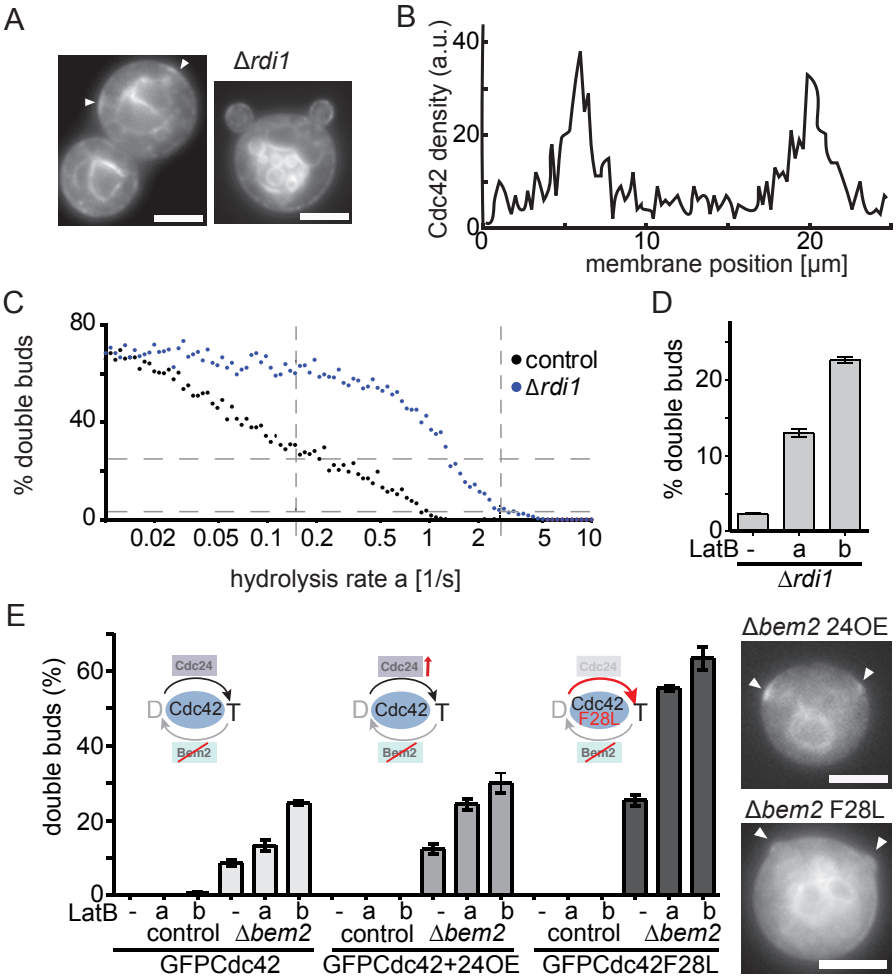

Figure 2.10: Formation of multiple polarization sites. A Examples of simultaneous formation of two Cdc42 caps (arrows) and buds in Δrdi1 cells. Scale bars: 4 μm. **B** Intensity profile illustrating formation of two caps in a simulated Δrdi1 cell. **C** Predicted effects of varying the rate of GTP hydrolysis on formation of multiple polarization sites in simulations of control and Δrdi1 cells. Fitted and estimated hydrolysis rates in control and ΔBem2 cells are indicated as vertical dashed gray lines. Percentage of double buds observed in Δbem2 cells after washing LatB out (25%) and in Δrdi1 cells (2.3%) are indicated as horizontal dashed gray lines. See also section 2.4.8. **D** Effect of washout of LatB on the percentage of Δrdi1 cells with two buds. Cells were treated with LatB for 20 min (a) or 40 min (b) before washout of the drug or without treatment (-). See Fig. 2.11 for experimental details. **E** Effect of Cdc42 activity level on the formation of double buds in control and ΔBem2 cells. Cells expressing GFP-Cdc42, GFP-Cdc42 and Cdc24-RFP or GFP-Cdc42^{F28L} were treated with LatB as in (D). Examples of double cap formation in Δbem2 cells expressing either GFP-Cdc42 or GFP-Cdc42^{F28L} are shown on the right. Bars represent means and SEM for three experiments with $>$ 100 cells each. Schematics illustrate changes in the Cdc42 GTPase cycle. Scale bars: 4μm.

if rates of GTP hydrolysis are reduced sufficiently (Fig. 2.10C, black curve). In contrast, Rdi1-mediated recycling of Cdc42 alone was unable to generate multiple stable caps in our

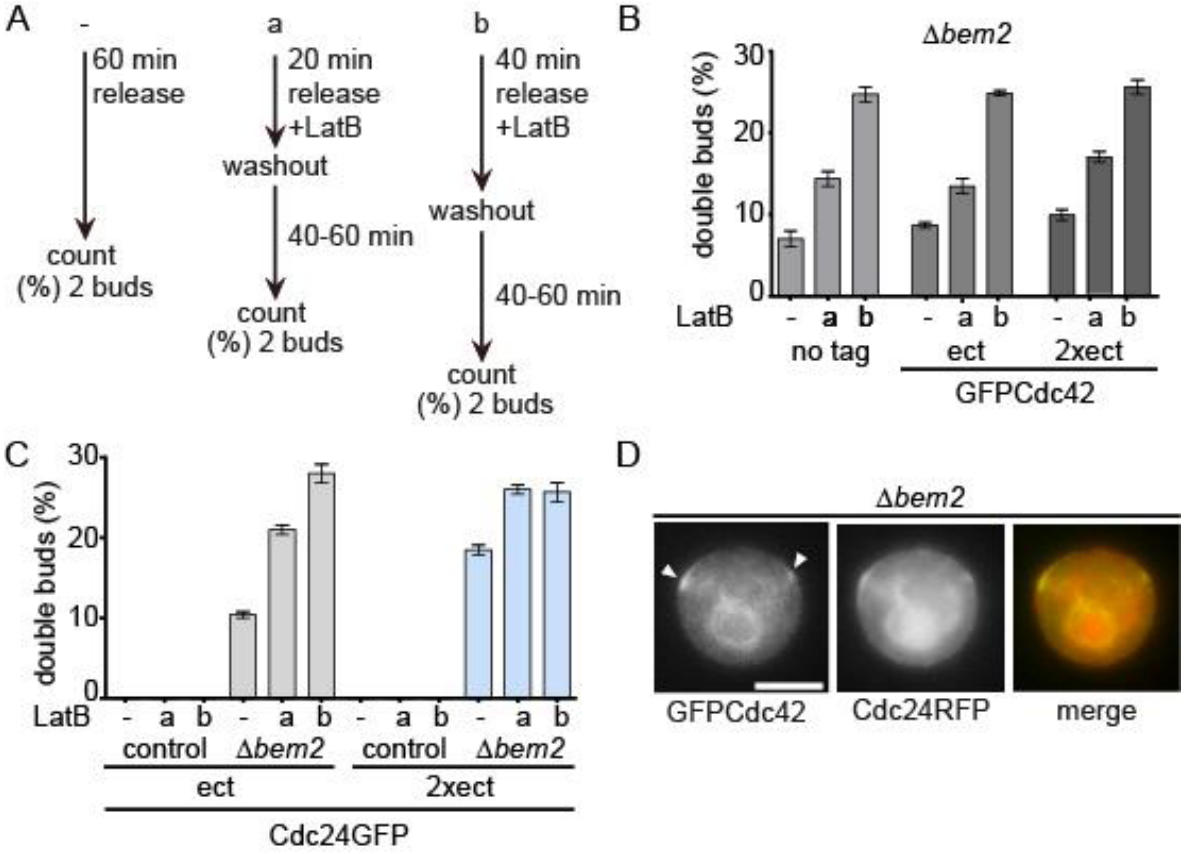

Figure 2.11: Delay of polarization causes formation of multiple polarization sites. A Schematic representation of the LatB washout procedure. **B** Effect of prior exposure to LatB (conditions for -, a and b as in (A)) on the percentage of cells with two buds formed by a ΔBem2 strain expressing one (untagged), two (GFP-Cdc42) or three (2xGFP-Cdc42) copies of CDC42. Buds were counted 60 min after removal of LatB. **C** Effect of prior exposure to LatB (conditions for -, a and b as in (A)) on the percentage of cells with two buds formed by control and Δbem2 strains expressing two (Cdc24-GFP) or three (2xCdc24-GFP) copies of CDC24. Buds were counted 60 min after removal of LatB washout. Bars in (B) and (C) represent means ± SD from three experiments with 100 cells each. **D** Colocalization of GFP-Cdc42 (green in merge) and Cdc24-RFP (red in merge) in two caps (arrowheads) in a Δbem2 cell. Scale bar: 4 μm.

simulations (section 2.4.3). The formation of multiple stable caps at lower hydrolysis rates can be explained by the reduction or loss of the ability of GDI-mediated recycling to restrict cap formation to a single polarization site and the enhanced nucleation of actin at higher levels of Cdc42-GTP. To increase Cdc42 activity in Δrdi1 cells, we exploited the known cell-cycle dependent activation of Cdc42 after the G1/S transition [35, 33]. We released Δrdi1 cells from G1 arrest in the presence of LatB to prevent immediate polarization and washed the drug out at different times thereafter to allow polarization with varying initial Cdc42 activity (Fig. 2.11A). As predicted, the number of cells with two polarization sites increased from 2.3% to 13% and 23% with increasing duration of drug treatment and hence increasing level of Cdc42 activity (Fig. 2.10D, section 2.4.8). Next, we again used Δbem2 cells to increase Cdc42 activity in the presence of Rdi1. We found that 8.7% of cells formed two buds (Fig. 2.10E,

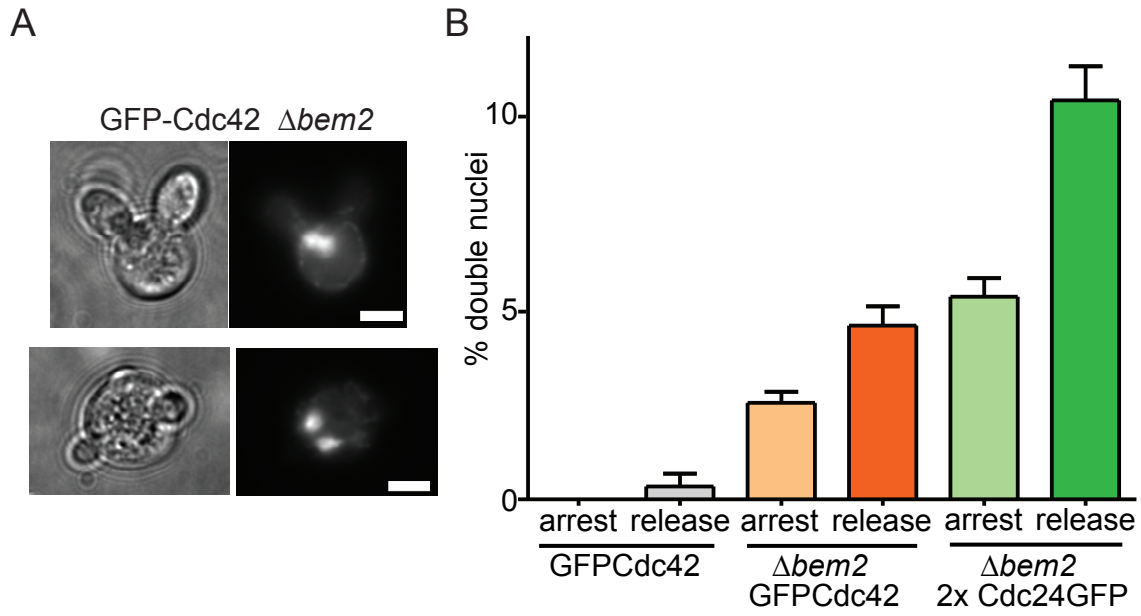

Figure 2.12: Multiple polarization sites and DNA segregation. **A** Examples of Δbem2 cells displaying two nuclei and two buds. Scale bars: 4 μm. **B** Percentage of cells with two nuclei in controls, and in Δbem2 cells expressing GFP-Cdc42 or two copies of Cdc24-GFP.

2.11C, section 2.4.8), similar to a previous report [35]. This frequency was not greatly affected by changes in Cdc42 expression level (Fig. 2.11B, section 2.4.7). We then further increased Cdc42 activity by either overexpressing the GEF Cdc24 (Fig. 2.11D) or expressing a Cdc42 mutant with a high intrinsic GDP release rate ($Cdc42^{F28L}$, [23]). Neither treatment induced formation of double buds in control cells (Fig. 2.10E, 2.11C). However, when a ΔBem2 strain was used, the number of cells forming multiple polarization sites increased significantly (Figs. 2.10E, 2.11C). Indeed, the combination of Δbem2 and $Cdc42^{F28L}$ resulted in double buds in more than 60% of cells (Fig. 2.10E). Taken together, our results indicate that actin-mediated recycling of Cdc42 is prone to creating multiple stable polarization sites, and that this effect is sensitive to the level of Cdc42 activity. Moreover, our results show that a perturbation of GDI-mediated polarization can induce the formation of multiple buds in otherwise wild-type cells.

While formation of two polarization sites in a small percentage of cells in a population might, at first sight, seem tolerable, even slight effects on cell division could translate into a strong evolutionary disadvantage. Indeed, we found that the formation of multiple buds directly correlated with an increased number of mis-segregated nuclei (Fig. 2.12A) and this effect was dependent on increased activity of Cdc42 (Fig. 2.12B). On average, more than 20% of cells with double buds also exhibited defects in nuclear segregation (compare Fig. 2.12B with Figs. 2.11 and 2.10E). Formation of multiple buds therefore likely leads to problems during mitosis and hence has a direct impact on cell survival.

2.3 Discussion

We have shown that yeast cells can spontaneously establish polarity by dynamically localizing the central polarity regulator Cdc42 through a combination of two recycling pathways with different kinetic properties and distinct biological implications.

GDI-dependent recycling of Cdc42 is fast (T/2 of 2 s) and is directly coupled to the GTPase cycle of Cdc42. Symmetry breaking in this pathway occurs via a combination of two positive feedback loops for activation and recruitment of Cdc42, and is governed by reaction-diffusion dynamics. GDI-mediated polarization is characterized by efficient formation of a unique polarization axis, but is at the same time sensitive to perturbations in the GTPase cycle of Cdc42.

In contrast, actin-mediated recycling of membrane bound Cdc42 is slower (T/2 of 10 s) and depends solely on Cdc42 activity [17]. The use of long-lived actin cables for directed delivery of Cdc42 to the PM leads to formation of very stable polarization sites. However, this stability comes with a significant risk of stochastically generating multiple stable polarization sites - something that becomes especially prominent if levels of Cdc42 are increased. By combining the two recycling pathways, yeast cells ensure reliable establishment of a unique polarity axis, which is essential for correct cell division.

To quantitatively describe and analyze the interplay between the two Cdc42 recycling pathways, we have built a detailed, particle-based mechanistic model for polarity establishment and performed extensive stochastic simulations. We took great care to keep the complexity of the model (number of parameters, reaction equations) at a level that was appropriately supported by experimental evidence. We used measurements from previous studies, as well as a variety of quantitative in vivo and in vitro experiments, to validate the underlying assumptions and constrain values for the remaining free parameters. This integrated approach allowed us to make detailed predictions concerning polarization efficiency, protein localization kinetics and number of polarization sites, which were successively verified with remarkable accuracy by experimental data.

Two key features in our mathematical model should be emphasized. First, we found that polarity establishment in yeast did not sensitively depend on the quantity of Cdc42 in the cell. This was also observed in our simulations, where even a 10-fold increase in Cdc42 concentration failed to prevent polarization. These findings contradict a recent study, in which stochastic polarization of Cdc42 was proposed to depend critically on low expression levels [73]. Instead, we find, as in our original study with constitutively active Cdc42 [17], that polarization depends on the level of Cdc42 activity, and hence on the concentration of the GEF present at the site of polarization, which ultimately drives both central feedback loops in the GDI-mediated polarization of Cdc42.

Second, because it separately implements positive feedback in Cdc42 activation (Cdc42GTP-GEF-Bem1-Cla4 interactions) and Cdc42 recruitment (GEF-GDI competition), our theoretical model does not depend on non-linear recruitment of the GEF Cdc24 as proposed by a previous Turing-type model [72] that was not supported by our experimental results.

Our results indicate that yeast cells did not simply evolve two redundant pathways for cell polarization in order to safeguard an essential process against random error. Instead they

combine the positive features of two pathways to simultaneously achieve reliability and spatial precision in cell polarization. Such an optimized interplay of pathways requires an appropiate selection of parameter values. Indeed, our results suggest that the GTPase cycle of Cdc42 plays a central role in coordinating pathways underlying polarity establishment. In particular, the Cdc42 hydrolysis rate is restricted to a rather narrow range between roughly 1 and 3/s. Faster rates of hydrolysis lead to a complete loss of polarization due to the lack of sufficient amounts of active Cdc42 in the cell (Fig. 2.9A), while slower hydrolysis leads to formation of multiple buds (Fig. 2.10C). The latter effect is a result of a reduced recycling speed and hence smaller contribution for the GDI pathway on the one hand (Fig. 2.9C) and a simultaneous failure of the actin pathway to focus polarization to a single site if Cdc42 activity is increased (Fig. 2.10C). GDI recycling therefore needs to be faster than the actin pathway to ensure that polarization is restricted to a single site and, according to our simulations, Cdc42 seems to indeed hydrolyze GTP with nearly maximal possible speed. At the other extreme, if the GDI pathway is deleted, cells become very prone to form multiple caps (Fig. 2.10C).

Our results provide a mechanistic link between the well established fast GTPase cycle and GDI-mediated recycling of Rho GTPases. Similar interactions have also been reported for small GTPases of the Rab family [100] that control intracellular membrane trafficking. The molecular mechanisms we identified for localization of Cdc42 during cell polarization might therefore also be applicable for other processes of spatial cellular organization.

Our proposed model for Cdc42 polarization was capable of reproducing all our experimental results and accurately and quantitatively predicted several experimentally validated phenotypes. However, there are still many open questions concerning mechanistic details of the biophysical and biochemical processes driving cell polarization. For example, it has recently been demonstrated that lipid composition at the polarized site, in particular negatively charged phospholipids, influence the association of Cdc42 (with its positively charged poly-basic region) with the plasma membrane and hence impact on cell polarity [54, 101]. Furthermore, while we assumed cell cycle-dependent activation of Cdc24 and inactivation of Bem2 in the LatB washout experiments (Fig. 2.10, 2.11), the detailed biochemistry of these regulatory processes is not fully understood and they were not included in the mathematical model. Finally, we did not consider potential regulation of GDI-Cdc42 interaction or GDI-membrane interaction by phosphorylation [102]. All these additional aspects provide ample scope for future improvements in both modelling and mechanistic understanding of cell polarization. As nicely summarized in a recent review, the value of a mathematical model should be judged "not by how complex and detailed it is, but by what could be learned from it" [103]. Our current model consequently incorporates the minimum degree of complexity compatible with the generation of meaningful forecasts, and was able to reflect and predict basic properties of cellular organization that will hopefully help to rationalize a variety of different biological processes.

2.4 Materials and methods

2.4.1 Test of Turing-like model of Goryachev and Pokhilko

To experimentally verify the polarization model proposed by Goryachev and Pokhilko [72] we considered the GEF Cdc24 dynamics predicted by this model. The model assumed that cytosolic Bem1-Cdc24 complexes (E_c) can attach to the membrane with a basal rate k_1 or attach by forming a complex M with Cdc42-GTP (T) on the membrane with rate k_7. Membrane-bound Bem1-Cdc24 (E_m) was allowed to detach with rate k_{-1} or to form a complex M with Cdc42-GTP with rate k_4. The opposite reaction of the complex formation was included with rate k_{-4}.

Given these reactions we concluded that for very low Cdc42-GTP concentrations all Bem1-Cdc24 on the membrane will be given in its Cdc42-GTP independent form E_m. In contrast, for high Cdc42-GTP concentrations the reactions k_7 and k_4 will strongly enhance the formation of M complexes on the expense of E_m and E_c. Therefore, the fraction of Cdc24 on the membrane, which can detach to the cytosol with rate k_{-1}, gets smaller at higher Cdc42-GTP concentrations.

In general, the time scale at which Cdc24 is removed from a membrane compartment is given by the fraction of the total Cdc24 number and the protein flux J_- out of this compartment, i.e. $\tau = (\int E_m + \int M)/J_-$. Neglecting the contribution of the small lateral membrane diffusion the exchange time τ is given by

$$\tau = \frac{\int E_m + \int M}{k_{-1} \int E_m} \tag{2.1}$$

where $\int$ denotes an integration over the whole compartment of the membrane. Hence, given the aforementioned dependence of M and E_m on Cdc42-GTP the model predicts that time τ depends on the concentration of Cdc42-GTP as well. To obtain a more quantitative expression for τ we used approximate expressions for E_m and M derived by Goryachev and Pokhilko assuming rapid cytosolic diffusion, fast reaction kinetics compared to the membrane diffusion, and separation of time scales. These expressions are given by

$$E_m = E_c \left(\frac{k_1}{k_{-1}} + \frac{k_7}{k_{-1}} T \right) , \quad M = E_c T \left(\frac{k_4 k_7}{k_{-1} k_{-4}} T + \frac{k_4 k_1}{k_{-4} k_{-1}} + \frac{k_7}{k_{-4}} \right) \tag{2.2}$$

where E_c is assumed to be constant due to rapid cytosolic diffusion. The term of M with quadratic dependence on T represents the core reaction of the model necessary for pattern formation. Using the parameters given by the authors [72, 66] we obtained

$$E_m = E_c \left(1 + \frac{T}{\mu M} \right) , \quad M = E_c \frac{T}{\mu M} \left(2 + \frac{T}{\mu M} \right) . \tag{2.3}$$

Accordingly, for the exchange time τ of Cdc24 we got

$$\tau = \frac{\int \left(1 + \frac{T}{\mu M}\right) + \int \frac{T}{\mu M}\left(2 + \frac{T}{\mu M}\right)}{k_{-1} \int \left(1 + \frac{T}{\mu M}\right)} . \tag{2.4}$$

Note that the concentration of membrane-bound proteins is measured per volume in a $10nm$ thick layer along the membrane [72]. Again we found that τ depends on the concentraction of active Cdc42. The time τ can approximately be determined using fluorescence recovery after photobleaching (FRAP) of Cdc24. Importantly, we found that the FRAP time of polarized Cdc24 did not change as we reduced the Cdc42 hydrolysis by deletion of GAP Bem2 (Fig. 2.6B) indicating that τ is not affected by changes of Cdc42-GTP concentrations. According to Eq. (2.4) the model by Goryachev and Pokhilko τ is only insensitive to changes in Cdc42-GTP concentration if $T \ll 1\mu M$ in the cluster. However, this condition implies that $M \ll E_m$, $M \sim T$ and $E_m = const.$ Hence, the model of Goryachev and Pokhilko implies that the Cdc24 FRAP is unaffected by changes of Cdc42 hydrolysis only if the total Cdc24 distribution $E_m + M$ is almost homogeneously distributed along the membrane. This clearly contradicts experiments showing that Cdc24 strongly localizes to the polarization site [65].

2.4.2 Stochastic model of cell polarity

To further elucidate the roles of Rdi1 and actin-dependent recycling pathways in polarization we built a stochastic particle-based model, and simulated the emergence of polarity in budding yeast. Our model explicitly includes as variables the active (T) and inactive (D) forms of Cdc42, which can be recruited to the plasma membrane and accumulate in caps. A pool of Cdc42 (T_{IM}, D_{IM}) can be found on internal membranes (IM) and is allowed to shuttle between plasma membrane and internal membranes via endocytosis and exocytosis. Cdc42 can also be extracted from the plasma membrane directly into a well-mixed pool of cytosolic Cdc42-GDP (D_{cyt}) by interaction with its GDI, Rdi1. We considered a two-dimensional model of a circular shaped cell with radius R. The membrane was split into $n = 100$ segments where reactions take place between particles on the same segment $i = 1, ..., n$. This approach allowed us to stochastically simulate the temporal evolution of the system using the Gillespie algorithm [104].

We fitted our model to recapitulate the emergence of Cdc42 caps in latrunculin-treated and in $\Delta rdi1$ cells, and tested its reliability by comparing the predictions of the combined model with our experimental results derived from wild-type cells and mutants altered in GTP hydrolysis.

Reactions incorporated into the model

To achieve and maintain polarization, Cdc42 must be continuously returned to the cap, as diffusion in the plasma membrane acts to flatten any inhomogeneities in protein distribution. We incorporated diffusion of Cdc42 in the plasma membrane as jumps between neighbouring segments with the stochastic rate constant k_D. The rate can be calculated from $k_D = (2\pi R/n)^2$, where D is the diffusion constant and R the cell radius [105].

The intrinsic GDP exchange activity of Cdc42 is increased by its only GEF, Cdc24, which is delivered to already active Cdc42 on the membrane by the effector Bem1 [42, 16]. However, recruitment of Cdc24 and Bem1 to the cap is bounded by limited availability of the molecules involved [65]. We employed an effective description of this bounded positive feedback such that the activation rate for the process

$$D_i \xrightarrow{b_1 F(\{T_i\})} T_i\,, \tag{2.5}$$

is given by a Michaelis-Menten law $F(\{T_i\}) = T_i/(c_{th} + \sum_i T_i)$ with amplitude b_1. Here D_i and T_i denote the number of passive and active Cdc42 respectively at site i. The denominator of $F(\{T_i\})$ effectively limits GEF recruitment if the total amount of active Cdc42 substantially exceeds the threshold c_{th}. Moreover, we used a similar functional form $F(\{T_i\})$ to account for GEF-mediated recruitment of Cdc42 from the cytosol with subsequent nucleotide-exchange

$$D_{cyt} \xrightarrow{c_1 F(\{T_i\})} T_i\,. \tag{2.6}$$

This term reflects direct or indirect competition for Cdc42 binding between GEF and GDI as shown in Fig. 2.5. The resulting displacement of the GDI by the GEF has been suggested previously for mammalian Rho and Rab GTPases [95, 96, 100]. In the absence of GEF, nucleotide-exchange and membrane attachment of Cdc42-GDP are assumed to occur at background rates b_2 and c_2.

Direct extraction of Cdc42-GDP from the plasma membrane is facilitated by interaction with its GDI Rdi1 (Fig. 2.4A and [52, 29]). We assumed that Rdi1 is present in large excess and diffuses rapidly in the cytosol. Therefore the extraction of Cdc42-GDP into the well-mixed cytosolic pool of Cdc42 is taken to occur with a constant rate d.

Since Rdi1 preferentially interacts with Cdc42-GDP (see Fig. 2.4A), the last reaction necessary for Rdi1-dependent polarization is hydrolysis of Cdc42-GTP. This we implemented as a first-order reaction with rate a. The reactions of the Rdi1-dependent polarization pathway are shown in Fig. 2.3C.

A second mechanism for Cdc42 recycling and cell polarization is provided by actin-mediated transport of exocytic and endocytic vesicles [17]. A promising approach to the modeling of this cycle, in which vesicles were explicitly taken into account, has been published recently [75, 62]. However, this approach do not provide polarization for measured diffusion constants [28] and make predictions which we could not confirm experimentally (cf. Fig. 2.3A) indicating that some molecular details are still incompletely understood. As we were mainly interested in how the distribution of Cdc42 affected the reorganization of the cytoskeleton, we heuristically modeled the effective protein dynamics induced by endocytosis and exocytosis. Details of the model are shown in Fig. 2.3B.

We assumed that the nucleotide bound to Cdc42 does not change during recycling as intrinsic nucleotide exchange and hydrolysis rates are very low [24] and the GAP and GEF for Cdc42 are expected to be mostly active on the plasma membrane where they are present at higher concentration in polar caps or patches [65]. Cdc42 caps are maintained by a dynamic

balance of focused exocytosis, dilution by lateral diffusion within the plasma membrane, and endocytosis [28]. We made the simplifying assumption that the total exocytic flux of Cdc42 remains the same before and after polarization for a given internal pool of cargo. The flux of Cdc42 from the internal membranes is equally spread over the whole plasma membrane in unpolarized cells but is slightly focused in polarized cells. We implemented this in our model by allowing the 'nucleation' of $N_A = 2$ sites of increased exocytosis on the plasma membrane similar to earlier models [17]. As actin reorganization is under control of Cdc42-GTP we modeled the nucleation of stable actin bundles as

$$A_{cyt} \xrightarrow{eT_i} A_i \,. \tag{2.7}$$

where A_{cyt} and A_i represent available and nucleated stable actin bundles, respectively, with $\sum A_i + A_cyt = N_A$. The exocytic flux is described by the reactions

$$T_{IM} \xrightarrow{f[A_i+G(A_i)]/h} T_i \,, \tag{2.8}$$

$$D_{IM} \xrightarrow{f[A_i+G(A_i)]/h} D_i \tag{2.9}$$

with $G(\{A_i\}) = (h - \sum_i A_i)/n$, where h describes a background exocytosis rate in regions not impinged upon by actin cables. This description allows for focused exocytosis along nucleated actin bundles while keeping total exocytosis constant. Finally, we approximated endocytosis of Cdc42 to internal membranes by a constant endocytosis rate g. All reactions of the agent-based model are summarized in Table 2.1.

reaction	formula
membrane diffusion	$T_i \xrightarrow{k_D} T_{i\pm1}$, $D_i \xrightarrow{k_D} D_{i\pm1}$
hydrolysis	$T_i \xrightarrow{a} D_i$
nucleotide-exchange	$D_i \xrightarrow{b_1 T_i/(c_{th}+\sum_j T_j)+b_2} T_i$
recruitment	$D_{cyt} \xrightarrow{c_1 T_i/(c_{th}+\sum_j T_j)} T_i$
	$D_{cyt} \xrightarrow{c_2} D_i$
extraction	$D_i \xrightarrow{d} D_{cyt}$
actin bundle nucleation	$A_{cyt} \xrightarrow{eT_i} A_i$
exocytosis	$T_{IM} \xrightarrow{f[A_i+(h-\sum_j A_j)/n]/h} T_i$,
	$D_{IM} \xrightarrow{f[A_i+(h-\sum_j A_j)/n]/h} D_i$
endocytosis	$T_i \xrightarrow{g} T_{IM}$
	$D_i \xrightarrow{g} D_{IM}$

Table 2.1: Model reactions

Parameter estimates

To fit our model we first separately considered LatB-treated wild-type and $\Delta rdi1$ cells. The diffusion constant D of Cdc42, the total number N_{42} of Cdc42 and the intrinsic activation rate b_2 were taken or estimated from published data [106, 28, 65, 24]. The average cell radius R was determined to be $3.95\mu m$. As LatB-treated wild-type cells show a Cdc42 mobility (FRAP) rate of approximately 0.28/s, we estimated the extraction rate d to be 0.5/s. As initial conditions for control and LatB-treated cells we distributed on average 20% of all Cdc42 to the plasma membrane, with the remaining Cdc42 being split equally between internal membranes and cytosol [65]. In simulations of $\Delta rdi1$ cells the cytosolic fraction was redistributed to the membranes, with one-third being allocated to the plasma membrane. To begin our simulation, we assumed that the GEF had just arrived at the plasma membrane, and started with an average fraction of active Cdc42 on all membranes determined by the ratio of intrinsic activation and hydrolysis. The activation threshold c_{th} limiting the total amount of active GEF was estimated to be 100, given that roughly 300 Cdc42 molecules are localized to steady-state caps [106, 65].

The remaining parameters were chosen such that the caps formed in LatB-treated and $\Delta rdi1$ cells satisfied a set of constraints over an average of 400 runs. We fitted the GEF-dependent activation and recruitment rates b_1 and c_1, and the hydrolysis and background insertion rates a and c_2 in LatB simulations assuming exocytosis and endocytosis to be zero. Using FRAP and fractionation experiments from [65] we estimated the fraction of Cdc42 in the cap at steady state to be 10%, with the same amount being distributed over the rest of the plasma membrane. From our data shown here (Fig. 2.7) and previous publications [28, 29] we estimated the height and width of Cdc42 caps to 10 times the background density and 10% of the circumference, respectively.

The fitting constraints were a Cdc42 FRAP time in steady-state LatB caps of 2-3 s, a total amount of Cdc42 on the plasma membrane of 15-25%, a cap height of 7-12 times the background, and a cap width of 8-12%. Each simulation was terminated after $t_{end} = 1300s$ internal simulation time - comparable to the duration of our experiments and the time cells take to polarize after GEF release from the nucleus [33, 34]. A cap was deemed to have formed if a spatially averaged profile of Cdc42 (over 5% of the membrane) was higher than twice its average value. At the end of the simulation the number of caps and the particle density of Cdc42 were determined and a Gaussian distribution was fitted to the Cdc42 profile to quantify its shape. We defined the cap width as twice the distance between the turning points of the fit.

To simulate FRAP values, at time $t_{frap} = 1200s$ the number of caps was determined. For simulations with a single cap, Cdc42 in a region corresponding to 20% of the plasma membrane and centered at the cap position was changed into a 'non-fluorescent' version of Cdc42. The migration of fluorescent Cdc42 into the cap was then monitored and the recovery halftime T/2 was calculated by fitting with a single exponential function.

After fitting the model to LatB-treated cells we used the parameters obtained and successively fitted the actin nucleation rate e, the exocytosis parameters f and h, and the endocytosis rate g for $\Delta rdi1$ cells. Model parameters for $\Delta rdi1$ cells were chosen such that steady-state caps had a FRAP recovery time of 10-12 s, with 30-40% of all Cdc42 on the plasma membrane,

a cap height of 7-12 times background, 0-10% cells with double caps and 90-100% total polarization.

For LatB-treated cells we obtained 19% of all Cdc42 on the plasma membrane, 40% on internal membranes, and 41% in the cytosol. For simulated $\Delta rdi1$ cells we found that 67% of all Cdc42 was distributed to internal membranes and 33% to the plasma membrane. For control cells we found 20% on the plasma membrane, 40% in the cytosol, and 40% on internal membranes.

The results shown in Figs. 2.7-2.10 were obtained from 400 runs for each point in parameter space, with the same simulation time and evaluation procedure as described for fitting the model above. Model parameters used in simulations are summarized in Table 2.2.

parameter	value	description
n	100	number of lattice sites
R	$3.95\mu m$	cell radius; from this work
D	$0.036\mu m^2/s$	diffusion constant [28]
k_D	$0.585/s$	corresponding model reaction rate
N_{42}	3000	Cdc42 per cell; estimate obtained by comparing the fraction of Cdc42 in the cytosol and the total amount of GDI per cell [106, 65]
N_A	2	number of assumed possible actin bundle nucleation sites
a	$2.74/s$	hydrolysis rate; fitted to provide latrunculin treated control cell properties
b_1	$63.1/s$	GEF-mediated nucleotide exchange rate; fitted to provide properties of LatB treated control cells
b_2	$0.0002/s$	intrinsic nucleotide exchange rate [24]
c_1	$0.04472/s$	GEF-mediated membrane attachment rate of cytosolic Cdc42; fitted to provide properties of LatB treated control cells
c_2	$0.0015/s$	basal membrane attachment rate of cytosolic Cdc42; fitted to provide properties of LatB treated control cells
d	$0.5/s$	Cdc42-GDP extraction rate; estimated from Cdc42 FRAP in this work
e	$0.000139/s$	actin bundle nucleation rate; fitted to provide properties of $\Delta rdi1$ cells
f	$0.02236/s$	rate describing the total exocytosis of Cdc42 to the membrane; fitted to provide properties of $\Delta rdi1$ cells
h	4	parameter defining rate of background exocytosis of Cdc42; fitted to provide properties of $\Delta rdi1$ cells
g	$0.04472/s$	endocytosis rate; fitted to provide properties of $\Delta rdi1$ cells
c_{th}	100	threshold of bounded feedback; estimate based on the approximate amount of Cdc42 in the polarity cluster

Table 2.2: Model parameters

2.4.3 Robustness of polarization dynamics

The GDI-dependent polarization pathway alone can be described in terms of deterministic dynamics by a set of partial differential equations. This set of reaction-diffusion equations allows growth of a small perturbation of the unpolarized state and hence pattern formation. Our stochastic simulations of this pathway show that only one stable cluster is established. We address this behavior to the Cdc42 number conservation similar to other mass conserved polarity models [107, 72]. To check for robustness of this behavior against parameter variations we changed each reaction rate separately between 1/2 and twice its control cell value and found that either a single stable polarity cluster was formed at the end of the simulations or that in some cases the polarization efficiency was lost as for example for a higher hydrolysis rate (Fig. 2.9A). This analysis showed that the formation of a single stable polarity cluster opposed to multiple stable clusters is indeed a robust property of GDI-mediated polarization. The actin-dependent polarization pathway alone is prone to production of multiple caps as there is always the possibility that actin bundles nucleate at two (or more) distant sites on the plasma membrane. However, the risk to form two distant polarization sites can be decreased by a reduction of the probability for actin bundle nucleation. This reduction provides the polarization site which is established first with more time to redistribute Cdc42 on the membrane and therefore enhances the probability to nucleate the second actin bundle in close vicinity to the first one. The actin bundle nucleation rate is given by the product of the local Cdc42-GTP concentration times rate constant e. Hence, a change of the hydrolysis rate allows to vary the probability for actin bundle nucleation. Indeed, we found that the number of double caps in simulated Δrdi1 cells is reduced at higher hydrolysis rates as can be seen in Fig. 2.10C. Once formed clusters of this polarization pathway are stable as we assumed an irreversible actin bundle nucleation. To test for robustness of the ability to form multiple clusters we changed each reaction rate of the actin-dependent polarization pathway separately between 1/2 and twice its control cell value. We found that the risk to form two stable clusters did not vanish in most cases. However, for some changes we found that the number of double caps was strongly reduced, e.g. for a higher hydrolysis rate as can be seen in Fig. 2.10C. These observations were accompanied by a simultaneous reduction of the general polarization efficiency (e.g. compare Figs. 2.9A, 2.10C) and arise due to an insufficient probability to reliably nucleate one or even two actin bundles in all cells within the simulation time of 20 minutes. We concluded that the ability to occasionally form multiple stable clusters is a robust property of actin-dependent polarization as long as the polarization sites are established at all. To check the robustness of unique control cell polarization we combined both polarization pathways and varied each model reaction rate separately between 1/2 and twice its control cell value. We found that the occurrence of multiple stable polarity clusters was inhibited or at least significantly reduced compared to the corresponding findings for the actin-dependent polarization pathway alone. Hence, the ability of control cells to suppress the establishment of multiple stable caps compared to Δrdi1 cells is a robust model property. Stronger parameter changes are necessary to weaken this ability as for example shown in Fig. 2.10C for different hydrolysis rates. In this case we observed that the occurring multiple clusters were stable and localized together with the actin bundles indicating that the stability of multiple clusters arises from the actin part of the model. The influence of the parameter variations is summarized in Fig. 2.13.

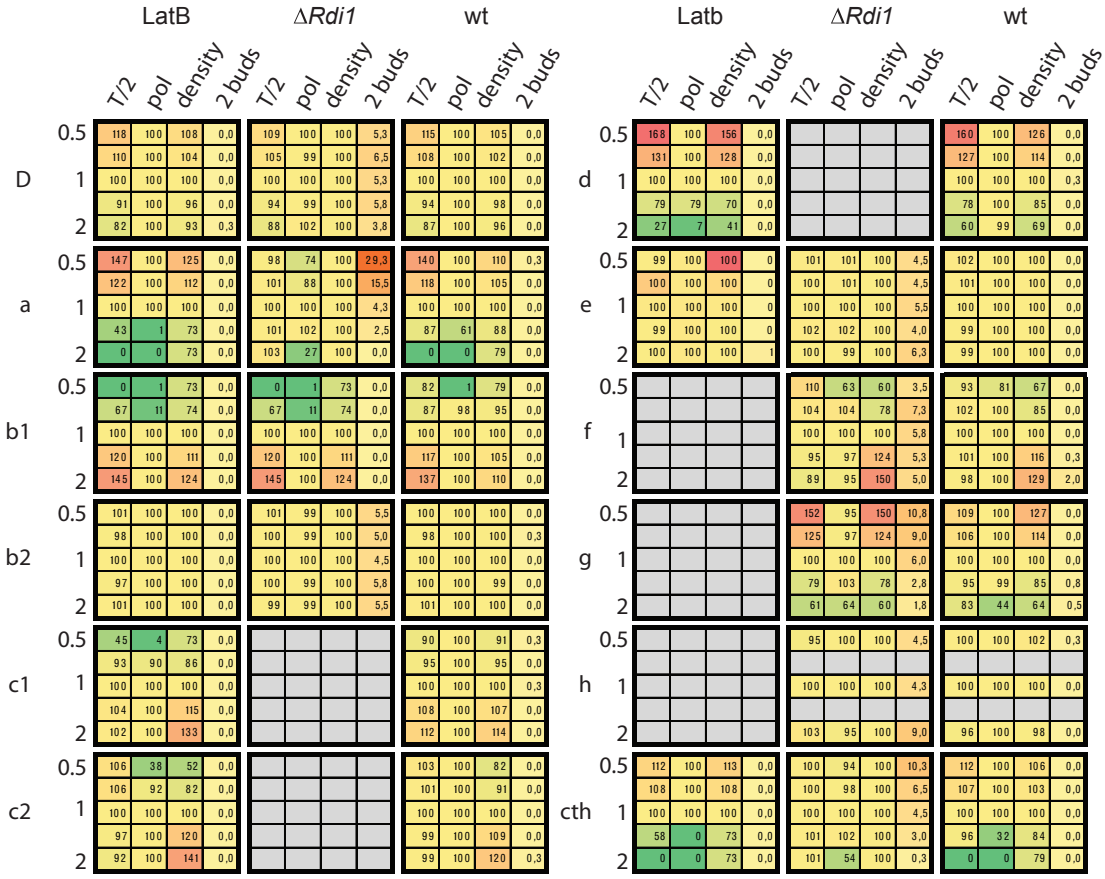

Figure 2.13: Results of parameter scan. Shown are the changes in various readouts (T/2: FRAP recovery halftime, pol: polarization efficiency, density: average Cdc42 density on plasma membrane, 2 buds: number of cells forming two buds) upon changing key parameters in our models between 2 and 0.5 fold. Parameters that are varied are indicated left of the respective matrices. For each parameter the scan results are shown for cells without actin (LatB), without the GDI (Δrdi1) or for control cells (wt). For the columns "T/2", "pol" and "density" all values are shown in % of the original parameter value (1). For the column "2 buds" the actual percentage of cells with double buds is shown. Color coding: greens indicate lower values, red/dark orange indicate higher values. Yellow/light orange indicate little change compared to the original parameter value.

2.4.4 Experimental procedures

Cell culture and plasmids

All strains used in this study are derived from RWS116, a strain in which only one G1 cyclin, CLN2, is expressed under the control of a methionine-repressible promoter [37]. Unless otherwise stated, cells were grown overnight at RT in standard SC medium containing 2% glucose but lacking methionine. To arrest logarithmically growing cells in the G1 phase of the cell cycle, methionine (3 mM) was added to the medium for 4 h. Cells were then released from cell cycle arrest by washing them three times and resuspending them in methionine-free

medium. At least 50 cells per time point were monitored for cap formation in at least three independent experiments. Mean percentages (SD) of polarized cells were plotted over time. Standard genomic manipulation procedures [108] were used for GFP integrations or gene deletions. Site-directed mutagenesis was performed as described [109]. Strains, plasmids and primers are listed at the end of this section.

Interaction screen

We used the following set of query proteins: Cdc42, its GEF Cdc24, its GAPs Bem2, Bem3, Rga1 and Rga2, and its GDI Rdi1. We also included the Cdc42 effectors Bem1 and Cla4. Physical and genetic interaction partners were collected from public databases (BioGRID [110], DIP [111] and MPACT [112]) and the literature. Physical interactions were inferred from data on affinity purification, co-crystallization, FRET, gel-retardation, PCA, protein-peptide interaction, reconstituted complexes and two-hybrid interactions. Genetic interactions were indicated by synthetic growth defects, haploinsufficiencies and synthetic lethality. We only considered negative interactions from Synthetic Genetic Array (SGA) screens in the context of the functional redundancy of pathways. We also performed an SGA screen with Rdi1 as described elsewhere [90] and identified two additional actin-related interaction partners, Gos1 and Bem2. These were verified by random spore analysis [113] and included in the final list. All interaction partners involved in actin-related processes were grouped in four sub-categories: actin general (involved in formation of actin patches or cables), early secretion (ER-to-Golgi transport), late secretion (Golgi-to-PM transport) and endocytic recycling. All identified genetic and physical interactions are listed in sections 2.4.5 and 2.4.6, respectively. For each query protein the numbers of interactions with members of each functional group were extracted. The number of unique interactions in each functional group served as a measure of the overall strength of interaction with that group and was colour-coded in a heat map (see Fig. 2.2A).

Microscopy and imaging

Coverslips were coated with 5 μl of 2 mg/ml ConA (Sigma) prior to sample observation. Raw images were used for all quantifications and analyses. Polarization and washout experiments were performed on a Zeiss Axio Imager.A1 upright microscope system with an 1.4 NA 100x objective, an X-Cite 120 light source (Lumen Dynamics) and an iXON DU-897 EMCCD camera (Andor) coupled to a 2x magnification ring. Images were acquired with Metamorph 7.0 software. Images for FRAP experiments were acquired by inclined illumination on a custom-built TIRF setup from Till Photonics based on a fully automated iMic stand with 1.45 NA 100x objective from Olympus. The 488 nm (Coherent Sapphire) and 561 nm (Cobolt Jive) lasers were directed through an AOTF and directly coupled into the iMic. A galvanometer-driven two-axis scanning head was used to adjust incidence angles. Separate filters for detection of green and red fluorophores were used to avoid spectral bleed-through. For FRAP of diffraction-limited spots at the cell equator, an additional galvanometer was used to switch between FRAP and inclined illumination modes. Caps were selected immediately after they had formed (10-20 min after release from G1 arrest). Five frames were acquired prior to the first bleaching event. Laser intensity was set to 50-100%, and bleaching

was performed for 30-50 ms. Images were collected with a cooled iXON DU-897 EMCCD camera (Andor). Acquisition was controlled by the Live Acquisition software package.

Analysis of the effects of varying Cdc42 expression levels on the efficiency of polarization

Fig. 2.1A: Cells expressing GM-Cdc42 (Cdc42 N-terminally tagged with GFP and Myc6) from the CDC42 promoter or a galactose-inducible promoter were grown overnight in SC-methionine and 2% glucose, washed three times with distilled water, diluted into SC-methionine containing 2% raffinose, and then arrested for 3 h in G1 in YPD supplemented with 2% raffinose and 3 mM methionine. Cells expressing GM-Cdc42 from the GAL promoter were induced for either 30 min or 90 min by addition of 2% galactose. To disrupt the actin cytoskeleton, cells were treated with 150 μM LatA during release from G1. Polarized cells were counted after 30 min and 60 min (cells expressing GM-Cdc42 under the CDC42 promoter) and after 30 min and 90 min (galactose-induced cells). Expression levels of GM-Cdc42 were determined by integrating fluorescence intensity for each cell.

Spotting Assay

To verify strain functionality, 3-fold serial dilutions of an equal amount of logarithmically growing cells were spotted as triplicate onto Sc-Met plates and incubated at room temperature, 30°C or 37°C for 2 days.

Growth Assay

Logarithmically growing cells were grown to an OD600 of 0.3, diluted 10 fold with medium and transferred to a 96-well flat-bottom plate (Corning). Growth rates were measured every 5 min at 30°C and OD620with a Multiscan FC 96-well reader (Thermo Scientific). Measurements of each strain were done in triplicates. Growth curves were analysed and fitted with Prism 4.0 (Graphpad).

Fluorescent Intensity measurements

Fluorescent intensities of logarithmically growing cells were measured using an INCell Analyzer 2000 (GE Healthcare) equipped with a 40x/0.6 air objective. Images of living yeast cells were automatically acquired from several positions per well with exposure times of 50 ms for the brightfield channel, 1800 ms for GFP fluorescence and 500 ms for RFP fluorescence using appropriate filter sets. 25 images with >100 cells were acquired per strain and channel and quantified using INCell Analyzer Workstation v3.7 software.

Drug treatments and staining

To disrupt all actin structures, cells were released from G1 arrest in medium containing 400 μM LatB. In washout experiments LatB treatment was performed for 20 min or 40 min, and

then removed by washing three times. Polarization (number of buds) was monitored 40-60 min later. Cells with single and double buds were counted in three independent experiments (n=100 cells each). For FM4-64 staining, cells were incubated in 0.32 μM FM4-64 for 2 min at RT, and visualized after a brief wash with distilled water. For DAPI-staining, cells were released from G1 arrest for 2-25 h and then fixed with formaldehyde. 16% formaldehyde was added to 1 ml of cells to an end concentration of 3%. Cells were incubated for 2 h at room temperature and then washed twice in PBS, resuspended in 30 μl PBS + 0.1% Triton. Fixed cells were then incubated with 0.1 μg/ml DAPI solution for 10 - 15 min and washed twice with PBS.

FRAP analysis

To quantify fluorescence recovery during FRAP experiments, automatic MATLAB (MathWorks, 2010a) routines were implemented. Intensities in the bleached region were corrected for background fluorescence (using intensities measured in a cell- free area) and efficiency of photobleaching (using a reference cell in the same image that had not been bleached). The recovery curve was normalized to the intensities before (1) and after (0) the FRAP event and fitted with the function $y_{fit}(t) = a(1 - b(\exp(-tc)) - d(\exp(-te))$. We used a double exponential fit to represent the two processes contributing to fluorescence recovery in the bleached region: fast recovery (due to rapid diffusion) of soluble Cdc42 bleached in the cytosol and slower recovery of the membrane-bound Cdc42 pool (via a combination of GDI- and actin-mediated mechanisms). The halftime for the slower component, $t^2_{1/2} = -log(0.5)/e$ was automatically extracted from the metadata provided by the acquisition software. Results were only included in the analysis if the data could be reliably fitted (residual sum of squares >0.95) and the residuals were randomly distributed below and above the curve. Means and SEMs were calculated from at least 10 independent FRAP experiments on different cells (see also Table 2.4.7).

Calculation of cap width and height

For measurements of cap width and height, GFP-Cdc42 caps were manually identified from medial cross-sections and a region R_{cap} was drawn around the perimeter of the cap. A background region R_{bg} was selected inside the same cell, avoiding bright internal membrane staining (vacuole etc.). In addition, background intensity I_0 from the camera chip was calculated from a region distant from any cell. The height H of the cap was then calculated as $H = (I(R_{cap}) - I_0)/(I(R_{bg}) - I_0)$. The cap width W was the size of the cap area R_{cap}. Total intensities I_{tot} of GFP-Cdc42 caps were calculated as $I_{tot} = H * W$.

Protein purification

Cdc42 was purified as a His6-tagged protein from baculovirus-infected Sf21 insect cells. All purification steps were performed at 4°C. Stirred 1-l cultures of Sf21 cells were infected for 48 h by Kinnakeet Biotechnology (Midlothian, VA). Cell pellets were resuspended in 40 ml of

hypotonic buffer (20 mM sodium borate pH 10.2, 5 mM $MgCl_2$, 200 μM PMSF, 1 μg/ml aprotinin and leupeptin) and disrupted by Dounce homogenization. The membrane-containing components of the lysate were spun down at 150,000×g in a Ti70 rotor (Beckman Coulter) for 20 min, after which the supernatant containing non-prenylated Cdc42 was discarded, while the pellet was resuspended in 50 ml of TBS-containing magnesium (TBSM; 50 mM Tris pH 7.5, 150 mM NaCl, and 5 mM $MgCl_2$). The procedure was repeated twice and the final pellet was resuspended in TBSM containing 1% Triton-X 100. The lysate was further homogenized and agitated for 30 min on a rotisserie, resulting in the solubilization of the geranylgeranylated Cdc42. The remaining insoluble fraction was pelleted in a tabletop centrifuge at 9,000×g for 20 min at 4°C and discarded. The supernatant containing detergent-solubilized, isoprenylated His6-tagged Cdc42 was incubated for 30 min with chelating Sepharose beads (Qiagen) charged with Ni^{2+}. Beads were then washed with 400 ml of high salt buffer (50 mM Tris pH 7.5, 700 mM NaCl, 5 mM $MgCl_2$, 0.1% CHAPS, and 20 mM imidazole) and protein was eluted with 10 ml of elution buffer (50 mM Tris pH 7.5, 150 mM NaCl, 5 mM $MgCl_2$, 0.1% CHAPS, 500 mM imidazole). The fractions containing Cdc42 were pooled and concentrated to a volume of 2 ml. His6-tagged prenylated Rac1 was purified in the same manner as Cdc42.

RhoGDI (human) and the limit GAP domain of Cdc42-GAP (human, residues 234-462) were purified from E. coli cells harbouring plasmids encoding N-terminal GST fused to each construct. The N-terminally His6-tagged DHR2C domain of human Dock180 (the limit guanine nucleotide exchange domain) was purified from E. coli cells bearing appropriate expression plasmids. Cells were grown at 37°C to OD 0.8. Protein expression was induced by adding 1 mM isopropyl 1-thio-D-galactopyranoside for 3 h before pelleting at 6,000×g for 10 min. Cell pellets were homogenized in TBSM and lysed by sonication. Cell debris was centrifuged at 20,000×g for 30 min, and the supernatant was used for purification. Supernatants containing GST-tagged proteins were incubated with glutathione beads (Amersham Biosciences) and equilibrated with TEDA buffer (20 mM Tris pH 8.0, 1 mM EDTA, 1 mM DTT, and 1 mM sodium azide) for 30 min at 4°C. The beads were then washed with several column volumes of TEDA-containing 500 mM NaCl. After a final rinse with TBSM, the protein was eluted with 10 mM glutathione in TBSM. The His6-tagged DHR2 domain was purified on chelating Sepharose beads (Qiagen) charged with Ni^{2+}, as described above. All proteins were concentrated in a 10 MWC Amicon Ultra concentrator (Fisher). Protein concentrations were determined using the Bio- Rad Protein Assay Kit with bovine serum albumin as standard.

Liposome binding assays

All liposome vesicles were prepared by extrusion using the Avanti mini-extruder. For fluorescence experiments smaller liposomes were prepared with 1 μm diameter membrane. For pelleting experiments larger liposomes were prepared using 8 μm membranes, followed by centrifugation at 16,000×g for 10 min and resuspension of pellets in TBSM. All lipids used were purchased from Avanti Polar Lipids, unless stated otherwise. The standard lipid composition in molar percentages was 35% PE, 25% PS, 5% PI, and 35% cholesterol (Nu Chek Preps).For fluorescence-based assays of Cdc42-liposome association a Varian Cary Eclipse fluorimeter was used in the counting mode. Excitation and emission wavelengths were 365 and 440 nm, respectively. Samples were stirred continuously at 25°C in TBSM. To prepare HAF (hexadecanoylaminofluorescein)-labelled lipids for FRET assays, 1.25 nmol of HAF (Molec-

ular Probes) was vortexed with 50 μl of lipids (1 mg/ml). In order to monitor the release of Cdc42 from liposomes, Cdc42 was preloaded with a methylanthraniloyl-modified (Mant) nucleotide (GTP, GDP or GMP-PNP) and incubated with 30 μl of HAF- containing liposomes at RT for 5 min. The mixture was added to the cuvette, bringing the final Cdc42 concentration to 40 nM. At the indicated time points, 50 nM RhoGDI and 10 nM Cdc42GAP were added, and fluorescence was recorded for 20 min. Traces monitored the changes in Mant fluorescence due to changes in FRET between Mant-nucleotide-bound Cdc42 and liposomes containing HAF.

Nucleotide exchange assay

Competition between GDI and the guanine nucleotide exchange factor Dock180 was measured with prenylated Rac1. Rac1 was preloaded with Mant-GDP in a 25-μl volume in the presence of 20 μl of unlabeled 1-μm liposomes. After transferring the mixture (containing 60 nM Rac1 and 500 nM Mant-GDP) to the cuvette, unlabeled GTP (10 μM) and GDI (80 nM) were added for 10 min. At the indicated times, different concentrations of the DHR2 domain of Dock180 were added. Traces monitored the loss of Mant fluorescence due to nucleotide exchange.

Statistics and data analysis

Curve fitting for polarization curves was done with Prism 4 (GraphPad Software, La Jolla) using a sigmoidal dose-response equation: $Y = Bottom + (Top - Bottom)/(1 + 10\hat{}((LogEC50 - X) * HillSlope))$. All averages are given as either geometric means SD or geometric means SEM. Unpaired two-tailed t-tests were performed to validate the significance of differences.

Yeast strains

Strain	Genotype*	Source/Reference
RWS116	MATa *cln1*::HisG *cln2*Δ *cln3*::HisG YipLac204-MET-CLN2::TRP1 *ura3 his3-11,15 ade2-1can1-100*	(Gulli et al., 2000)
RWS119	pGal-myc-GFP-CDC42::URA3 (RWC108)	this study
RWS794	pCDC24-CDC24-GFP::hphNT1	this study
RWS1023	pCDC42-myc-GFP-CDC42^{D57Y}::URA3 (RWC686)	this study
RWS1024	pCDC42-myc-GFP-CDC42^{R66E}::URA3 (RWC689)	this study
RWS1028	Δ*bem2*::G418	this study
RWS1029	Δ*bem2*::G418 pCDC24-CDC24-GFP::LEU2 (RWC153)	this study
RWS1031	Δ*bem2*::G418 pCDC42-myc-GFP-CDC42::URA3 (RWC108) p42-GFP-Cdc42::LEU2 (RWC151)	this study
RWS1034	pCDC42-GFP-CDC42::cloNAT	this study
RWS1035	Δ*bem2*::G418 pCDC42-myc-GFP-CDC42::URA3 (RWC108)	this study
RWS1036	pCDC42-myc-GFP-CDC42^{G60A}::URA3 (RWC688)	this study
RWS1037	pCDC42-myc-GFP-CDC42^{G12V}::URA3 (RWC687)	this study
RWS1038	Δ*vps27*::G418 pCDC42-myc-GFP-CDC42::URA3 (RWC108)	this study
RWS1039	Δ*rdi1*::LEU2 Δ*vps27*::G418 pCDC42-myc-GFP-CDC42::URA3 (RWC108)	this study
RWs1040	pCDC24-CDC24-GFP::LEU2 (RWC153) pCDC24-CDC24-GFP::URA(RWC146)	this study
RWS1041	Δ*bem2*::G418 pCDC24-CDC24-GFP::LEU2 (RWC153) pCDC24-CDC24-GFP::URA(RWC146)	this study
RWS1047	*myo2-16* pCDC42-myc-GFP-CDC42::URA3 (RWC108)	this study
RWS1048	*myo2-16* Δ*rdi1*::LEU2 pCDC42-myc-GFP-CDC42::URA3 (RWC108)	this study
RWS1088	pCDC42-myc-GFP-CDC42::URA(RWC108) pCdc24Cdc24mRFP-Ruby::LEU2 (RWC723)	this study
RWS1099	pCDC42-myc-GFP-CDC42::URA3(RWC108) p42-GFP-Cdc42::LEU2 (RWC151)	this study
RWS1135	pCDC42-myc-GFP-CDC42^{F28L}::URA3 (RWC790)	this study
RWS1136	Δ*bem2*::G418 pCDC42-myc-GFP-CDC42^{F28L}::URA3 (RWC790)	this study
RWS1421	pCDC42-myc-GFP-CDC42::URA3 (RWC108)	this study
RWS1422	pCDC24-CDC24::LEU2 (RWC153)	this study
RWS1423	Δ*rdi1*::LEU2 pCDC42-myc-GFP-CDC42::URA3 (RWC108)	this study
RWS1424	Δ*bem2*::G418 pCDC42-myc-GFP-CDC42::URA(RWC108) pCdc24Cdc24mRFP-Ruby::LEU2 (RWC723)	this study

*all strains were made in the RWS 116 background

Plasmids

Plasmid	Origin	Description	Source/Reference
RWC21	pRS306	GFP-CDC42 under the control of Gal promoter in a pRS306 backbone for integration into the URA3 locus after linearization	(Wedlich-Soldner et al., 2004)
RWC108	pRS306	GFP-CDC42 under the control of the endogenous CDC42-promoter in a pRS306 backbone for integration into the URA3 locus after linearization	(Wedlich-Soldner et al., 2004)
RWC146	pRS316	CDC24-GFP under the control of the endogenous CDC24-promoter in a pRS316 backbone URA3-CEN plasmid	this study
RWC148	pRS305	pRS305 backbone for integration into the LEU2 locus after linearization	this study
RWC151	pRS305	GFP-CDC42 under the control of the endogenous CDC42-promoter in a pRS305 backbone for integration into the LEU2 locus after linearization	this study
RWC153	pRS305	CDC24-GFP under the control of the endogenous CDC24-promoter in a pRS305 backbone for integration into the LEU2 locus after linearization	(Wedlich-Soldner et al., 2004)
RWC233	pYM-25	Plasmid for C-terminal direct tagging, hphNT1.	(Janke et al., 2004)
RWC257	pYM-N4	Plasmid for N-terminal direct tagging, clonNAT.	(Janke et al., 2004)
RWC550	pYM-N4	Plasmid for N-terminal direct tagging, clonNAT under the control of the endogenous CDC42 promoter	(Janke et al., 2004)
RWC686	pRS306	GFP-CDC42D57Y under the control of the endogenous CDC42-promoter in a pRS306 backbone for integration into the URA3 locus after linearization	this study
RWC687	pRS306	GFP-CDC42G12V CDC42D57Y under the control of the endogenous CDC42-promoter in a pRS306 backbone for integration into the URA3 locus after linearization	this study
RWC688	pRS306	GFP-CDC42G60A CDC42D57Y under the control of the endogenous CDC42-promoter in a pRS306 backbone for integration into the URA3 locus after linearization	this study
RWC689	pRS306	GFP-CDC42R66E CDC42D57Y under the control of the endogenous CDC42-promoter in a pRS306 backbone for integration into the URA3 locus after linearization	this study
RWC723	pRS305	CDC24-mRFP CDC42D57Y under the control of the endogenous CDC24-promoter in a pRS305 backbone for integration into the LEU2 locus after linearization	this study
RWC790	pRS306	GFP-CDC42F28L under the control of the endogenous CDC42-promoter in a pRS306 backbone for integration into the URA3 locus after linearization	this study

Primer

Primer	Sequence 5'→3'	use
RWS650	AGCAAAACTTATAAAACAAGAAATAAACGTATTAGCTCT TCCACAAAATGcgtacgctgcaggtcgac*	Cdc42 genomic GFP integration
RWS651	CACGTTTTCCCAACAGCACCATCACCGACAACAACACAC TTTAGCGTTTGCatcgatgaattctctgtcg	Cdc42 genomic GFP integration
RWS618	TCCGGATTTGTGGAAGAGCTAATACGTTTATTTC	Cdc42 promoter with BspEI
RWS617	GAGCTCCAGGCCGGAACTCAAAAGG	Cdc42 promoter with SacI
RWS655	AAGAAATGTTGGCGGAAAACAATGAGAAATTCTTGAAC ATTCGTCTGTAT cgtacgctgcaggtcgac	Cdc24 genomic GFP integration
RWS654	GTTTTTTTCTTGAATTATTTAGTATTTGCTGTATACTAGTT TTATTTATCA atcgatgaattcgagctcg	Cdc24 genomic GFP integration
RWS347	AGGCAAGAGATCAGGCGGAAAGA	amplification of KanMX-cassette
RWS346	AGAAGCAAGCTACGTTGCAGCCA	amplification of KanMX-cassette
RWS885	CAGGTTTCATTGGAGGTGC	Bem2 deletion test primer
RWS265	GGTGCTCAACAATTCAGTTCT	Bem2 deletion test primer
RWS352	TGCACCAACATACCGTTTTGC	Bem2 deletion test primer
RWS351	TGATGGTAAATCCCGTCCTGC	Bem2 deletion test primer
RWS98	CACGGAGCCTACCTTTTAG	Vps27 deletion test primer
RWS97	GTTCGTGTGGTTAGACAAC	Vps27 deletion test primer
RWS207	TGATGCTTTGTAGCTGTTGCTC	Vps27 deletion test primer
RWS206	AGAGAAGCTGAAGAAGCGAAGC	Vps27 deletion test primer
RWS343	TGAAATGCTTCTGAGCGAAGC	Vps27 deletion test primer
RWS342	TCAAATGCCTTGCTGACCACT	Vps27 deletion test primer
RWS1112	GAGCGCAACGCAATTAATG	Cdc42 amplification from RWC 21
RWS73	CTGCCCTTTCGAAAGATC	Cdc42 amplification from RWC 21
RWS1110	GATATGACAAGGGTCTCAATTCATCGTAATCTTCTTGACC G	R66E mutation primer
RWS1109	GAAGATTACGATGAATTGAGACCCTTGTCATATC	R66E mutation primer
RWS1112	GAGCGCAACGCAATTAATG	Cdc42 amplification from RWC 21
RWS73	CTGCCCTTTCGAAAGATC	Cdc42 amplification from RWC 21
RWS1540	GGAACATAGTCGGCTGGCAATTGATTCGTTGTATAG	F28L mutation primer
RWS1539	CTATACAACGAATCAATTGCCAGCCGACTATGTTCC	F28L mutation primer
RWS48	GTATTCTGGGCCTCCATG	KanMX test primer
RWS47	GATACTAACGCCGCCATC	KanMX test primer
RWS1247	TGAGCTGCGCACGTCAAG	KanMX test primer
RWS1246	TGGTCGCTATACTGCTGTC	KanMX test primer

* restriction endonuclease sites are underlined; homology regions for direct integration are depicted in small letters

2.4.5 Genetic Interactions

Query	Interactor	Experiment	Interactor Category
BEM1	RSR1	(This study)	CDC42 SIGNALING
BEM1	VPS9	(This study)	ENDOCYTIC RECYCLING
RDI1	GOS1	(This study)	EARLY SECRETION
BEM2	RDI1	(This study)	CDC42 Module
CDC42	MSB3	SYNTHETIC GROWTH DEFECT	LATE SECRETION
CDC42	CAP1	SYNTHETIC GROWTH DEFECT	ENDOCYTIC RECYCLING
CDC42	BUD6	SYNTHETIC GROWTH DEFECT	ACTIN GENERAL
CDC42	GIC2	SYNTHETIC GROWTH DEFECT	CDC42 SIGNALING
CDC42	CAP2	SYNTHETIC GROWTH DEFECT	ACTIN GENERAL
BEM2	PXL1	SYNTHETIC GROWTH DEFECT	ACTIN GENERAL
CLA4	RGA1	SYNTHETIC GROWTH DEFECT	CDC42 Module
CLA4	RGA2	SYNTHETIC GROWTH DEFECT	CDC42 Module
BEM2	GET2	SYNTHETIC GROWTH DEFECT	EARLY SECRETION
BEM2	GET1	SYNTHETIC GROWTH DEFECT	EARLY SECRETION
BEM2	BEM3	SYNTHETIC GROWTH DEFECT	CDC42 Module
CLA4	RVS161	SYNTHETIC GROWTH DEFECT	ACTIN GENERAL
CLA4	PEA2	SYNTHETIC GROWTH DEFECT	ACTIN GENERAL
RGA1	RIC1	SYNTHETIC GROWTH DEFECT	ENDOCYTIC RECYCLING
CLA4	RVS167	SYNTHETIC GROWTH DEFECT	ACTIN GENERAL
CLA4	ICE2	SYNTHETIC GROWTH DEFECT	EARLY SECRETION
CDC42	SPA2	SYNTHETIC GROWTH DEFECT	ACTIN GENERAL
CDC42	RSR1	SYNTHETIC GROWTH DEFECT	CDC42 SIGNALING
CLA4	CHS6	SYNTHETIC GROWTH DEFECT	LATE SECRETION
CLA4	CHS5	SYNTHETIC GROWTH DEFECT	LATE SECRETION
BEM1	ACT1	SYNTHETIC HAPLOINSUFFICIENCY	ACTIN GENERAL
BEM2	ACT1	SYNTHETIC HAPLOINSUFFICIENCY	ACTIN GENERAL
BEM2	SMY1	SYNTHETIC LETHALITY	LATE SECRETION
CLA4	CHS5	SYNTHETIC LETHALITY	LATE SECRETION
CLA4	SMY1	SYNTHETIC LETHALITY	LATE SECRETION
CLA4	EDE1	SYNTHETIC LETHALITY	ENDOCYTIC RECYCLING
CLA4	CHS6	SYNTHETIC LETHALITY	LATE SECRETION
CLA4	BNI1	SYNTHETIC LETHALITY	ACTIN GENERAL
CLA4	BEM4	SYNTHETIC LETHALITY	CDC42 SIGNALING
CLA4	ARP2	SYNTHETIC LETHALITY	ACTIN GENERAL
BEM1	BBC1	SYNTHETIC LETHALITY	ACTIN GENERAL
BEM2	TPM1	SYNTHETIC LETHALITY	ACTIN GENERAL
CLA4	BUD6	SYNTHETIC LETHALITY	ACTIN GENERAL
CLA4	RVS167	SYNTHETIC LETHALITY	ACTIN GENERAL
CLA4	RVS161	SYNTHETIC LETHALITY	ACTIN GENERAL
CLA4	VAC14	SYNTHETIC LETHALITY	ENDOCYTIC RECYCLING

BEM2	CHS5	SYNTHETIC LETHALITY	LATE SECRETION
CLA4	SPA2	SYNTHETIC LETHALITY	ACTIN GENERAL
CLA4	MYO2	SYNTHETIC LETHALITY	LATE SECRETION
BEM2	SAC6	SYNTHETIC LETHALITY	ACTIN GENERAL
CLA4	FAB1	SYNTHETIC LETHALITY	ENDOCYTIC RECYCLING
BEM2	MYO2	SYNTHETIC LETHALITY	LATE SECRETION
BEM1	ARP2	SYNTHETIC LETHALITY	ACTIN GENERAL
CLA4	PEA2	SYNTHETIC LETHALITY	ACTIN GENERAL
CDC42	PEA2	SYNTHETIC LETHALITY	ACTIN GENERAL
CDC24	SEC15	SYNTHETIC LETHALITY	LATE SECRETION
CDC42	MSB3	SYNTHETIC LETHALITY	LATE SECRETION
CDC42	SEC10	SYNTHETIC LETHALITY	LATE SECRETION
CDC42	RSR1	SYNTHETIC LETHALITY	CDC42 SIGNALING
BEM1	BNI1	SYNTHETIC LETHALITY	ACTIN GENERAL
CDC42	BUD6	SYNTHETIC LETHALITY	ACTIN GENERAL
CDC42	BEM4	SYNTHETIC LETHALITY	CDC42 SIGNALING
CDC42	BNI1	SYNTHETIC LETHALITY	ACTIN GENERAL
CDC42	GIC2	SYNTHETIC LETHALITY	CDC42 SIGNALING
CDC42	CAP2	SYNTHETIC LETHALITY	ACTIN GENERAL
CDC42	SEC8	SYNTHETIC LETHALITY	LATE SECRETION
CDC42	SEC66	SYNTHETIC LETHALITY	EARLY SECRETION
CDC42	SEC5	SYNTHETIC LETHALITY	LATE SECRETION
CLA4	ARC40	SYNTHETIC LETHALITY	ACTIN GENERAL
CDC42	SPA2	SYNTHETIC LETHALITY	ACTIN GENERAL
CDC42	SEC9	SYNTHETIC LETHALITY	LATE SECRETION
CDC42	SEC2	SYNTHETIC LETHALITY	LATE SECRETION
CDC42	SEC15	SYNTHETIC LETHALITY	LATE SECRETION
CDC42	CAP1	SYNTHETIC LETHALITY	ENDOCYTIC RECYCLING
CDC24	BEM4	SYNTHETIC LETHALITY	CDC42 SIGNALING
CDC42	SEC3	SYNTHETIC LETHALITY	LATE SECRETION
CDC42	SEC4	SYNTHETIC LETHALITY	LATE SECRETION
BEM2	BNI1	SYNTHETIC LETHALITY	ACTIN GENERAL
BEM2	ARC40	SYNTHETIC LETHALITY	ACTIN GENERAL
RGA1	RIC1	SYNTHETIC LETHALITY	ENDOCYTIC RECYCLING
BEM2	CDC24	SYNTHETIC LETHALITY	CDC42 Module
BEM2	RGA1	SYNTHETIC LETHALITY	CDC42 Module
BEM2	ARP2	SYNTHETIC LETHALITY	ACTIN GENERAL
BEM2	CLA4	SYNTHETIC LETHALITY	CDC42 Module
BEM1	ARC40	SYNTHETIC LETHALITY	ACTIN GENERAL
BEM1	CDC42	SYNTHETIC LETHALITY	CDC42 Module
BEM1	CDC24	SYNTHETIC LETHALITY	CDC42 Module
BEM1	BEM2	SYNTHETIC LETHALITY	CDC42 Module
BEM2	ACT1	SYNTHETIC LETHALITY	ACTIN GENERAL
BEM1	SMY1	SYNTHETIC LETHALITY	LATE SECRETION
BEM1	CLA4	SYNTHETIC LETHALITY	CDC42 Module

BEM3	CDC24	SYNTHETIC LETHALITY	CDC42 Module
CDC24	CDC42	SYNTHETIC LETHALITY	CDC42 Module
CDC42	CLA4	SYNTHETIC LETHALITY	CDC42 Module
BEM1	MYO2	SYNTHETIC LETHALITY	LATE SECRETION
CDC24	CDC42	SYNTHETIC LETHALITY (CONDITIONAL)	CDC42 Module
BEM1	RDI1	(Costanzo et al., 2010)	CDC42 Module
BEM1	CDC42	(Costanzo et al., 2010)	CDC42 Module
BEM1	BOI1	(Costanzo et al., 2010)	CDC42 SIGNALING
BEM1	CAP2	(Costanzo et al., 2010)	ACTIN GENERAL
BEM1	CHS6	(Costanzo et al., 2010)	LATE SECRETION
CDC42	SRO7	(Costanzo et al., 2010)	LATE SECRETION
CDC42	TPM1	(Costanzo et al., 2010)	ACTIN GENERAL
BEM1	ACT1	(Costanzo et al., 2010)	ACTIN GENERAL
CLA4	RGA1	(Costanzo et al., 2010)	CDC42 Module
BEM1	BEM4	(Costanzo et al., 2010)	CDC42 SIGNALING
CDC42	SPA2	(Costanzo et al., 2010)	ACTIN GENERAL
BEM1	AIP1	(Costanzo et al., 2010)	ACTIN GENERAL
BEM2	CLA4	(Costanzo et al., 2010)	CDC42 Module
CDC42	GIC2	(Costanzo et al., 2010)	CDC42 SIGNALING
BEM3	RGA1	(Costanzo et al., 2010)	CDC42 Module
BEM2	RGA1	(Costanzo et al., 2010)	CDC42 Module
BEM1	BUD6	(Costanzo et al., 2010)	ACTIN GENERAL
BEM2	BEM3	(Costanzo et al., 2010)	CDC42 Module
CDC42	CAP1	(Costanzo et al., 2010)	ENDOCYTIC RECYCLING
BEM1	ARC18	(Costanzo et al., 2010)	ACTIN GENERAL
BEM1	CAP1	(Costanzo et al., 2010)	ENDOCYTIC RECYCLING
BEM2	CDC42	(Costanzo et al., 2010)	CDC42 Module
CDC42	CAP2	(Costanzo et al., 2010)	ACTIN GENERAL
CLA4	SHE4	(Costanzo et al., 2010)	LATE SECRETION
RDI1	YCK2	(Costanzo et al., 2010)	ENDOCYTIC RECYCLING
CLA4	RVS161	(Costanzo et al., 2010)	ACTIN GENERAL
RDI1	VRP1	(Costanzo et al., 2010)	ACTIN GENERAL
BEM1	ARF1	(Costanzo et al., 2010)	EARLY SECRETION
CLA4	PEA2	(Costanzo et al., 2010)	ACTIN GENERAL
CLA4	CHS5	(Costanzo et al., 2010)	LATE SECRETION
RGA1	ACT1	(Costanzo et al., 2010)	ACTIN GENERAL
BEM1	ARF3	(Costanzo et al., 2010)	ENDOCYTIC RECYCLING
CLA4	YEL1	(Costanzo et al., 2010)	ENDOCYTIC RECYCLING
CLA4	TPM1	(Costanzo et al., 2010)	ACTIN GENERAL
RDI1	TOS2	(Costanzo et al., 2010)	CDC42 SIGNALING
RDI1	BEM4	(Costanzo et al., 2010)	CDC42 SIGNALING
RDI1	PEA2	(Costanzo et al., 2010)	ACTIN GENERAL
CLA4	SMY1	(Costanzo et al., 2010)	LATE SECRETION
CLA4	SLA1	(Costanzo et al., 2010)	ACTIN GENERAL
CLA4	SPA2	(Costanzo et al., 2010)	ACTIN GENERAL

RDI1	VPS27	(Costanzo et al., 2010)	ENDOCYTIC RECYCLING
RGA1	SRO7	(Costanzo et al., 2010)	LATE SECRETION
CLA4	BUD6	(Costanzo et al., 2010)	ACTIN GENERAL
CLA4	CAP2	(Costanzo et al., 2010)	ACTIN GENERAL
CLA4	CAP1	(Costanzo et al., 2010)	ENDOCYTIC RECYCLING
RGA2	GET1	(Costanzo et al., 2010)	EARLY SECRETION
CLA4	BEM4	(Costanzo et al., 2010)	CDC42 SIGNALING
RGA1	VPS9	(Costanzo et al., 2010)	ENDOCYTIC RECYCLING
RGA1	VRP1	(Costanzo et al., 2010)	ACTIN GENERAL
RGA1	BUD14	(Costanzo et al., 2010)	ACTIN GENERAL
BEM1	ATG8	(Costanzo et al., 2010)	EARLY SECRETION
CLA4	EDE1	(Costanzo et al., 2010)	ENDOCYTIC RECYCLING
RGA1	CMD1	(Costanzo et al., 2010)	ACTIN GENERAL
CLA4	ICE2	(Costanzo et al., 2010)	EARLY SECRETION
RGA1	SLA1	(Costanzo et al., 2010)	ACTIN GENERAL
RGA1	SLY41	(Costanzo et al., 2010)	EARLY SECRETION
BEM1	BBC1	(Costanzo et al., 2010)	ACTIN GENERAL
CLA4	CHS6	(Costanzo et al., 2010)	LATE SECRETION
BEM2	CCZ1	(Costanzo et al., 2010)	ENDOCYTIC RECYCLING
BEM2	BUL1	(Costanzo et al., 2010)	ENDOCYTIC RECYCLING
BEM2	BUD6	(Costanzo et al., 2010)	ACTIN GENERAL
BEM2	BUD14	(Costanzo et al., 2010)	ACTIN GENERAL
BEM2	CCZ1	(Costanzo et al., 2010)	ENDOCYTIC RECYCLING
BEM2	CAP2	(Costanzo et al., 2010)	ACTIN GENERAL
BEM2	CAP1	(Costanzo et al., 2010)	ENDOCYTIC RECYCLING
BEM2	BST1	(Costanzo et al., 2010)	EARLY SECRETION
BEM2	APL1	(Costanzo et al., 2010)	ENDOCYTIC RECYCLING
BEM2	ACT1	(Costanzo et al., 2010)	ACTIN GENERAL
BEM1	SEC61	(Costanzo et al., 2010)	LATE SECRETION
BEM2	BNI1	(Costanzo et al., 2010)	ACTIN GENERAL
BEM2	ARF1	(Costanzo et al., 2010)	EARLY SECRETION
BEM2	APS2	(Costanzo et al., 2010)	ENDOCYTIC RECYCLING
CDC24	RIC1	(Costanzo et al., 2010)	ENDOCYTIC RECYCLING
BEM1	FAR10	(Costanzo et al., 2010)	CDC42 SIGNALING
BEM1	GIC1	(Costanzo et al., 2010)	CDC42 SIGNALING
BEM2	GCS1	(Costanzo et al., 2010)	EARLY SECRETION
BEM2	MYO2	(Costanzo et al., 2010)	LATE SECRETION
BEM2	ICE2	(Costanzo et al., 2010)	EARLY SECRETION
BEM2	GIC1	(Costanzo et al., 2010)	CDC42 SIGNALING
BEM2	ERV14	(Costanzo et al., 2010)	EARLY SECRETION
BEM2	CLC1	(Costanzo et al., 2010)	ENDOCYTIC RECYCLING
BEM2	CHS6	(Costanzo et al., 2010)	LATE SECRETION
BEM2	CHS5	(Costanzo et al., 2010)	LATE SECRETION
BEM2	COG7	(Costanzo et al., 2010)	EARLY SECRETION
BEM2	COG6	(Costanzo et al., 2010)	EARLY SECRETION

BEM2	CMD1	(Costanzo et al., 2010)	ACTIN GENERAL
BEM1	RVS167	(Costanzo et al., 2010)	ACTIN GENERAL
BEM1	RVS161	(Costanzo et al., 2010)	ACTIN GENERAL
BEM1	RUD3	(Costanzo et al., 2010)	EARLY SECRETION
BEM1	SEC3	(Costanzo et al., 2010)	LATE SECRETION
BEM1	SEC15	(Costanzo et al., 2010)	LATE SECRETION
BEM1	SEC10	(Costanzo et al., 2010)	LATE SECRETION
BEM1	KES1	(Costanzo et al., 2010)	EARLY SECRETION
BEM1	PEA2	(Costanzo et al., 2010)	ACTIN GENERAL
BEM1	MYO2	(Costanzo et al., 2010)	LATE SECRETION
BEM1	KIN1	(Costanzo et al., 2010)	LATE SECRETION
BEM1	RHB1	(Costanzo et al., 2010)	EARLY SECRETION
BEM1	RGP1	(Costanzo et al., 2010)	ENDOCYTIC RECYCLING
BEM1	PXL1	(Costanzo et al., 2010)	ACTIN GENERAL
BEM1	YPT31	(Costanzo et al., 2010)	LATE SECRETION
BEM1	VPS74	(Costanzo et al., 2010)	EARLY SECRETION
BEM1	VPS51	(Costanzo et al., 2010)	ENDOCYTIC RECYCLING
BEM1	VPS17	(Costanzo et al., 2010)	ENDOCYTIC RECYCLING
BEM1	YEL1	(Costanzo et al., 2010)	ENDOCYTIC RECYCLING
BEM1	VRP1	(Costanzo et al., 2010)	ACTIN GENERAL
BEM1	GIC2	(Costanzo et al., 2010)	CDC42 SIGNALING
BEM1	TPM1	(Costanzo et al., 2010)	ACTIN GENERAL
BEM1	SHE4	(Costanzo et al., 2010)	LATE SECRETION
BEM1	SEC72	(Costanzo et al., 2010)	EARLY SECRETION
BEM1	SEC63	(Costanzo et al., 2010)	LATE SECRETION
BEM1	SYT1	(Costanzo et al., 2010)	LATE SECRETION
BEM1	SPA2	(Costanzo et al., 2010)	ACTIN GENERAL
BEM1	SMY1	(Costanzo et al., 2010)	LATE SECRETION
CDC24	CAP2	(Costanzo et al., 2010)	ACTIN GENERAL
CDC24	CAP1	(Costanzo et al., 2010)	ENDOCYTIC RECYCLING
CDC24	BUD6	(Costanzo et al., 2010)	ACTIN GENERAL
CDC24	PEA2	(Costanzo et al., 2010)	ACTIN GENERAL
CDC24	GIC2	(Costanzo et al., 2010)	CDC42 SIGNALING
CDC24	COG7	(Costanzo et al., 2010)	EARLY SECRETION
CDC24	BEM4	(Costanzo et al., 2010)	CDC42 SIGNALING
BEM3	EDE1	(Costanzo et al., 2010)	ENDOCYTIC RECYCLING
BEM3	CHS5	(Costanzo et al., 2010)	LATE SECRETION
BEM2	SPA2	(Costanzo et al., 2010)	ACTIN GENERAL
BEM3	SMY1	(Costanzo et al., 2010)	LATE SECRETION
BEM3	SLA1	(Costanzo et al., 2010)	ACTIN GENERAL
BEM3	SHE4	(Costanzo et al., 2010)	LATE SECRETION
CDC42	BEM4	(Costanzo et al., 2010)	CDC42 SIGNALING
CDC24	VPS41	(Costanzo et al., 2010)	ENDOCYTIC RECYCLING
CDC24	VAM7	(Costanzo et al., 2010)	ENDOCYTIC RECYCLING
CDC24	VAM6	(Costanzo et al., 2010)	ENDOCYTIC RECYCLING

CDC24	YPT7	(Costanzo et al., 2010)	ENDOCYTIC RECYCLING
CDC24	YPT32	(Costanzo et al., 2010)	LATE SECRETION
CDC24	YJL206C-A	(Costanzo et al., 2010)	LATE SECRETION
CDC24	VAM3	(Costanzo et al., 2010)	ENDOCYTIC RECYCLING
CDC24	SPA2	(Costanzo et al., 2010)	ACTIN GENERAL
CDC24	SNX41	(Costanzo et al., 2010)	ENDOCYTIC RECYCLING
CDC24	RSR1	(Costanzo et al., 2010)	CDC42 SIGNALING
CDC24	TPM1	(Costanzo et al., 2010)	ACTIN GENERAL
CDC24	TLG2	(Costanzo et al., 2010)	EARLY SECRETION
CDC24	SPH1	(Costanzo et al., 2010)	LATE SECRETION
BEM2	SHE4	(Costanzo et al., 2010)	LATE SECRETION
BEM2	SEC72	(Costanzo et al., 2010)	EARLY SECRETION
BEM2	SEC66	(Costanzo et al., 2010)	LATE SECRETION
BEM2	SNC2	(Costanzo et al., 2010)	LATE SECRETION
BEM2	SMY1	(Costanzo et al., 2010)	LATE SECRETION
BEM2	SHE4	(Costanzo et al., 2010)	LATE SECRETION
BEM2	SEC3	(Costanzo et al., 2010)	LATE SECRETION
BEM2	RSR1	(Costanzo et al., 2010)	CDC42 SIGNALING
BEM2	PXL1	(Costanzo et al., 2010)	ACTIN GENERAL
BEM1	ERV41	(Costanzo et al., 2010)	EARLY SECRETION
BEM2	SEC15	(Costanzo et al., 2010)	LATE SECRETION
BEM2	SEC10	(Costanzo et al., 2010)	LATE SECRETION
BEM2	RUD3	(Costanzo et al., 2010)	EARLY SECRETION
BEM3	BNI1	(Costanzo et al., 2010)	ACTIN GENERAL
BEM2	YCK1	(Costanzo et al., 2010)	ENDOCYTIC RECYCLING
BEM2	VPS74	(Costanzo et al., 2010)	EARLY SECRETION
BEM2	VPS51	(Costanzo et al., 2010)	EARLY SECRETION
BEM3	ARC15	(Costanzo et al., 2010)	ACTIN GENERAL
BEM2	YPT32	(Costanzo et al., 2010)	LATE SECRETION
BEM2	YCK2	(Costanzo et al., 2010)	ENDOCYTIC RECYCLING
BEM2	VPS30	(Costanzo et al., 2010)	ENDOCYTIC RECYCLING
BEM2	SYT1	(Costanzo et al., 2010)	LATE SECRETION
BEM2	SSO2	(Costanzo et al., 2010)	LATE SECRETION
BEM2	SSO1	(Costanzo et al., 2010)	LATE SECRETION
BEM2	VPS21	(Costanzo et al., 2010)	ENDOCYTIC RECYCLING
BEM2	VAC14	(Costanzo et al., 2010)	ENDOCYTIC RECYCLING
BEM2	TPM1	(Costanzo et al., 2010)	ACTIN GENERAL

*: only negative genetic interactions were included

2.4.6 Physical Interactions

Query	Interactor	Experiment	Interactor Category
BEM1	ACT1	AFFINITY CAPTURE-WESTERN	ACTIN GENERAL
BEM1	ACT1	AFFINITY PRECIPITATION	ACTIN GENERAL
BEM1	ACT1	PHYSICAL INTERACTION	ACTIN GENERAL
BEM1	ACT1	TWO HYBRID	ACTIN GENERAL
BEM1	LAS17	AFFINITY CAPTURE-WESTERN	ACTIN GENERAL
BEM1	LAS17	PHYSICAL INTERACTION	ACTIN GENERAL
BEM2	BUD14	AFFINITY CAPTURE-MS	ACTIN GENERAL
BEM2	BUD14	PHYSICAL INTERACTION	ACTIN GENERAL
BEM2	SPA2	AFFINITY CAPTURE-MS	ACTIN GENERAL
CDC42	BNI1	PHYSICAL INTERACTION	ACTIN GENERAL
CDC42	BNI1	TWO HYBRID	ACTIN GENERAL
CLA4	ABP1	PHYSICAL INTERACTION	ACTIN GENERAL
CLA4	ABP1	TWO HYBRID	ACTIN GENERAL
CLA4	SLA2	PHYSICAL INTERACTION	ACTIN GENERAL
CLA4	SLA2	TWO HYBRID	ACTIN GENERAL
RGA1	CMD1	AFFINITY CAPTURE-MS	ACTIN GENERAL
BEM1	BOI1	AFFINITY CAPTURE-MS	CDC42 SIGNALING
BEM1	BOI1	AFFINITY PRECIPITATION	CDC42 SIGNALING
BEM1	BOI1	PCA	CDC42 SIGNALING
BEM1	BOI1	PHYSICAL INTERACTION	CDC42 SIGNALING
BEM1	BOI1	TWO HYBRID	CDC42 SIGNALING
BEM1	BOI2	AFFINITY CAPTURE-MS	CDC42 SIGNALING
BEM1	BOI2	PHYSICAL INTERACTION	CDC42 SIGNALING
BEM1	BOI2	RECONSTITUTED COMPLEX	CDC42 SIGNALING
BEM1	BOI2	TWO HYBRID	CDC42 SIGNALING
BEM1	FAR1	AFFINITY CAPTURE-WESTERN	CDC42 SIGNALING
BEM1	FAR1	AFFINITY CHROMATOGRAPHY	CDC42 SIGNALING
BEM1	FAR1	PHYSICAL INTERACTION	CDC42 SIGNALING
BEM1	FAR1	RECONSTITUTED COMPLEX	CDC42 SIGNALING
BEM1	FAR1	TWO HYBRID	CDC42 SIGNALING
BEM1	RSR1	AFFINITY CHROMATOGRAPHY	CDC42 SIGNALING
BEM1	RSR1	PHYSICAL INTERACTION	CDC42 SIGNALING
BEM1	RSR1	RECONSTITUTED COMPLEX	CDC42 SIGNALING
BEM3	BEM4	PHYSICAL INTERACTION	CDC42 SIGNALING
BEM3	BEM4	TWO HYBRID	CDC42 SIGNALING
CDC24	BEM4	PHYSICAL INTERACTION	CDC42 SIGNALING
CDC24	BEM4	TWO HYBRID	CDC42 SIGNALING
CDC24	BOI1	AFFINITY CAPTURE-MS	CDC42 SIGNALING
CDC24	BOI1	AFFINITY CAPTURE-WESTERN	CDC42 SIGNALING
CDC24	BOI2	AFFINITY CAPTURE-MS	CDC42 SIGNALING
CDC24	BOI2	AFFINITY CAPTURE-WESTERN	CDC42 SIGNALING
CDC24	BOI2	PHYSICAL INTERACTION	CDC42 SIGNALING
CDC24	FAR1	AFFINITY CAPTURE-WESTERN	CDC42 SIGNALING

BEM2	CHS5	SYNTHETIC LETHALITY	LATE SECRETION
CLA4	SPA2	SYNTHETIC LETHALITY	ACTIN GENERAL
CLA4	MYO2	SYNTHETIC LETHALITY	LATE SECRETION
BEM2	SAC6	SYNTHETIC LETHALITY	ACTIN GENERAL
CLA4	FAB1	SYNTHETIC LETHALITY	ENDOCYTIC RECYCLING
BEM2	MYO2	SYNTHETIC LETHALITY	LATE SECRETION
BEM1	ARP2	SYNTHETIC LETHALITY	ACTIN GENERAL
CLA4	PEA2	SYNTHETIC LETHALITY	ACTIN GENERAL
CDC42	PEA2	SYNTHETIC LETHALITY	ACTIN GENERAL
CDC24	SEC15	SYNTHETIC LETHALITY	LATE SECRETION
CDC42	MSB3	SYNTHETIC LETHALITY	LATE SECRETION
CDC42	SEC10	SYNTHETIC LETHALITY	LATE SECRETION
CDC42	RSR1	SYNTHETIC LETHALITY	CDC42 SIGNALING
BEM1	BNI1	SYNTHETIC LETHALITY	ACTIN GENERAL
CDC42	BUD6	SYNTHETIC LETHALITY	ACTIN GENERAL
CDC42	BEM4	SYNTHETIC LETHALITY	CDC42 SIGNALING
CDC42	BNI1	SYNTHETIC LETHALITY	ACTIN GENERAL
CDC42	GIC2	SYNTHETIC LETHALITY	CDC42 SIGNALING
CDC42	CAP2	SYNTHETIC LETHALITY	ACTIN GENERAL
CDC42	SEC8	SYNTHETIC LETHALITY	LATE SECRETION
CDC42	SEC66	SYNTHETIC LETHALITY	EARLY SECRETION
CDC42	SEC5	SYNTHETIC LETHALITY	LATE SECRETION
CLA4	ARC40	SYNTHETIC LETHALITY	ACTIN GENERAL
CDC42	SPA2	SYNTHETIC LETHALITY	ACTIN GENERAL
CDC42	SEC9	SYNTHETIC LETHALITY	LATE SECRETION
CDC42	SEC2	SYNTHETIC LETHALITY	LATE SECRETION
CDC42	SEC15	SYNTHETIC LETHALITY	LATE SECRETION
CDC42	CAP1	SYNTHETIC LETHALITY	ENDOCYTIC RECYCLING
CDC24	BEM4	SYNTHETIC LETHALITY	CDC42 SIGNALING
CDC42	SEC3	SYNTHETIC LETHALITY	LATE SECRETION
CDC42	SEC4	SYNTHETIC LETHALITY	LATE SECRETION
BEM2	BNI1	SYNTHETIC LETHALITY	ACTIN GENERAL
BEM2	ARC40	SYNTHETIC LETHALITY	ACTIN GENERAL
RGA1	RIC1	SYNTHETIC LETHALITY	ENDOCYTIC RECYCLING
BEM2	CDC24	SYNTHETIC LETHALITY	CDC42 Module
BEM2	RGA1	SYNTHETIC LETHALITY	CDC42 Module
BEM2	ARP2	SYNTHETIC LETHALITY	ACTIN GENERAL
BEM2	CLA4	SYNTHETIC LETHALITY	CDC42 Module
BEM1	ARC40	SYNTHETIC LETHALITY	ACTIN GENERAL
BEM1	CDC42	SYNTHETIC LETHALITY	CDC42 Module
BEM1	CDC24	SYNTHETIC LETHALITY	CDC42 Module
BEM1	BEM2	SYNTHETIC LETHALITY	CDC42 Module
BEM2	ACT1	SYNTHETIC LETHALITY	ACTIN GENERAL
BEM1	SMY1	SYNTHETIC LETHALITY	LATE SECRETION
BEM1	CLA4	SYNTHETIC LETHALITY	CDC42 Module

RGA1	ENT1	AFFINITY CAPTURE-WESTERN	ENDOCYTIC RECYCLING
RGA2	ENT1	AFFINITY CAPTURE-WESTERN	ENDOCYTIC RECYCLING
BEM1	SEC10	RECONSTITUTED COMPLEX	LATE SECRETION
BEM1	SEC15	AFFINITY CAPTURE-WESTERN	LATE SECRETION
BEM1	SEC15	PHYSICAL INTERACTION	LATE SECRETION
BEM1	SEC15	RECONSTITUTED COMPLEX	LATE SECRETION
BEM1	SEC15	TWO HYBRID	LATE SECRETION
BEM1	SEC5	PCA	LATE SECRETION
BEM1	SEC5	RECONSTITUTED COMPLEX	LATE SECRETION
BEM1	SEC8	AFFINITY CAPTURE-WESTERN	LATE SECRETION
CDC24	SEC15	PHYSICAL INTERACTION	LATE SECRETION
CDC24	SEC15	TWO HYBRID	LATE SECRETION
CDC42	MSB3	RECONSTITUTED COMPLEX	LATE SECRETION
CDC42	MSB4	RECONSTITUTED COMPLEX	LATE SECRETION
CDC42	SEC3	PHYSICAL INTERACTION	LATE SECRETION
CDC42	SEC3	RECONSTITUTED COMPLEX	LATE SECRETION
CLA4	SEC23	AFFINITY CAPTURE-MS	LATE SECRETION
RGA1	MLC1	AFFINITY CAPTURE-MS	LATE SECRETION
BEM1	CDC24	AFFINITY CAPTURE-MS	CDC42 Module
BEM1	CDC24	AFFINITY CAPTURE-WESTERN	CDC42 Module
BEM1	CDC24	AFFINITY PRECIPITATION	CDC42 Module
BEM1	CDC24	PCA	CDC42 Module
BEM1	CDC24	PHYSICAL INTERACTION	CDC42 Module
BEM1	CDC24	PROTEIN-PEPTIDE	CDC42 Module
BEM1	CDC24	RECONSTITUTED COMPLEX	CDC42 Module
BEM1	CDC24	TWO HYBRID	CDC42 Module
BEM1	CDC42	AFFINITY CAPTURE-WESTERN	CDC42 Module
BEM1	CDC42	PHYSICAL INTERACTION	CDC42 Module
BEM1	CDC42	RECONSTITUTED COMPLEX	CDC42 Module
BEM1	CDC42	TWO HYBRID	CDC42 Module
BEM1	CLA4	AFFINITY CAPTURE-WESTERN	CDC42 Module
BEM1	RGA2	AFFINITY CAPTURE-MS	CDC42 Module
BEM3	CDC42	TWO HYBRID	CDC42 Module
BEM3	CLA4	PHYSICAL INTERACTION	CDC42 Module
BEM3	CLA4	TWO HYBRID	CDC42 Module
CDC24	CDC42	AFFINITY CAPTURE-WESTERN	CDC42 Module
CDC24	CDC42	AFFINITY PRECIPITATION	CDC42 Module
CDC24	CDC42	PHYSICAL INTERACTION	CDC42 Module
CDC24	CDC42	RECONSTITUTED COMPLEX	CDC42 Module
CDC24	CDC42	TWO HYBRID	CDC42 Module
CDC24	CLA4	AFFINITY CAPTURE-WESTERN	CDC42 Module
CDC24	RGA2	AFFINITY CAPTURE-MS	CDC42 Module
CDC24	RGA2	AFFINITY CAPTURE-WESTERN	CDC42 Module
CDC42	CDC24	AFFINITY CAPTURE-WESTERN	CDC42 Module
CDC42	CDC24	AFFINITY PRECIPITATION	CDC42 Module

CDC42	CDC24	PHYSICAL INTERACTION	CDC42 Module
CDC42	CDC24	RECONSTITUTED COMPLEX	CDC42 Module
CDC42	CDC24	TWO HYBRID	CDC42 Module
CDC42	CLA4	AFFINITY CAPTURE-WESTERN	CDC42 Module
CDC42	CLA4	PHYSICAL INTERACTION	CDC42 Module
CDC42	CLA4	RECONSTITUTED COMPLEX	CDC42 Module
CDC42	CLA4	TWO HYBRID	CDC42 Module
CDC42	RDI1	AFFINITY CAPTURE-WESTERN	CDC42 Module
CDC42	RDI1	AFFINITY PRECIPITATION	CDC42 Module
CDC42	RDI1	FRET	CDC42 Module
CDC42	RDI1	PHYSICAL INTERACTION	CDC42 Module
CDC42	RDI1	TWO HYBRID	CDC42 Module
CDC42	RGA1	PHYSICAL INTERACTION	CDC42 Module
CDC42	RGA1	RECONSTITUTED COMPLEX	CDC42 Module
CDC42	RGA1	TWO HYBRID	CDC42 Module
CDC42	RGA2	TWO HYBRID	CDC42 Module
CLA4	RGA1	PHYSICAL INTERACTION	CDC42 Module
CLA4	RGA1	TWO HYBRID	CDC42 Module

2.4.7 FRAP values

Strain	N	T/2	SEM
Cdc42 (1x)	24	2.03	0.15
Cdc42 (2x)	56	2.19	0.08
Cdc42 (3x)	10	2.32	0.16
Cdc42 (1x) + LatB	11	2.77	0.12
Cdc42 (2x) + LatB	24	2.55	0.07
Cdc42 (3x) + LatB	12	3.26	0.25
Δ*rdi1* Cdc42 (2x)	20	10.56	0.45
$Cdc42^{R66E}$	11	9.14	0.66
Δ*bem2* Cdc42 (2x)	20	6.65	0.39
Δ*bem2* Cdc42 (2x) + LatB	12	9.61	0.57
$Cdc42^{G12V}$	16	33.44	2.20
$Cdc42^{D57Y}$	16	11.93	0.68
$Cdc42^{G60A}$	11	6.76	0.40
Cdc24 (1x)	10	2.12	0.14
Cdc24 (2x)	20	2.10	0.15
Cdc24 (3x)	11	2.22	0.14
Cdc24 (2x) + LatB	14	2.17	0.12
Cdc24 (3x) + LatB	17	2.05	0.09
Δ*bem2* Cdc24 (2x)	10	2.06	0.15
Δ*bem2* Cdc24 (3x)	10	2.26	0.18
Δ*bem2* Cdc24 (3x) + LatB	11	1.96	0.10

2.4.8 Double buds

Strain	LatB*	N	% 2 buds	SD
control (GM-Cdc42)	/	300	0.0	0.0
	a	300	0.0	0.0
	b	300	0.7	0.6
2x GFP-Cdc42 (2x integr. Plasmid)	/	500	0.0	0.0
	a	300	0.0	0.0
	b	300	0.3	0.6
GM-Cdc42 + Cdc24OE	/	900	0.0	0.0
	a	300	0.0	0.0
	b	300	0.0	0.0
GFP-Cdc42F28L	/	500	0.0	0.0
	a	300	0.0	0.0
	b	300	0.0	0.0
Δ*rdi1*	/	400	2.3	0.5
	a	300	13.0	1.0
	b	300	23.0	0.6
Δ*bem2* (no tag)	/	200	7.0	1.4
	a	300	14.0	1.5
	b	300	25.0	1.5
Δ*bem2*	/	600	8.7	0.8
	a	300	13.0	1.5
	b	300	25.0	0.6
Δ*bem2* 2x GM-Cdc42	/	500	9.8	1.5
	a	300	17.0	1.2
	b	300	26.0	1.5
Δ*bem2* GFP-Cdc42 + Cdc24OE	/	900	12.0	1.3
	a	300	24.0	1.5
	b	300	30.0	2.6
Δ*bem2* GFP-Cdc42F28L	/	500	25.0	1.5
	a	300	55.0	0.6
	b	300	63.0	3.1
Cdc24-GFP	/	700	0.0	0.0
	a	300	0.0	0.0
	b	300	0.0	0.0
2xCdc24-GFP (integr.+CEN-Pl)	/	700	0.0	0.0
	a	300	0.0	0.0
	b	300	0.0	0.0
Δbem2 Cdc24-GFP	/	1000	10.0	1.3
	a	300	21.0	1.0
	b	300	28.0	2.0
Δbem2 2x Cdc24-GFP	/	600	19.0	1.5
	a	300	26.0	1.0
	b	300	26.0	2.1

* /: no washout, a: washout after 20 min LatB, b: washout after 40 min LatB

3 Cell polarization in yeast optimizes spatial and temporal control of Cdc42 signaling

This chapter is based on a manuscript originating from a cooperation with the experimental group of Roland Wedlich-Söldner for which I contributed all theoretical results [138].

3.1 Introduction

Cell polarization is a fundamental cellular process that defines a single orientation within prokaryotic or eukaryotic cells and is often referred to as symmetry breaking. This mechanism is a prerequisite for many developmental and pathogenic processes such as cell migration, maintenance of epithelial tissue integrity, asymmetric stem cell division, or tumor development [121, 123, 129].

In the yeast *Saccharomyces cerevisiae*, the GTPase Cdc42 regulates cell polarization to determine the position of a new growth or bud site. A collection of different proteins under control of Cdc42 accumulates within a restricted region of the plasma membrane to initiate several downstream events at the desired position. These clusters arise even in the absence of any spatial cues [16] and are characterized by a dynamic equilibrium where clusters remain stable although individual proteins exchange between plasma membrane and cytoplasm [65]. Two pathways for Cdc42 localization have been identified that independently generate cell polarization [16, 65]. One pathway involves targeted exocytosis of membrane-bound Cdc42 along actin cables [17, 124], while the other relies on fast recycling of Cdc42 through the cytosol by the guanine nucleotide dissociation inhibitor (GDI) Rdi1 [29]. Constitutively active or inactive Cdc42 cannot polarize without actin [65] indicating that the ability of Cdc42 to cycle between its active GTP-bound and inactive GDP-bound state is crucial for actin-independent polarization. Moreover, polarization has been shown to rely on a positive feedback loop of Cdc42-GTP recruiting its activator, the guanine nucleotide exchange factor (GEF) Cdc24, to the membrane [41, 42, 16, 38]. Although many studies have focused on identifying polarity regulators and their interactions, the fundamental mechanisms responsible for spontaneous polarization without help of actin structures still remain controversial. Altschuler and colleagues put forward a conceptual model for yeast polarity establishment relying on a single positive feedback loop of a polarity protein locally enhancing its own membrane attachment [73]. The model predicts stochastic unstable polarization with reduced polarization efficiency at higher particle numbers where stochastic effects become smaller. This approach was questioned by a recent study where expression levels of Cdc42 did not influence the polarization efficiency [49]. In a more mechanistic approach Goryachev and Pokhilko developed a mathematical model for cell polarization in yeast including putative molecular interactions for which

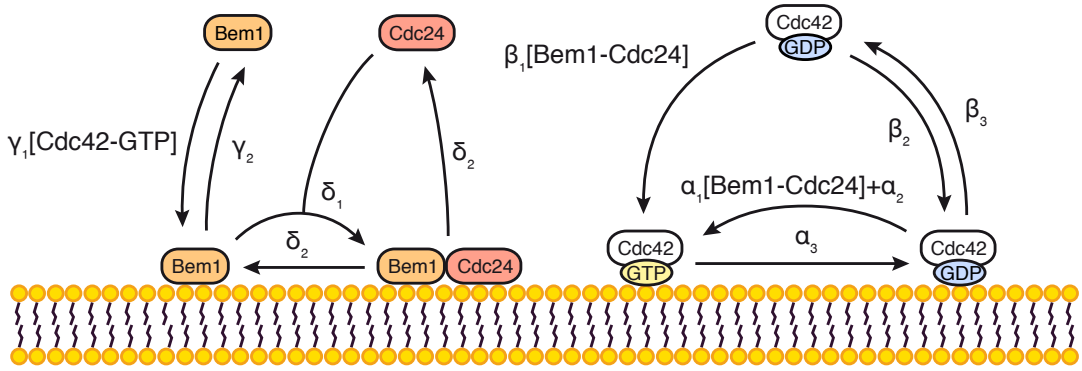

Figure 3.1: Details of the mechanistic model for GDI-mediated cell polarization in yeast. Schematic representation of model reactions. A list of all model reactions is given in section 3.4.1.

experimental evidence is lacking. The authors proposed a Turing-type mechanism for GDI-mediated polarization, which predicts that several transient clusters arise that then merge into a single cluster due to competition for limited amounts of proteins. However, multiple transient caps could so far only be detected in a small subpopulation of wild-type cells and it has not been clarified whether these caps rather rely on actin than the GDI-mediated pathway [66, 49]. This makes it at present difficult to draw definite conclusions from the wild-type polarization dynamics on the GDI-mediated mechanisms of polarization. In addition, the role of the cell cycle in polarity regulation remains incompletely understood.

The coexistence of two independent polarization pathways with unresolved interactions and unclear polarization dynamics prompted us to investigate the fundamental features of GDI-mediated polarization in more detail and to develop a minimal mechanistic model for this polarization pathway. Our results provide strong evidence that GDI-mediated polarization is mainly driven by deterministic reaction-diffusion dynamics. The model provides a unified and comprehensive understanding of several known mutant phenotypes and predicts several phenotypes, which we could verify experimentally. In addition, we identify the enhancement of positive feedback loops in Cdc42 activation and recruitment as the molecular mechanism which facilitates cell cycle control of GDI-mediated polarization. A detailed analysis of the polarization dynamics as well as systematic parameter variations reveal an optimization of GDI-mediated polarization with respect to spatial and temporal control of Cdc42-GTP production. Taken together, our combined theoretical and experimental analysis reveals the fundamental design principles that allow GDI-mediated cell polarization to reliably initiate developmental processes at a specific time and place.

3.2 Results

For our theoretical analysis we first developed a minimal mechanistic model of GDI-mediated polarization. We considered a yeast cell as a spherically shaped cytosolic volume surrounded

by a plasma membrane boundary. Proteins were allowed to either attach to the inner side of the plasma membrane or to remain in the soluble cytosolic pool. Cdc42, its GEF Cdc24 and effector Bem1 have been shown to act together to locally amplify the activation and accumulation of Cdc42 [41, 42]. We therefore explicitly included the spatial distribution of these polarity proteins in terms of their concentrations as model variables. We allowed all proteins to freely diffuse with diffusion constants of $D_2 = 0.03\mu m^2/s$ on the membrane [28] and $D_3 = 11\mu m^2/s$ in the cytosol [137]. To estimate the amount of cellular Cdc42 we took into account that GDIs and GTPases form stoichiometric complexes in the cytosol [96]. Hence, with an average number of 1650 molecules of the yeast Rho GDI per cell [106] and a cytosolic fraction of Cdc42 of roughly 50% [65] we estimated the total cellular amount of Cdc42 to $N_{42} = 3000$. We determined the average cell radius for G1-arrested cells used in this study to $R = 3.95 \pm 0.05\mu m$ (n=63) and used the previously determined protein numbers per cell [106] of Bem1 ($N_B = 6500$) and Cdc24 ($N_{24} = 1000$). A schematic representation of the model reactions discussed below is shown in Fig. 3.1.

While Cdc42 is anchored to the membrane via a prenylation site and polybasic region irrespective of the bound nucleotide, extraction by the GDI preferentially occurs for the inactive GDP-bound form (Fig. 2.4, [52, 30]), which we implemented with rate β_3. Next we included a set of reactions describing a positive feedback loop recruiting the GEF Cdc24 towards Cdc42-GTP [41, 42]. Details of this feedback loop still remain controversial [38, 48, 39]. However, Bem1 and p21-activated kinase Cla4 likely contribute to the feedback loop as they interact with Cdc42, Cdc24 and each other [37, 41, 127]. We made the conservative assumption that the Cdc24 concentration on the membrane is proportional to the amount of Cdc42-GTP at the respective site and implemented Bem1-mediated recruitment of Cdc24 towards active Cdc42 (Fig. 3.1). Cytosolic Bem1 attaches to the membrane with a rate equal to the local Cdc42-GTP concentration times a rate constant γ_1. This reaction effectively describes targeting of Bem1 to the membrane by interaction with Cdc42-GTP or other Cdc42-GTP-bound proteins such as Cla4 [41, 42] and subsequently bind to the membrane using their PX domain [38]. Cytosolic Cdc24 then binds to membrane-bound Bem1 with a rate δ_1 and forms a complex on the membrane; this accounts for the fact that Bem1 recruits Cdc24 to the membrane [41, 42], activates it [40] and maintains it there [47]. The corresponding reverse detachment reactions of Bem1 and Cdc24 are included with rates γ_1 and δ_1, respectively, as both proteins rapidly exchange between polarity cluster and cytosol [65]. We implemented hydrolysis of GTP on Cdc42 by GTPase-activating proteins (GAPs) [24, 25, 26, 27] with a constant rate α_3. Nucleotide-exchange of membrane-bound Cdc42-GDP takes place with a constant intrinsic rate α_2 and a rate proportional to the local concentration of membrane bound Cdc24 times a constant α_1, representing GEF-catalyzed nucleotide-exchange [24]. Cytosolic Cdc42-GDP attaches to the membrane with a low constant background rate β_2 [30]. Moreover, it attaches in GTP-bound form with a rate equal to the local membrane-bound Cdc24 concentration times constant β_1. We included the latter reaction to effectively describe a GEF-mediated displacement of Cdc42 from its GDI Rdi1 and subsequent nucleotide-exchange based on experimental evidence of GEF-mediated displacement of the GTPases Rac1 and Rab from their GDI (Fig. 2.5, [96, 100]). To conclude, the key mechanism of our model is a Bem1-Cdc24-mediated positive feedback loop of Cdc42-GTP locally enhancing the activation and recruitment of further Cdc42. A detailed description of all model reaction rates is given in section 3.4.2.

Mathematically, the spatio-temporal protein dynamics in the plasma membrane and the cy-

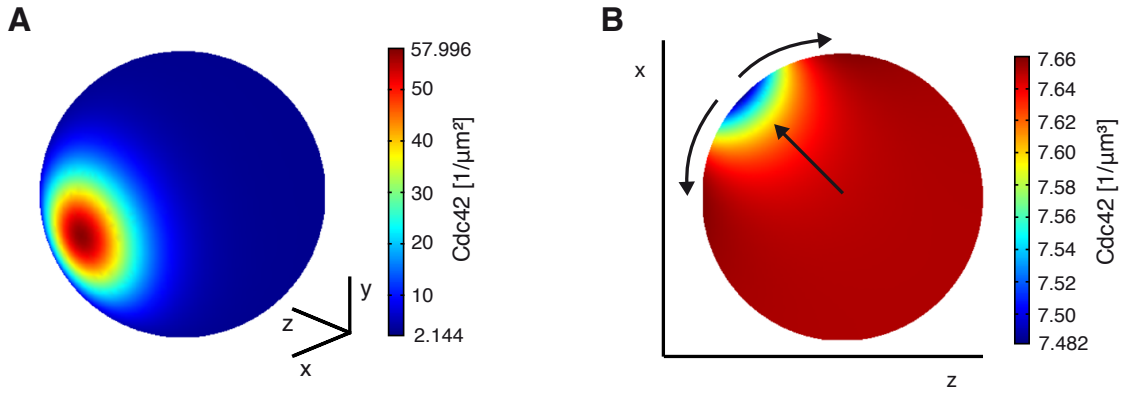

Figure 3.2: Steady state Cdc42 distribution. **A** Numerically obtained polarized Cdc42 distribution on the membrane for wild-type conditions. **B** Corresponding cytosolic distribution of Cdc42 in the x-z plane. Arrows indicate the protein flux.

tosol resulting from a combination of all above reactions and protein diffusion can be cast in the form of a set of partial differential equations (section 3.4.1). We employed analytical as well as numerical methods to solve these equations and thereby determined the polarization efficiency and cluster dynamics for different genetic backgrounds.

3.2.1 Stable cell polarization with continuous exchange of proteins

Initially we set out to characterize the properties of control cells. To this end we numerically simulated the protein dynamics starting from an unpolarized state and found that the system was able to efficiently evolve into a polarized steady state. Cdc42, Bem1 and Cdc24 accumulate in a cluster on the plasma membrane while the corresponding cytosolic concentrations remain almost homogeneous due to the rapid cytosolic diffusion. An example for the simulated spatial Cdc42 distribution in control cells is shown in Fig. 3.2A,B. Directly below the cluster a volume with slightly reduced cytosolic concentrations is flanked by regions with slightly higher cytosolic concentrations (Fig. 3.2B). Both deviations are caused by a continuous exchange of proteins from and into the cluster. A net flux of proteins from the cytosol to the membrane is established at the center of the cluster which is balanced by an opposite flux of proteins at the periphery keeping the total amount of proteins in the cluster constant. Hence, proteins are continuously redistributed to the cluster center to counteract lateral diffusion along the plasma membrane (arrows in Fig. 3.2B) similar to other mass conserved polarity models [107, 72].

3.2.2 Polarization initially emerges as a single broad cap which narrows over time

The initial emergence of polarity can be effectively studied in terms of a linear stability analysis of our model. To this end we extended a previously developed approach for systems with protein exchange between membrane and cytosol [116] to include the spherical symmetry of

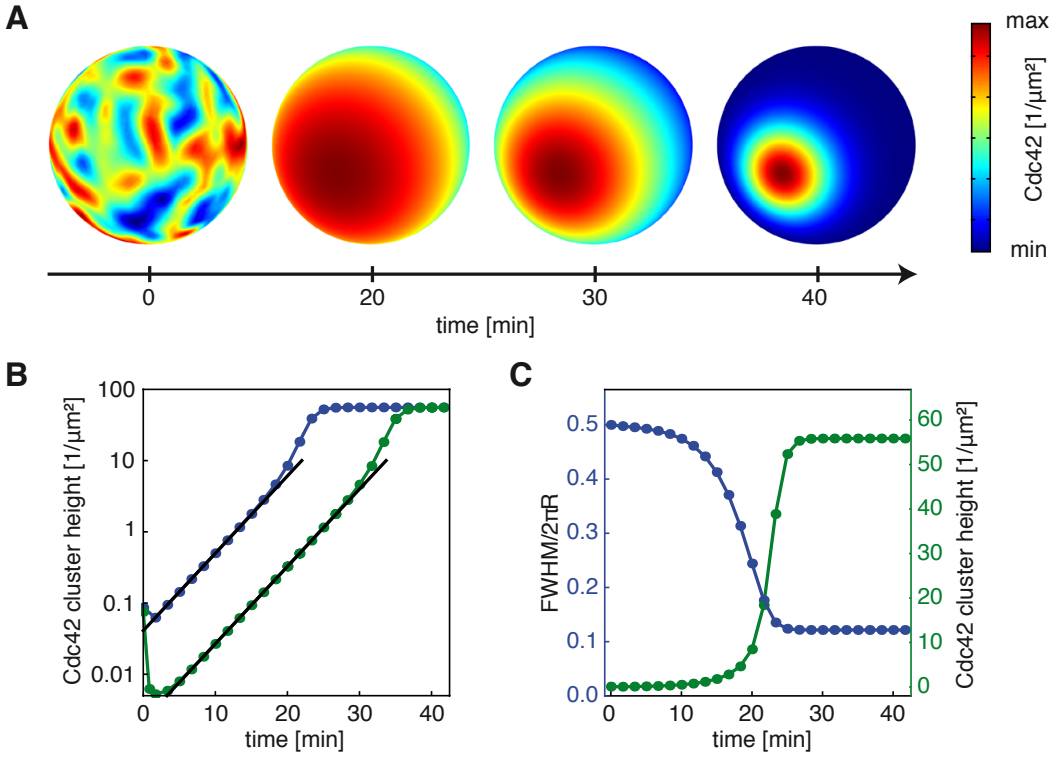

Figure 3.3: Predicted dynamics of GDI-mediated polarization. A Cdc42 density on the plasma membrane for different polarization time points as obtained from numerical simulations starting from the unpolarized homogenous solution disturbed by a small random perturbation using wild-type parameters. **B** Development of simulated Cdc42 cluster height (maximum density over background) over time starting with a random initial perturbation (red curve) or using a broad cap as initial perturbation (blue curve). The black lines correspond to a growth rate of the corresponding cluster of 0.00417/s as predicted from the linear stability analysis. **C** Full width at half maximum (FWHM) of simulated Cdc42 cluster height measured along a great circle through the cap center over circumference $2\pi R$ (blue) and simulated Cdc42 cluster height (green) with the same broad faint cap as initial perturbation as in (B) for different time points.

the cell and the catalyzed membrane attachment of polarity factors. In a linear stability analysis one introduces a small random perturbation to an unpolarized homogenous state of polarity proteins and calculates the time evolution of this protein distribution. Such perturbations represent small concentration fluctuations in protein levels which arise from the Brownian movement of proteins in the cell [115]. Growth of the perturbation implies that the unpolarized state is unstable and that an inhomogeneous pattern arises.

For control cells the linear stability analysis predicted that small random perturbations of the unpolarized state grow and thereby directly evolve into a unique polarity cluster (Fig. 3.12, section 3.4.4). This was in contrast to the previously made prediction of multiple emerging clusters [72]. Importantly, the stability analysis also predicted that random perturbations always directly evolve towards a single growing cluster when we modified each individual model parameter over more than two orders of magnitude (section 3.4.5).

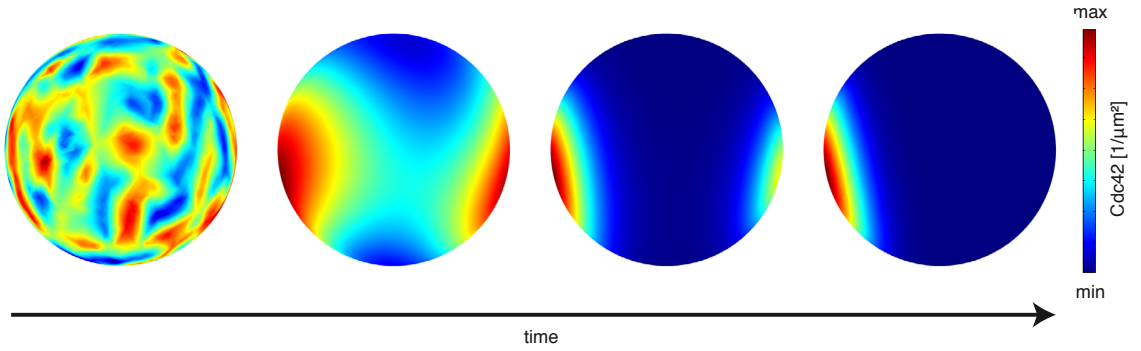

Figure 3.4: Unphysiological polarization dynamics. Numerically obtained relative Cdc42 protein concentration for different time points of a polarizing cell with a Cdc24 protein number 10 times its wild-type value. The initial random perturbation was generated as for control cells and is described in section 3.4.3.

In general, two qualitatively different patterns can arise as the growing perturbation reaches a macroscopic size. If the initial perturbation is sufficiently small, the emerging pattern will be determined by the linear stability analysis. Conversely, if the initial perturbation is too large, a random pattern emerges that depends on the initial perturbation. By numerical evaluation of the full polarization dynamics we found that even considerable perturbations with an amplitude of 1% of the corresponding average concentration (section 3.4.3) directly evolved into a single cluster as we varied each model parameter between 1/3 and 3 times its control value. Only for parameters values that were well outside this physiologically relevant range we observed that small perturbations could also evolve into multiple clusters before coalescing into a single polarization site due to competition for limited amounts of proteins similar to previous models (see also [107, 72]). An example for formation of multiple caps is shown in Fig. 3.4. In summary, our model predicts that small random perturbations robustly induce the direct formation of a single polarity cluster as opposed to coarsening dynamics.

Given the complex circuitry underlying GDI-mediated polarization we sought to identify characteristic properties of the process which could be verified experimentally. When we examined the temporal evolution of polarization sites in our simulations (section 3.4.3) we could identify two distinct phases. Initially, the random protein distribution was gradually replaced by a single broad cap with exponentially growing amplitude consistent with the prediction from the linear stability analysis (Figs. 3.3A, 3.12). In the second phase, the single broad cluster narrowed until it reached a final steady state distribution. To better quantify the narrowing of the cluster we performed simulations with a faint broad cap as an initial perturbation. A single cluster emerged, which showed the same dynamics and shape as those started from random perturbations, confirming that polarization was robust to considerable changes of the initial conditions (Fig. 3.3B). As expected, only the time to reach the final state did depend on the amplitude of the initial perturbation. The numerically obtained cluster shape and growth rate corresponded to the predicted ones from the linear stability analysis (black lines in Figs. 3.3B, 3.12). Nonlinear effects enhanced the growth rate when the cluster reached a threshold size (Fig. 3.3B). The time window where these nonlinear effects became significant coincided with the regime where most of the narrowing of the cluster occurred (Fig. 3.3C). In addition, this was accompanied by most of the absolute increase of the cluster

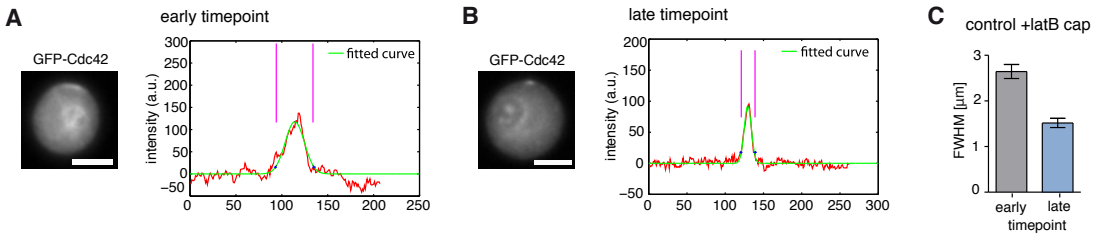

Figure 3.5: Experimental characterization of narrowing dynamics. A,B Representative images and cap intensity profiles of latrunculin treated control cells expressing GFP-Cdc42 at an early (20-30 min after release, A) and late (30-50 min after release, B) time point during polarization. **C** Comparison of full width at half maximum (FWHM) of GFP-Cdc42 + latrunculin caps at early (N=13, SEM=0.15) and late time points (N=28, SEM=0.10).

height (Fig. 3.3C). In summary, our model predicts that one characteristic property of direct single site polarization is the steady narrowing of emerging polarity clusters.

To validate our prediction in experiments we released a synchronized population of latrunculin B-treated yeast cells expressing GFP-Cdc42 from G1 arrest and compared their cluster widths at early and late time points (Fig. 3.5A,B). In accordance with our model prediction the clusters were significantly broader shortly after release, compared to the much more focused caps at later time point (Fig. 3.5C). We also directly monitored the establishment of polarity clusters in latrunculin B-treated cells expressing GFP-Cdc42 or Bem1-GFP. Polarity clusters first emerged as single and faint broad caps which then progressively became narrower and brighter in the time course of several minutes (Fig. 3.6A-D). Note that the high contrast of Bem1-GFP caps allowed the observation of very early broad-caped states (Fig. 3.6C,E) that were not detectable with the weaker Cdc42 signal (Fig. 3.6A,B). The vast majority of cells directly developed a unique polarization site. Only in 3.8% of 209 latrunculin B treated cells expressing GFP-Cdc42 we observed intermediate states with multiple clusters during polarization. Hence, our findings indicate that the observed narrowing of clusters is a characteristic signature for the direct emergence of unique polarization site. The formation of narrow caps did neither depend on the presence of actin structures nor on the formation of a septin diffusion barrier as they also arise in the absence of septin structures [126]. Moreover, our findings suggest that the previously described narrowing of caps in untreated control cells [66] may arise from the dynamics of the GDI-dependent polarization mechanism.

The two-stage process of GDI-mediated polarization identified above allows yeast cells to directly and robustly generate a unique localized Cdc42-GTP cluster and provides an efficient mechanism to initiate processes downstream of Cdc42 like actin reorganization at a desired position with a minimum risk of transmitting the signal at wrong or multiple positions. Without the direct formation of a single cluster GDI-mediated polarization would instead actively generate several transient clusters with high Cdc42-GTP concentration and enhance the risk to initiate irreversible processes such as budding at several places on the membrane. For example, the increased occurrence of transient multiple caps in cells strongly overexpressing Bem1 is accompanied by an occasional formation of multiple buds [66].

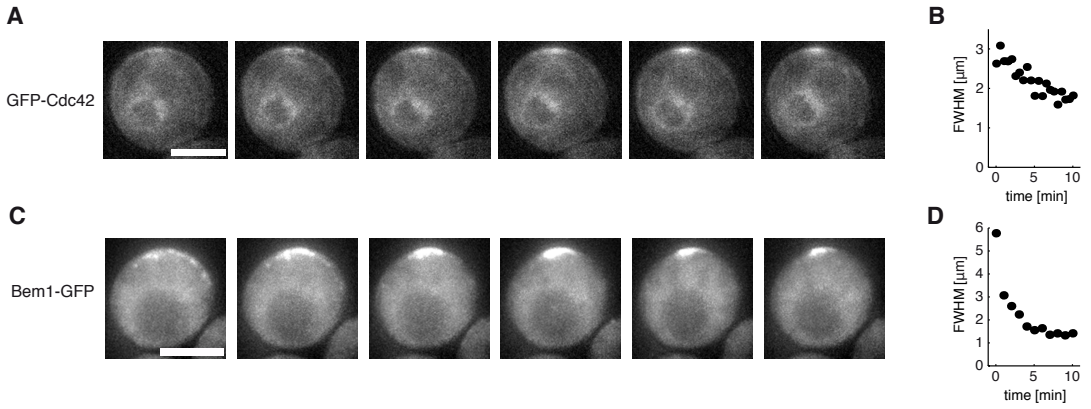

Figure 3.6: Time evolution of polarizing yeast cells. **A** Time series showing GFP-Cdc42 cap establishment in a control cell treated with latrunculin (60s time steps between frames). **B** Time evolution of full width at half maximum of GFP-Cdc42 cap shown in (A) (first frame of (A) corresponds to width at 1min). **C** Time series showing Bem1-GFP cap establishment in a cell treated with latrunculin (60s time steps between frames). **D** Time evolution of full width at half maximum of Bem1-GFP cap shown in (C) (first frame of (C) corresponds to width at 0min). Scale bar: 4 μm

3.2.3 Cell cycle induced changes provide temporal control over GDI-mediated polarization

We next asked how changes of system parameters influence GDI-mediated polarization. We focused on parameters which were experimentally accessible and which directly affected the regulation of Cdc42, such as the rates of GTP hydrolysis and membrane extraction rates of Cdc42 as well as concentrations of the GEF and Bem1. Note that we limited our study to moderately increased protein concentrations in order to avoid the generation of unspecific protein-protein interactions that might occur at non-physiological densities.

Our analysis showed that reduced values for any of the chosen parameters prevented polarization (Fig. 3.7A,B). Importantly, a distinction can be made with regard to the fold change needed to induce this loss. The polarization efficiency was sensitive to a reduction of Cdc24 or Bem1 expression levels but robust to an increase of both. In contrast, we found that while polarization was sensitive to moderately increased Cdc42 hydrolysis and extraction rates, a high fold reduction of both rates was necessary to cause loss of polarization. These results shed new light on previous observations on polarization of mutants in the absence of actin. Cells expressing non-hydrolysable Cdc42 and cells without the GDI Rdi1 represent limiting cases of cells with low Cdc42 hydrolysis and membrane extraction rates, respectively. As predicted by our model, cells cannot polarize in either case (Figs. 3.7A,B, [17, 29]). Moreover, yeast cells without Bem1 [65], with reduced amounts of available Cdc24 [33], or overexpressing the GAP Bem3 (increased Cdc42 hydrolysis, [35]) were not able to polarize. Hence, our model provides a generalized and unified description of these mutant phenotypes.

An important feature emerging from our simulations is the ability of yeast cells to regulate polarization in a switch-like manner when crossing a threshold in Cdc24 concentration or Cdc42 hydrolysis rate (Fig. 3.7A). These two parameters are also regulated during the yeast

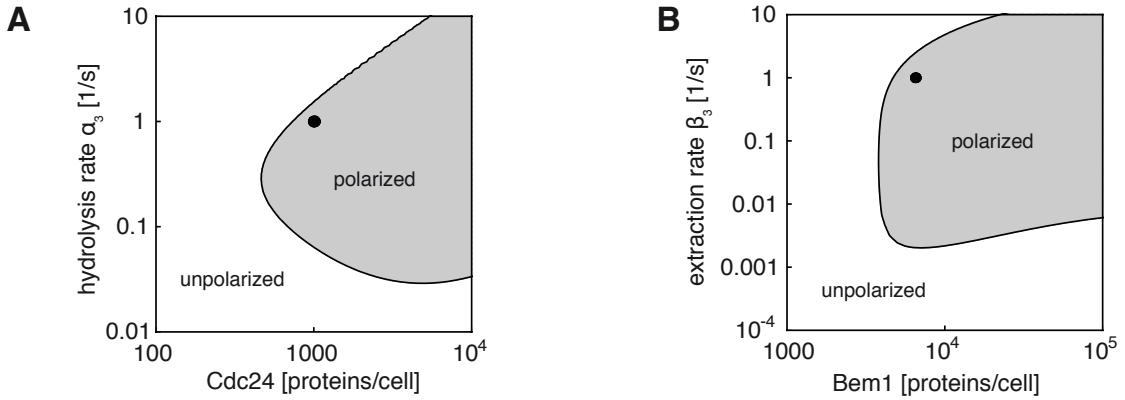

Figure 3.7: Parameters affecting polarization efficiency. A,B Polarization capability predicted from the linear stability analysis shown for different concentrations of the GEF Cdc24 and Cdc42 hydrolysis rates (A) as well as for different concentrations of Bem1 protein and Cdc42 extraction rates (B). Black dots indicate values in control cells.

cell cycle: On the one hand, Cdc24 is sequestered in the nucleus in unpolarized G1 cells and released into the cytosol at the G1-S transition [33, 34]. Inhibition of this relocation process leads to inhibition of cell polarization. On the other hand, reduction of Cdc42 hydrolysis at the G1-S transition by phosphorylation of the Cdc42 GAPs Bem2 and Bem3 has been shown to be crucial for polarization [35]. Hence, our results indicate that GDI-mediated polarization is switched on during the cell cycle by a simultaneous increase in GEF concentrations and reduction of the Cdc42 hydrolysis rate.

Given these findings, we wanted to better understand the choice of parameters in control cells and the cell cycle-dependent regulation of polarity. In the following sections we therefore studied the features defining polarized and unpolarized states in more detail.

3.2.4 Enhancing the positive feedback loops provides simultaneous switch-like regulation of polarization and Cdc42 activation

To reveal the mechanism for the failure of GDI-dependent polarization we next investigated the membrane-cytosol ratio of Cdc42 in unpolarized cells for different parameter regimes and asked whether failure to polarize is correlated with loss of active Cdc42 on the cell membrane. Interestingly, we found that the regimes with significant amounts of active Cdc42 overlapped but did not coincide with the polarization regimes identified above (Fig. 3.8A,B). For hydrolysis rates much lower and GEF concentrations much higher than the control cell values, there were significant amounts of active Cdc42 even in cells which were unable to polarize (Fig. 3.8A). In this regime the positive feedback loops were still active but the protein transport to the membrane was too slow to counter lateral diffusion on the plasma membrane, and therefore unable to cause cap formation. Consistent with these results, non-hydrolysable Cdc42 has been shown to accumulate on the plasma membrane but is unable to polarize through the GDI-mediated polarization mechanism (Fig, 3.8A, [65]). A similar

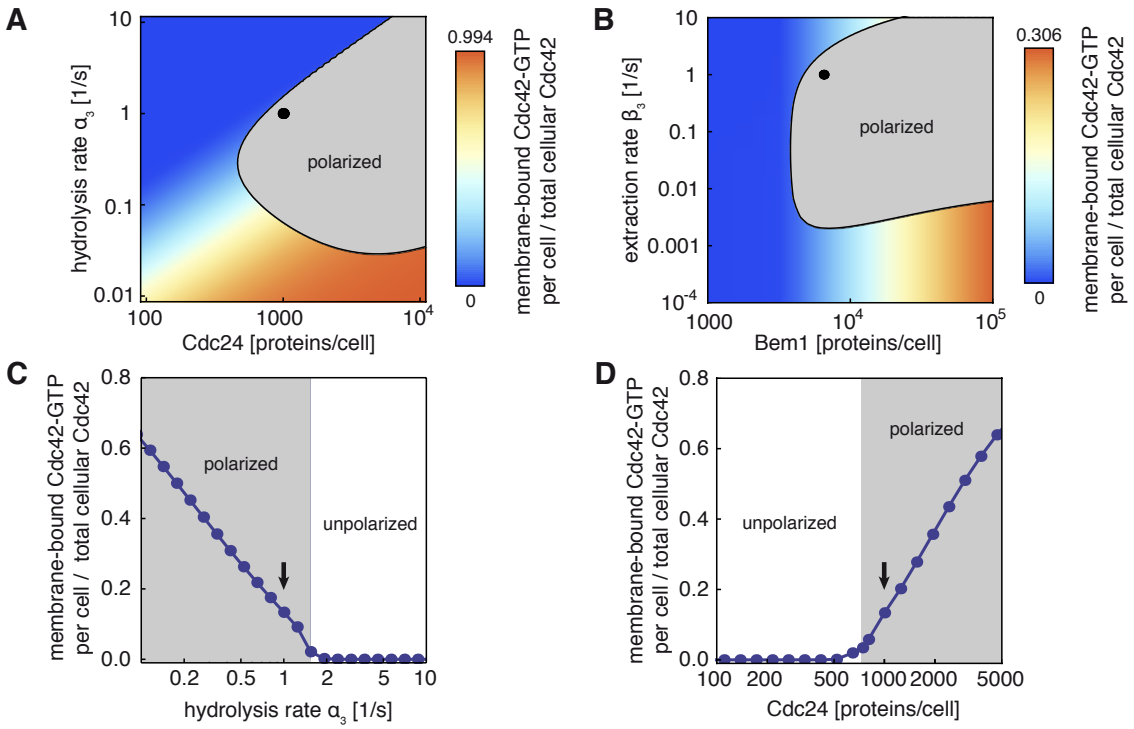

Figure 3.8: Cdc42 activation for changing parameters. A,B Plots as in Fig. 3.7 but in addition indicating concentration of membrane-bound Cdc42-GTP (as fraction of total cellular Cdc42) in unpolarized cells. Black dots indicate values in control cells. **C,D** Concentration of membrane-bound Cdc42-GTP for different Cdc24 protein numbers per cell (C) and Cdc42 hydrolysis rates (D) The arrows indicate the control cell values.

behavior is found for increasing Bem1 concentrations at low extraction rates (Fig. 3.8B).

These findings stand in contrast to the behavior close to the control cell values at the upper boundary of the polarization regime, where cell cycle induced parameter changes switch cells into an unpolarized state with very low Cdc42-GTP levels (Fig. 3.8A,B). To further analyze the cells properties at this boundary we calculated the final concentration of active Cdc42 for changing Cdc24 expression levels and Cdc42 hydrolysis rates in the vicinity of the wild-type values (Fig. 3.8C,D). Our results reveal that the production of active Cdc42 is almost completely switched off when polarization breaks down. Hence, cell cycle induced changes simultaneously regulate polarity and the ability for Cdc42-GTP production in a switch-like manner. The GDI-mediated polarization mechanism not only allows selecting a spatially restricted region for Cdc42 to initiate further downstream processes, it also controls the transmission of the Cdc42 signal itself. This switch-like response is genuinely different from the response in a hypothetical system without feedback loops. In the latter case, instead of an abrupt change at a threshold, one would expect the amount of active Cdc42 to gradually increase with the activator concentration (and decrease with the hydrolysis rate) over the whole parameter range such that much higher changes of regulators would be necessary to effectively suppress Cdc42 activity in unpolarized cells. To better understand the origin of the observed switch-like behavior we systematically varied several system parameters, which

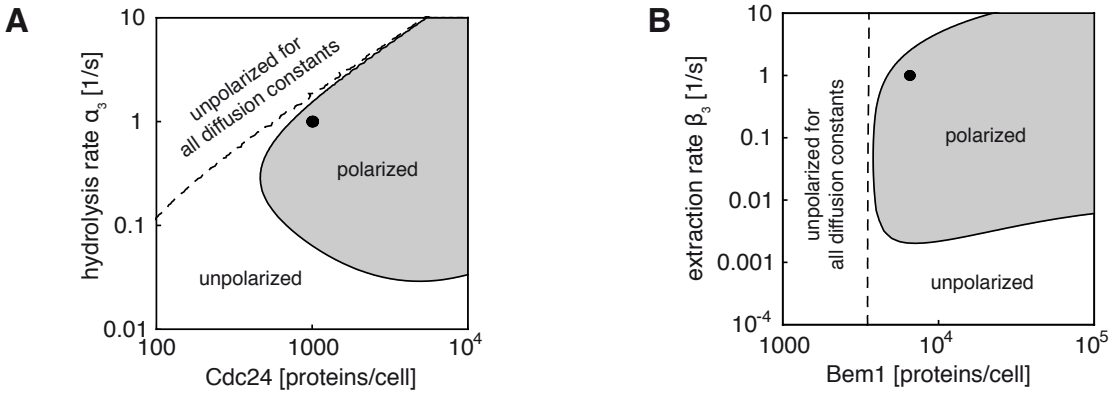

Figure 3.9: Polarization efficiency for changing diffusion constants. A,B Plots as in Fig. 3.7 but additionally indicating parameter regions where polarization cannot be rescued by a change of the diffusion constants D_2, D_3. Black dots indicate values in control cells.

we assumed to be essential for the pattern formation process. We have previously shown that polarity clusters are maintained by continuous redistribution of polarity factors to counteract the lateral membrane diffusion. Therefore, we expected that loss of polarity might be rescued by a change of the diffusion constants. However, for large parts of the parameter regions considered above we found that loss of polarization could not be rescued in this way (Fig. 3.9A,B). This indicates that loss of polarization in these regimes depends on the nonlinear dynamics of the protein reaction network itself and not solely from insufficient redistribution of proteins. Notably, the diffusion-insensitive parameter regions also coincided with the loss of almost all Cdc42-GTP on the membrane, compare with Figs. 3.8A,B. Hence, we concluded that in these regimes the positive feedback loops of Cdc42 activation and membrane attachment fail and can therefore no longer locally enhance the accumulation of Cdc42-GTP on the membrane as needed for pattern formation. These results provide a unified mechanistic understanding of several loss of polarity mutants: Reduced GEF or Bem1 concentrations or enhanced Cdc42 hydrolysis weaken the positive feedback loops of Cdc42 production on the membrane until they fail to operate.

In summary, the GDI-mediated polarization mechanism provides yeast cells with the ability to establish a polarized Cdc42 cluster at a specific membrane position, and at the same time allows an immediate change into an unpolarized state via a feedback switch where Cdc42 signaling is suppressed.

3.2.5 Cell cycle regulated temporal control induces a direct and robust change into highly localized polarization

To shed more light on the consequences of the control cell parameter choice, we studied the final shape of polarity clusters under varying system parameters. Starting form control cell values we numerically calculated the final Cdc42 cluster width for varying Cdc24 and Bem1 concentrations as well as different Cdc42 extraction and hydrolysis rates. When we increased the Bem1 or Cdc24 concentrations towards the control cell values we observed that directly a

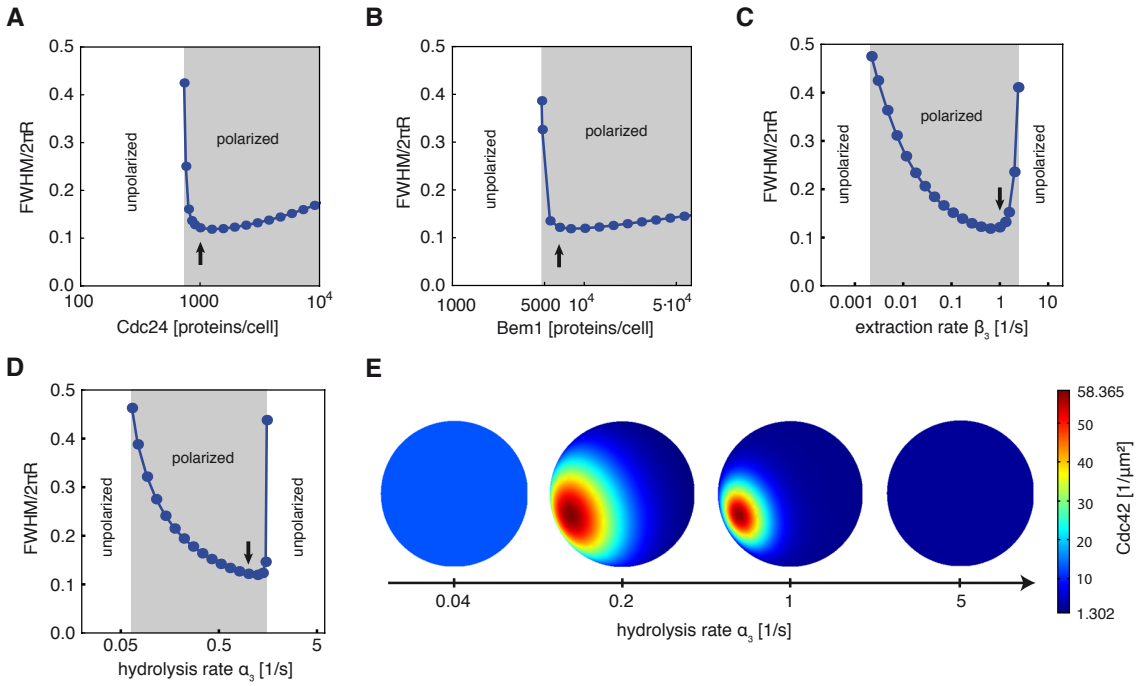

Figure 3.10: Predicted cluster widths for changing parameters. A-D Full width at half maximum of Cdc42 density as obtained in Fig. 3.3 for different Cdc24 protein numbers per cell (A) and Bem1 (B) concentrations and for different Cdc42 extraction (C) and hydrolysis (D) rates. The arrows indicate the corresponding control cell value. **E** Examples of Cdc42 cluster density calculated for different hydrolysis rates.

narrow final cluster was produced as polarization set in (Fig. 3.10A,B). In contrast, if Cdc42 extraction or hydrolysis rates were increased, polarized clusters were initially very broad and only gradually became narrower (Fig. 3.10C,D). However, these narrow final clusters were directly lost when the rates were increased slightly beyond the control cell values (Fig. 3.10C,D). Remarkably, the control cell values estimated from experiments were all situated in parameter regions that resulted in an almost optimal narrow cluster width (arrows in Fig. 3.10A-D). In summary, we find that the cell cycle dependent concomitant increase of cytosolic Cdc24 and decrease of GAP activity allows yeast cells to directly and robustly switch from an unpolarized state into a highly polarized state, thus ensuring the emergence of a narrow polarity cluster.

One quantitative prediction of our model is that a reduction of the Cdc42 hydrolysis or extraction rates would cause polarity clusters to become less focused compared to the wild-type situation (Fig. 3.10C,D). Cdc42 is then expected to spend more time on the plasma membrane and to diffuse over longer distances before Rdi1 extracts it into the cytosol. Numerical solutions of our mechanistic model show the Cdc42 concentration profile on the plasma membrane expected for different hydrolysis rates (Fig. 3.10E). Very low hydrolysis rates were only able to sustain patterns much larger than a yeast cell and therefore resulted in unpolarized cells. With increasing hydrolysis rates first broad caps appeared that spanned over the whole cell. Upon further increase of the rate caps became progressively narrower until a critical

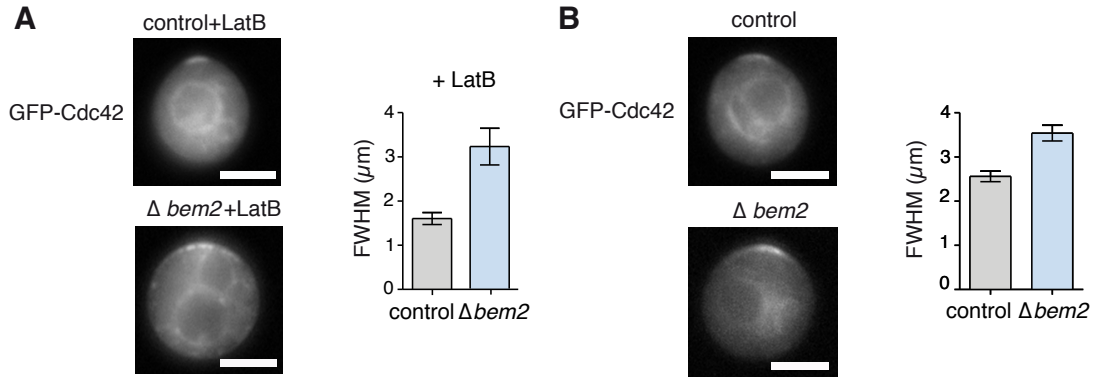

Figure 3.11: Experimental verification of predicted cluster widths. A, B Images and quantification of GFP-Cdc42 cap widths in control and Δbem2 cells in the presence (A) or absence (B) of latrunculin B. Bar graphs correspond to mean SEM. Scale bars: 4 μm.

value was reached above which the positive feedback loops failed to reinforce themselves. To verify the predicted broad clusters at low hydrolysis rates we used a yeast strain where the Cdc42 GAP Bem2 was deleted. We then treated these cells with latrunculin B and compared the width of the formed polar caps with those in similarly treated control cells. As predicted, Bem2 cells formed significantly broader caps with nearly twice the width of those in control cells (Fig. 3.11A). A slightly weaker effect on cap width was also observed in cells not treated with latrunculin, suggesting that GDI-mediated polarization may also contribute to the broadening of caps observed between control and Bem2 cells (Fig. 3.11B).

These results show that the cell cycle induced reinforcement of the positive feedback loops enables yeast cells to directly and robustly form a highly localized cluster out of an unpolarized state with only slight changes in parameter values. The finding that reduced hydrolysis broadens polarity clusters suggests that the polarity reaction network is optimized by rapid GTPase cycling to achieve maximally focused polarization. This focusing in turn might help to optimally organize morphogenetic processes downstream of Cdc42, such actin reorganization or septin ring formation [124, 126].

3.3 Discussion

Our results indicate that deterministic reaction-diffusion dynamics optimize spatial and temporal control of Cdc42-GTP production during yeast cell polarization. The mechanistic model introduced in this work belongs to the class of reaction-diffusion driven pattern-forming systems, and robustly provides direct emergence of a unique polarization site with characteristic narrowing dynamics as confirmed by our experiments. We found that two GEF-mediated positive feedback loops in Cdc42 activation and membrane recruitment arise as core mechanisms. In contrast to our findings, a previous model predicted GDI-mediated polarization via multiple transient competing clusters [72]. However, such polarization dynamics would increase the risk to accidentally initiate downstream signaling through Cdc42 at several places

before competition is finished, e.g. budding at several places on the membrane. Our findings suggest the following function of the GDI-mediated polarization pathway: It directly forms a unique polarization site and thereby counteracts the formation of multiple clusters, which might arise from actin-dependent polarization [17], strong particle fluctuations, or due to protein interaction with spatial cues. This does not exclude the occasional emergence of transient multiple clusters at random membrane positions [66, 49]. However, our findings show that the GDI-mediated polarization mechanism itself does not actively form multiple clusters but, in contrast, acts to suppress them and hence reduces the risk of misguided Cdc42 signaling in wild-type cells.

Furthermore, we have shown that enhancement of the positive feedback loops is the key mechanism that initiates polarization. Its characteristic feature is a switch-like change from an unpolarized state to a highly localized polarization site. For example, slight changes in Cdc24 or Bem1 protein concentration are sufficient to directly and robustly induce the formation of a narrow final polarity cluster. The mechanism of this switch lies in the success or failure of the positive feedback loops to self-enhance, and is not related to the ability to counteract lateral membrane diffusion. In addition, the switch to the polarized state is accompanied by a strong increase of activated Cdc42 levels.

Both release of the GEF Cdc24 from the nucleus and reduction of Cdc42 hydrolysis by phosphorylation of GAPs have been shown to contribute to activation of Cdc42 and subsequent polarity establishment [35, 34, 33]. Our results provide strong evidence that these changes are used for temporal control of GDI-mediated cell polarity as both parameter changes can induce polarization by enhancement of the positive feedback loops. Our findings provide a mechanistic understanding of how polarity establishment in yeast is regulated by the cell cycle. In wild-type cells, the GDI-mediated polarization mechanism fulfills a two-fold function. On the one hand, it provides a highly polarized cluster of Cdc42-GTP on the membrane. On the other hand, it safely keeps Cdc42 inactive in unpolarized cells. Thereby yeast cells acquire the ability to initiate Cdc42 signaling in a controlled switch-like manner in a spatially confined region of the plasma membrane. This has to be distinguished from other perturbations of the system where a loss of GDI-mediated polarity does not necessarily abolish Cdc42 signaling. For example, within our model we predict that a reduction of the Cdc42 membrane extraction rate (e.g. by deletion of the GDI RDI1) induces a loss of GDI-mediated polarity but still allows the production of significant amounts of active Cdc42 on the plasma membrane. This is reaffirmed by recent experiments with Δrdi1 cells which cannot polarize via the GDI-dependent pathways but still produce sufficient amounts of active Cdc42 to trigger polarization via actin structures [29]. Our model also predicted that polarity clusters would broaden if the Cdc42 extraction or hydrolysis rates were reduced. Consistently, we found that deletion of the GAP Bem2 led to significant broader clusters in latrunculin-treated cells indicating that the biochemical reaction network is indeed optimized to robustly provide a narrow final cluster.

By combining all results of our study we find that the following key features characterize the polarization process under physiological conditions: (i) GDI-mediated polarity operates in a parameter regime where polarization is accompanied by a significant fold change in Cdc42-GTP amounts. (ii) The pattern-forming mechanism directly produces a single cluster and not several intermediate clusters which then merge into a single cluster. (iii) Cell cycle induced changes in Cdc42 activation directly lead to the robust formation of a narrow final cluster with

only very small changes in Cdc24 concentrations or hydrolysis rates. Our results indicate that under typical physiological conditions in yeast cells all of the listed aspects are simultaneously optimized in order to provide controlled Cdc42 signaling with a minimized risk of accidentally initiating further processes downstream of Cdc42 at the wrong time or position.

The simultaneous optimization of the aforementioned aspects of polarity provides evidence for the GEF-mediated positive feedback loops of Cdc42 activation [42] and membrane attachment [96, 100] to be the key molecular mechanisms of GDI-mediated cell polarization suggesting a new perspective on how cell polarity can be established with a minimum set of polarity factors.

Given the high conservation of involved genes we expect GDI-mediated polarization throughout the animal kingdom to show a similar behavior as in yeast. The characteristic finding that reducing the hydrolysis of the polarity GTPase broadens polarity clusters in yeast provides an easily testable prediction to identify similar polarity mechanisms in other eukaryotes. As one example, deletion of the Rop (plant Rho GTPase) GAP Ren-1 defocused polarization of GTPase ROP1 in *Arabidopsis thaliana* pollen tubes [120].

3.4 Materials and methods

3.4.1 Reaction-diffusion equations

The set of partial differential equations describing the time evolution of protein concentrations given in the main text reads in spherical coordinates r, θ, ϕ

$$\begin{aligned}
\partial_t m_T &= (\alpha_1 m_{BG}+\alpha_2) m_D - \alpha_3 m_T + \beta_1 m_{BG} c_D + D_2 \Delta_{\theta,\phi} m_T\big|_{r=R}\,, && (3.1)\\
\partial_t m_D &= -(\alpha_1 m_{BG}+\alpha_2) m_D + \alpha_3 m_T + \beta_2 c_D - \beta_3 m_D + D_2 \Delta_{\theta,\phi} m_D\big|_{r=R}\,, && (3.2)\\
\partial_t m_B &= \gamma_1 m_T c_B - \gamma_2 m_B - \delta_1 m_B c_G + \delta_2 m_{BG} + D_2 \Delta_{\theta,\phi} m_B\big|_{r=R}\,, && (3.3)\\
\partial_t m_{BG} &= \delta_1 m_B c_G - \delta_2 m_{BG} + D_2 \Delta_{\theta,\phi} m_{BG}\big|_{r=R}\,, && (3.4)\\
\partial_t c_D &= D_3 \Delta c_D\,, && (3.5)\\
\partial_t c_B &= D_3 \Delta c_B\,, && (3.6)\\
\partial_t c_G &= D_3 \Delta c_G\,, && (3.7)
\end{aligned}$$

where $\Delta_{\theta,\phi}$ stands for the angular part of the spherical Laplace operator Δ. The membrane concentrations of Cdc42-GTP, Cdc42-GDP, Bem1, and Bem1-Cdc24 complexes at radial position $r = R$ are denoted by m_T, m_D, m_B, and m_{BG}, whereas c_D, c_B, and c_G describe the cytosolic concentrations of Cdc42-GDP, Bem1, and Cdc24. The cytosolic flux of proteins to the membrane is facilitated by the boundary conditions

$$D_3\partial_r c_D\big|_{r=R} = -(\beta_1 m_{BG}+\beta_2)c_D+\beta_3 m_D\big|_{r=R}\,, \tag{3.8}$$
$$D_3\partial_r c_B\big|_{r=R} = -\gamma_1 m_T c_B+\gamma_2 m_B\big|_{r=R}\,, \tag{3.9}$$
$$D_3\partial_r c_G\big|_{r=R} = -\delta_1 m_B c_G+\delta_2 m_{BG}\,.\big|_{r=R}\,. \tag{3.10}$$

The determined wild-type parameters are $D_2 = 0.03\mu m^2 s^{-1}$, $D_3 = 11\mu m^2 s^{-1}$, $R = 3.95\mu m$, $N_{42} = 3000$, $N_B = 6500$, $N_{24} = 1000$, $\alpha_1 = 0.2\mu m^2 s^{-1}$, $\alpha_2 = 0.12 min^{-1}$, $\alpha_3 = 1s^{-1}$, $\beta_1 = 0.266\mu m^3 s^{-1}$, $\beta_2 = 0.28\mu m s^{-1}$, $\beta_3 = 1s^{-1}$, $\gamma_1 = 0.2667\mu m^3 s^{-1}$, $\gamma_2 = 0.35s^{-1}$, $\delta_1 = 0.00297\mu m^3 s^{-1}$, and $\delta_2 = 0.35s^{-1}$.

3.4.2 Determination of reaction rates

The detachment rates of Bem1 and Cdc24, γ_2 and δ_2, were estimated with $0.35s^{-1}$ using fluorescence recovery after photobleaching (FRAP) experiments (section 2.4.7, unpublished data) and the intrinsic nucleotide-exchange rate $\alpha_2 = 0.12 min^{-1}$ was taken from literature [24]. Given a Cdc42 FRAP rate of 0.28/s (section 2.4.7) and taking into account that Cdc42 needs to be hydrolyzed before it gets extracted we estimated the hydrolysis and extraction rates α_3 and β_3 to $1s^{-1}$. To fit our model we used an estimate for the fraction of Cdc42 present in the cluster of 10-20% taken from literature [29]. Given that 50-70% of all Cdc42 are found in the inner compartments of the cell [29], we estimated the amount of Cdc42 on the plasma membrane outside the cluster to be equal to the amount inside the cluster. The fractions of Bem1 and Cdc24 in the cluster were estimated to 50% and 10%, respectively, based on fluorescence recovery experiments [65]. As ∼10% of on average 1000 Cdc24 molecules are found in the polarity cluster, which occupies roughly 10% of the membrane [29], we expect an average Cdc24 density of $\sim 5/\mu m^2$ within the cluster. Based on this estimate we chose a GEF-dependent nucleotide-exchange rate α_1, which provides an effective nucleotide-exchange rate of $1s^{-1}$ on the same order as hydrolysis and extraction rates in a cluster. The remaining attachment rates β_1, β_2, γ_1, and δ_1 were then chosen to approximately achieve fractions of 10% Cdc24, 50% Bem1, and 30% Cdc42 on the membrane of polarized cells based on the estimates given above.

3.4.3 Simulations

Simulations were performed using Comsol Multiphysics 3.5a. To generate random initial perturbations we took a random number from the interval [-1,1] for each site of a cubic lattice in space with a spacing of $1\mu m$. This lattice was then used to produce a continuous perturbation function f(x,y,z) using Comsols interpolation routine to define functions from a set of random data points. We assumed that pattern formation in our simulations is initiated by small random perturbations with an amplitude of 1% of the corresponding unpolarized protein concentration. The perturbations were generated by multiplying the initial unpolarized concentration of all membrane-bound proteins with (1+0.01*f(x,y,z)). Broad caps as initial perturbations were generated by adding a function with linear dependence on one spatial

direction to the unpolarized initial concentration of all membrane-bound proteins assuming that the function changes sign at the center of the cell.

3.4.4 Linear stability analysis

The initial dynamics of emerging polarity clusters can be studied using a linear stability analysis for problems with cytosol-membrane coupling [116]. Using this framework we ask how a small perturbation of the spatially homogenous steady state distribution of proteins would evolve in time. A decay of the perturbation implies that the homogenous state is stable and no polarization occurs. The advantage of this approach lies in the use of developed standard methods for systems of linear differential equations. The ability of the system to polarize for a certain set of parameters can be tested by finding the roots of polynomials instead of simulating the full dynamics each time. For all cases tested we found perfect agreement between linear stability analysis and simulation in predicting the spontaneous polarization efficiency. The full set of reaction-diffusion equations from the main text reads in spherical coordinates r, θ, ϕ

$$\begin{aligned}
\partial_t m_T &= (\alpha_1 m_{BG}+\alpha_2)m_D-\alpha_3 m_T+\beta_1 m_{BG}c_D+D_2\Delta_{\theta,\phi}m_T\big|_{r=R}\,, && (3.11)\\
\partial_t m_D &= -(\alpha_1 m_{BG}+\alpha_2)m_D+\alpha_3 m_T+\beta_2 c_D-\beta_3 m_D+D_2\Delta_{\theta,\phi}m_D\big|_{r=R}\,, && (3.12)\\
\partial_t m_B &= \gamma_1 m_T c_B-\gamma_2 m_B-\delta_1 m_B c_G+\delta_2 m_{BG}+D_2\Delta_{\theta,\phi}m_B\big|_{r=R}\,, && (3.13)\\
\partial_t m_{BG} &= \delta_1 m_B c_G-\delta_2 m_{BG}+D_2\Delta_{\theta,\phi}m_{BG}\big|_{r=R}\,, && (3.14)\\
\partial_t c_D &= D_3\Delta c_D\,, && (3.15)\\
\partial_t c_B &= D_3\Delta c_B\,, && (3.16)\\
\partial_t c_G &= D_3\Delta c_G\,, && (3.17)
\end{aligned}$$

where $\Delta_{\theta,\phi}$ stands for the angular part of the spherical Laplace operator Δ. The diffusive flux to the membrane is incorporated by the boundary conditions

$$\begin{aligned}
D_3\partial_r c_D\big|_{r=R} &= -(\beta_1 m_{BG}+\beta_2)c_D+\beta_3 m_D\big|_{r=R}\,, && (3.18)\\
D_3\partial_r c_B\big|_{r=R} &= -\gamma_1 m_T c_B+\gamma_2 m_B\big|_{r=R}\,, && (3.19)\\
D_3\partial_r c_G\big|_{r=R} &= -\delta_1 m_B c_G+\delta_2 m_{BG}\,.\big|_{r=R}\,. && (3.20)
\end{aligned}$$

As long as the perturbation is small compared to the homogenous steady state solution one considers a linearized version of the full set of reaction-diffusion equations as a good approximation for describing the time evolution of perturbations. The linearized version of full reaction-diffusion equations (3.11)-(3.20) for the perturbations δm_x, δc_x reads

$$\begin{aligned}
\partial_t \delta m_T &= (D_2\Delta_{\theta,\phi}-\alpha_3)\delta m_T+(\alpha_1 m^0_{BG}+\alpha_2)\delta m_D+(\alpha_1 m^0_D+\beta_1 c^0_D)\delta m_{BG} \\
&\quad +\beta_1 m^0_{BG}\delta c_D\big|_{r=R}\,, && (3.21)\\
\partial_t m_D &= \alpha_3 m_T+(D_2\Delta_{\theta,\phi}-\alpha_1 m^0_{BG}-\alpha_2-\beta_3)\delta m_D-\alpha_1 m^0_D\delta m_{BG}+\beta_2\delta c_D\big|_{r=R}\,, && (3.22)\\
\partial_t m_B &= \gamma_1 c^0_B\delta m_T+(D_2\Delta_{\theta,\phi}-\gamma_2-\delta_1 c^0_G)\delta m_B+\delta_2\delta m_{BG}+\gamma_1 m^0_T\delta c_B-\delta_1 m^0_B\delta c_G\big|_{r=R}\,, && (3.23)\\
\partial_t m_{BG} &= \delta_1 c^0_G\delta m_B+(D_2\Delta_{\theta,\phi}-\delta_2)\delta m_{BG}+\delta_1 m^0_B\delta c_G\big|_{r=R}\,, && (3.24)\\
\partial_t \delta c_D &= D_3\Delta\delta c_D\,, && (3.25)\\
\partial_t \delta c_B &= D_3\Delta\delta c_B\,, && (3.26)\\
\partial_t \delta c_G &= D_3\Delta\delta c_G\,. && (3.27)
\end{aligned}$$

For the linearized boundary conditions one gets

$$\begin{aligned}
D_3\partial_r\delta c_D\big|_{r=R} &= \beta_3\delta m_D-\beta_1 c^0_D\delta m_{BG}-(\beta_1 m^0_{BG}+\beta_2)\delta c_D\big|_{r=R}\,, && (3.28)\\
D_3\partial_r\delta c_B\big|_{r=R} &= -\gamma_1 c^0_B\delta m_T+\gamma_2\delta m_B-\gamma_1 m^0_T\delta c_B\big|_{r=R}\,, && (3.29)\\
D_3\partial_r\delta c_G\big|_{r=R} &= -\delta_1 c^0_G\delta m_B+\delta_2\delta m_{BG}-\delta_1 m^0_B\delta c_G\big|_{r=R}\,. && (3.30)
\end{aligned}$$

The constants m^0_x, c^0_x denote the values of m_x, c_x of the physical spatially homogenous steady state solution of equations (3.11)-(3.20). Note that these quantities depend on the particle numbers. To solve (3.21)-(3.30) we make use of the spherical symmetry. We expand the perturbations in a series of real spherical harmonics $Y_{l,m}(\theta,\phi)$ [131], assume an exponential time dependence, and use the ansatz

$$\delta m_x(t,\theta,\phi)=\sum_{l=0}^{\infty}\sum_{m=-l}^{l}\delta m_x^{l,m}Y_{l,m}(\theta,\phi)e^{\omega_{l,m}t}\,, \tag{3.31}$$

$$\delta c_x(t,r,\theta,\phi)=\sum_{l=0}^{\infty}\sum_{m=-l}^{l}A^{l,m}(r)Y_{l,m}(\theta,\phi)e^{\omega_{l,m}t}\,. \tag{3.32}$$

The aim of the following calculation is to find the largest real part $\mathrm{w_{l,m}}$ of all rates $\omega_{l,m}$ as a positive value implies a growth of pattern induced by a small perturbation. By combining (3.32) with (3.25)-(3.27) and using $r^2\Delta_{\theta,\phi}Y_{l,m}(\theta,\phi)=-l(l+1)Y_{l,m}(\theta,\phi)$ [132] we arrive at

$$0=\left[r^2\frac{\partial^2}{\partial r^2}+2r\frac{\partial}{\partial r}-l(l+1)-\frac{\omega_{l,m}r^2}{D_3}\right]A^{l,m}(r) \tag{3.33}$$

for each mode l,m. Physical solutions of this equation are the modified spherical Bessel functions of the first kind $i_l(r\sqrt{\omega_{l,m}/D_3})$ [130]. For the cytosolic perturbations we get

$$\delta c_x(t,r,\theta,\phi) = \sum_{l=0}^{\infty}\sum_{m=-l}^{l} \delta c_x^{l,m} i_l(r\sqrt{\omega_{l,m}/D_3}) Y_{l,m}(\theta,\phi) e^{\omega_{l,m}t}\,. \tag{3.34}$$

By putting putting (3.34) and (3.31) into the linearized boundary conditions we get for each mode l,m

$$\begin{aligned}
D_3\delta c_D^{l,m}\partial_r i_l(r\sqrt{\omega_{l,m}/D_3})\big|_{r=R} &= \beta_3\delta m_D^{l,m} - \beta_1 c_D^0 \delta m_{BG}^{l,m} \\
&\quad -(\beta_1 m_{BG}^0+\beta_2)\delta c_D^{l,m} i_l(R\sqrt{\omega_{l,m}/D_3})\,, &(3.35)\\
D_3\delta c_B^{l,m}\partial_r i_l(r\sqrt{\omega_{l,m}/D_3})\big|_{r=R} &= -\gamma_1 c_B^0\delta m_T^{l,m} + \gamma_2\delta m_B^{l,m} - \gamma_1 m_T^0 \delta c_B^{l,m} i_l(R\sqrt{\omega_{l,m}/D_3})\,, &(3.36)\\
D_3\delta c_G^{l,m}\partial_r i_l(r\sqrt{\omega_{l,m}/D_3})\big|_{r=R} &= -\delta_1 c_G^0\delta m_B^{l,m} + \delta_2\delta m_{BG}^{l,m} - \delta_1 m_B^0 \delta c_G^{l,m} i_l(R\sqrt{\omega_{l,m}/D_3})\,. &(3.37)
\end{aligned}$$

Using these equations we reexpress the cytosolic perturbations (3.34) in terms of the membrane perturbation amplitudes $\delta m_x^{l,m}$ as

$$\begin{aligned}
\delta c_D(t,r,\theta,\phi) &= \sum_{l=0}^{\infty}\sum_{m=-l}^{l} \frac{(\beta_3\delta m_D^{l,m} - \beta_1 c_D^0\delta m_{BG}^{l,m}) i_l(r\sqrt{\omega_{l,m}/D_3}) Y_{l,m}(\theta,\phi) e^{\omega_{l,m}t}}{D_3\partial_r i_l(r\sqrt{\omega_{l,m}/D_3})\big|_{r=R} + (\beta_1 m_{BG}^0+\beta_2) i_l(R\sqrt{\omega_{l,m}/D_3})}\,, &(3.38)\\
\delta c_B(t,r,\theta,\phi) &= \sum_{l=0}^{\infty}\sum_{m=-l}^{l} \frac{(-\gamma_1 c_B^0\delta m_T^{l,m} + \gamma_2\delta m_B^{l,m}) i_l(r\sqrt{\omega_{l,m}/D_3}) Y_{l,m}(\theta,\phi) e^{\omega_{l,m}t}}{D_3\partial_r i_l(r\sqrt{\omega_{l,m}/D_3})\big|_{r=R} + \gamma_1 m_T^0 i_l(R\sqrt{\omega_{l,m}/D_3})}\,, &(3.39)\\
\delta c_G(t,r,\theta,\phi) &= \sum_{l=0}^{\infty}\sum_{m=-l}^{l} \frac{(-\delta_1 c_G^0\delta m_B^{l,m} + \delta_2\delta m_{BG}^{l,m}) i_l(r\sqrt{\omega_{l,m}/D_3}) Y_{l,m}(\theta,\phi) e^{\omega_{l,m}t}}{D_3\partial_r i_l(r\sqrt{\omega_{l,m}/D_3})\big|_{r=R} + \delta_1 m_B^0 i_l(R\sqrt{\omega_{l,m}/D_3})}\,. &(3.40)
\end{aligned}$$

These expressions together with (3.32) now allow us to reduce the linearized set of reaction-diffusion equations (3.21)-(3.30) to four equations with four independent variables $\delta m_x^{l,m}$. After introducing the abbreviations

$$\begin{aligned}
A(\omega_{l,m}) &= \frac{1}{D_3\partial_r i_l(r\sqrt{\omega_{l,m}/D_3})\big|_{r=R}/i_l(R\sqrt{\omega_{l,m}/D_3}) + \beta_1 m_{BG}^0 + \beta_2}\,, &(3.41)\\
B(\omega_{l,m}) &= \frac{1}{D_3\partial_r i_l(r\sqrt{\omega_{l,m}/D_3})\big|_{r=R}/i_l(R\sqrt{\omega_{l,m}/D_3}) + \gamma_1 m_T^0}\,, &(3.42)\\
C(\omega_{l,m}) &= \frac{1}{D_3\partial_r i_l(r\sqrt{\omega_{l,m}/D_3})\big|_{r=R}/i_l(R\sqrt{\omega_{l,m}/D_3}) + \delta_1 m_B^0} &(3.43)
\end{aligned}$$

we combine all results and arrive at

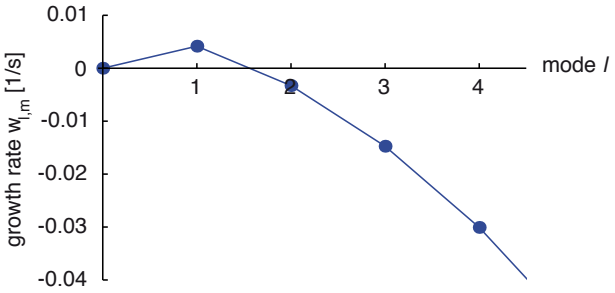

Figure 3.12: Dispersion relation for control cells. Plot of the growth rate $w_{l,m}$ determined from the linear stability analysis using control cell parameters for different modes l. The first mode corresponds to a growing single cluster whereas the higher modes decay.

$$
\begin{aligned}
0 &= [-D_2 l(l+1)/R^2 - \alpha_3 - \omega_{l,m}]\delta m_T^{l,m} + [\alpha_1 m_{BG}^0 + \alpha_2 + \beta_1 m_{BG}^0 \beta_3 A(\omega_{l,m})]\delta m_D^{l,m} \\
&\quad + \{\alpha_1 m_D^0 + \beta_1 c_D^0 [1 - \beta_1 m_{BG}^0 A(\omega_{l,m})]\}\delta m_{BG}^{l,m}, \qquad (3.44) \\
0 &= \alpha_3 m_T^{l,m} + \{-D_2 l(l+1)/R^2 - \alpha_1 m_{BG}^0 - \alpha_2 - \beta_3 [1 - \beta_2 A(\omega_{l,m})] - \omega_{l,m}\}\delta m_D^{l,m} \\
&\quad + [-\alpha_1 m_D^0 - \beta_2 \beta_1 c_D^0 A(\omega_{l,m})]\delta m_{BG}^{l,m}, \qquad (3.45) \\
0 &= \gamma_1 c_B^0 [1 - \gamma_1 m_T^0 B(\omega_{l,m})]\delta m_T^{l,m} + \{-D_2 l(l+1)/R^2 - \gamma_2 [1 - \gamma_1 m_T^0 B(\omega_{l,m})] \\
&\quad - \delta_1 c_G^0 [1 - \delta_1 m_B^0 C(\omega_{l,m})] - \omega_{l,m}\}\delta m_B^{l,m} + \delta_2 [1 - \delta_1 m_B^0 C(\omega_{l,m})]\delta m_{BG}^{l,m}, \qquad (3.46) \\
0 &= \delta_1 c_G^0 [1 - \delta_1 m_B^0 C(\omega_{l,m})]\delta m_B^{l,m} \\
&\quad + \{-D_2 l(l+1)/R^2 - \delta_2 [1 - \delta_1 m_B^0 C(\omega_{l,m})] - \omega_{l,m}\}\delta m_{BG}^{l,m} \qquad (3.47)
\end{aligned}
$$

for each mode l, m. The rates $\omega_{l,m}$ of nontrivial solutions can be found by setting the determinant of the coefficient matrix of this set of equations equal to zero. The growth rates $w_{l,m}$ we are interested in are the maximum real part of all possible $\omega_{l,m}$ for a certain mode l, m and were calculated using Mathematica 8. Note that $w_{l,m}$ and $\omega_{l,m}$ only depend on l. In general, random perturbations will be made of a superposition of all possible modes. Under physiological conditions only the first modes $1, m$ have a positive growth rate and the initial shape of emerging wild-type clusters is predicted to be a superposition of the first real spherical harmonics (Fig. 3.12). The wild-type parameters are given in section 3.4.1.

3.4.5 Robustness of the polarization dynamics

Next we asked whether the direct evolution of initial perturbations towards a single cluster is a robust property of polarization. We varied each model parameter separately and found that only for large changes of some parameters the linear stability analysis predicts higher modes ($l = 2, 3, 4, \dots$) to have the largest growth rate. The changes from the wild-type values needed to induce this behavior are 16x for N_{24}, 46x for N_B, 0.031x for D_2, and 86x for δ_1.

However, given that also higher modes have a positive growth rate it is possible that a perturbation reaches a size where nonlinear effects become important before a single mode

dominates its shape. This is the case if the initial perturbation is too large for the given differences of growth rates. To address this issue we numerically simulated the full polarization dynamics starting with different realizations of the perturbation function f(x,y,z) defined in section 3.4.3. We found that the initial small perturbations still directly evolved into a single cluster as we varied each model parameter separately from 1/3 to 3 times its wild-type value.

3.4.6 Experimental procedures

Strain constructions and growth conditions

Techniques for yeast cell culture and genetics were performed as described previously [133]. All yeast strains are described in section 3.4.7. The genotypes of the yeast strains are as follows: MATa cln1::HisG cln2Δ cln3::HisG YipLac204-MET-CLN2::TRP1 ura3 his3-11.15 ade2-1 can1-100 (gift from M. Peter). For the polarization assay logarithmically growing triple cln cells (in SC-Methionine and 2% glucose medium) were arrested in G1 by growth for 4h in SC-all medium supplemented with 3mM Methionine. LatB was added at 400μM with release. For time-lapse microscopy cells were transferred to glass bottom dishes (Mat Tek) 1h prior to G1 release.

Plasmid constructions and genomic tagging

pRS 306 was used for N-terminal plasmid construction (section 3.4.8). All primers used within this study are listed in section 3.4.9.

Microscopy and Imaging

Coverslips or glass bottom dishes were coated with 5μl 2mg/ml ConA (Sigma) prior to sample observation. Raw images were used for quantifications and analyses. Depicted images were background-subtracted and light- and contrast-optimized for better visualization. Single pictures of cells were taken on a Zeiss Imager A1 upright microscope system with an Olympus 1.3NA 100x Objective Lense, an X-Cite Halogen lamp from Visitron Systems, and an AndoriXON EM CCD Camera. Images were acquired with Metamorph 7.O software. Time lapse movies of Bem1-GFP were acquired on a custom TIRF setup from Till photonics based on a fully automated iMic-stand with 1.45 NA 100x objective from Olympus. The 488 nm (Coherent Saphire) laser was directed through an AOTF and directly coupled into the iMic. A galvanometer driven 2-axis scan head was used to adjust the TIRF angle and an additional galvanometer was used to switch between regular fluorescence and TIRF mode. Images were collected with a cooled AndoriXON DU-897 EM CCD camera. Acquisition was controlled by the Live-Acquisition software package. Oblique illumination [128] was used for time lapse microscopy. Acquisition of Bem1-GFP+LatB cells was taken with 60ms exposure, 60s frame rate and 60% laser power and maximum projection of 3 z-stacks, increment 0.4μm. Cells expressing GFP-Cdc42 were arrested, released and latrunculin treated in an ONIX (cellASIC) microfluidics device. Acquisition of GFP-Cdc42-GFP+LatB cells was taken with 30ms exposure, 30s frame rate, 40% laser power, and maximum projection of 3 z-stacks, increment 0.2μm.

Experimental cap width determination

Microscopy images of the cell equator (with cap located on the equator) were used to determine cap expansions. A line scan was manually drawn along the cell membrane (including the cap). For automatic analysis of the caps used for Figs. 3.5C, 3.11A,B the raw images were processed with a Gaussian blur with a 3x3 matrix to mimic average intensities along the line scan. Intensities along the line scan were retrieved for each position on the cell membrane. A Gaussian was then fitted on the intensities and the cap width was determined as the full width at half maximum.

3.4.7 Yeast strains

Strain	Genotype*	Source/Reference
RWS116	MATa cln1::HisG cln2Δ cln3::HisG YipLac204-MET-CLN2::TRP1 ura3 his3-11.15 ade2-1 can1-100	Gulli et al., 2000
RWS1028	Δbem2::G418	Freisinger et al.
RWS1035	Δbem2::G418 pCDC42-myc-GFP-CDC42::URA3 (RWC108)	Freisinger et al.
RWS1421	pCDC42-myc-GFP-CDC42::URA3 (RWC108)	Freisinger et al.
RWS1045	pBem1-Bem1-GFP::URA3 (RWC138)	This study

*all strains were made in RWS 116 background

3.4.8 Plasmids

Plasmid	Origin	Description	Source/Reference
RWC108	pRS306	GFP-CDC42 under the control of the endogenous CDC42-promoter in a pRS306 backbone for integration into the URA3 locus after linearization	Wedlich et al. 2004
RWC138	pRS306	Bem1-GFP under the control of the endogenous Bem1-promoter in a pRS306 backbone for integration into the URA3 locus after linearization	Gift from Mathias Peter

3.4.9 Primers

Primer	Sequence 5'→3'
RWS347	AGGCAAGAGATCAGGCGGAAAGA
RWS346	AGAAGCAAGCTACGTTGCAGCCA
RWS885	CAGGTTTCATTGGAGGTGC
RWS265	GGTGCTCAACAATTCAGTTCT
RWS352	TGCACCAACATACCGTTTTGC
RWS351	TGATGGTAAATCCCGTCCTGC
RWS48	GTATTCTGGGCCTCCATG
RWS47	GATACTAACGCCGCCATC

4 Minimal mass-conserving model of cell polarity

4.1 Introduction

Cell polarization is a fundamental developmental process that defines symmetry axes or selects directions of growth. Signaling molecules accumulate in a restricted region of the inner site of a cell's plasma membrane where they initiate further developmental processes. For example, the polarized signaling molecule Cdc42 in the yeast *Saccharomyces cerevisiae* guides the reorganization of cytoskeletal structures resulting in directed transport of further proteins to the prospective construction site [135]. Similarly, cell polarity also plays an important role in stem cell division [123] or plant growth processes such as pollen tube or root hair development [134, 136]. Theoretical approaches to describe cell polarity often rely on reaction-diffusion dynamics [119]. Mass conserved models of this kind have been introduced in order to describe the formation of a unique polarization site via coalescence of multiple growing polarity clusters due to competition for limited amounts of proteins [107, 72].

Here we develop a minimal conceptual model of cell polarity including only its central features. Still it shows the phenomenological complexity of more detailed models. The simplicity of our approach allows a thorough theoretical analysis revealing basic principles of the polarization dynamics.

4.2 Results

We consider cell polarity to rely on nonlinear protein dynamics in a finite system which consists of a spherical cytosolic volume and a surrounding plasma membrane. Proteins can diffuse in both compartments and exchange between cytosol and membrane. As the simplest case we include only a single protein species and enforce mass conservation as particle production and decay occur on time scales much larger than the protein dynamics.

The set of partial differential equations describing the time evolution of this system reads in spherical coordinates r, θ, ϕ

$$\partial_t M = f(M,C)|_{r=R} + D_2 \Delta_{\theta,\phi} M \,, \tag{4.1}$$

$$\partial_t C = D_3 \Delta C \,. \tag{4.2}$$

Here M and C account for the membrane and cytosol concentration, respectively, whereas R denotes the cell radius. The function $f(M,C)|_{r=R}$ describes the sum of reactions for cytosol membrane exchange, D_2 and D_3 are diffusion constants, and $\Delta_{\theta,\phi}$ is the angular part of the Laplace operator Δ in spherical coordinates. The diffusive flux between cytosol and membrane is facilitated by the boundary condition

$$D_3\partial_r C|_{r=R} = -f(M,C)|_{r=R} \tag{4.3}$$

which also enforces the particle conservation $\int dVC + \int dAM = N$. Here A and V denote surface area and volume of the cell.

To elucidate which conditions allow spontaneous cell polarization we apply a linear stability analysis and extend a previously developed approach for systems with membrane-cytosol coupling [116] to describe spherical geometries and nonlinear membrane attachment. Using this analysis we calculate the time evolution of a small perturbation δM, δC of a stable homogeneous fix point M_0, C_0. We expand Eqs. (4.1)-(4.3) around M_0, C_0 and neglect terms which are nonlinear with respect to δM, δC. We arrive at

$$\begin{aligned}
\partial_t \delta M &= \alpha_M \delta M + \alpha_C \delta C\big|_{r=R} + D_2 \Delta_{\theta,\phi}\delta M\,, && (4.4)\\
\partial_t \delta C &= D_3 \Delta \delta C\,, && (4.5)\\
D_3 \partial_r \delta C\big|_{r=R} &= -\alpha_M \delta M - \alpha_C \delta C\big|_{r=R} && (4.6)
\end{aligned}$$

with the Jacobi coefficients $\alpha_M = \partial_M f(M,C_0)|_{M=M_0}$ and $\alpha_C = \partial_C f(M_0,C)|_{C=C_0}$. Eqs. (4.4) and (4.5) can be solved using the ansatz

$$\delta M(t,\theta,\phi) = \sum_{l=0}^{\infty}\sum_{m=-l}^{l} \delta m^{l,m} Y_{l,m}(\theta,\phi) e^{\omega_{l,m} t}, \tag{4.7}$$

$$\delta C(r,\theta,\phi,t) = \sum_{l=0}^{\infty}\sum_{m=-l}^{l} \delta c^{l,m} i_l(r\sqrt{\omega_{l,m}/D_3}) Y_{l,m}(\theta,\phi) e^{\omega_{l,m} t} \tag{4.8}$$

where $Y_{l,m}(\theta,\phi)$ and $i_l(x)$ denote real spherical harmonics [131] and modified spherical Bessel functions of the first kind [130], respectively. Using the Eqs. (4.6)–(4.8) we reexpress the cytosolic expansion coefficients $\delta c^{l,m}$ in terms of the membrane expansion coefficients $\delta m^{l,m}$. This relation together with Eqs. (4.7) and (4.8) allows us to reduce Eq. (4.4) to an equation for the membrane perturbation coefficients $\delta m^{l,m}$ which has nonzero solutions only if the growth rates satisfy

$$\omega_{l,m} = -\frac{D_2 l(l+1)}{R^2} + \frac{\alpha_M D_3 \partial_r i_l(r\sqrt{\omega_{l,m}/D_3})\big|_{r=R} / i_l(R\sqrt{\omega_{l,m}/D_3})}{D_3 \partial_r i_l(r\sqrt{\omega_{l,m}/D_3})\big|_{r=R} / i_l(R\sqrt{\omega_{l,m}/D_3}) + \alpha_C}\,. \tag{4.9}$$

In the following we limit our study to a reasonable range of parameters to simplify our calculations. In budding yeast it was shown that polarization occurs on a time scale of several minutes and that the emerging polarity clusters do not oscillate along the cell membrane indicating that the imaginary part of the growth rate is negligible ([65, 66], Fig. 3.6). The cytosolic diffusion constant in yeast is typically of the order of $10\mu m^2/s$ [29] and its cell radius is about $5\mu m$ [65]. Hence, we can assume that perturbations grow with a real growth rate much smaller than the rate at which cytosolic proteins diffuse through the whole cell, i.d.

$$\max_{l,m}[\omega_{l,m}] \ll D_3/R^2\,. \tag{4.10}$$

In this limit we can simplify (4.9) further. We use the series representation of the modified spherical Bessel function [130] to derive an approximate expression for $[\partial_x i_l(x)]/i_l(x)$ in the limit $|x|\ll 1$. This allows us to approximate the growth rates (4.9) in the limit $|\omega_{l,m}|\ll D_3/R^2$. To leading order we get the dispersion relation

$$\omega_{l,m} = -\frac{D_2 l(l+1)}{R^2} + \frac{\alpha_M l D_3/R}{l D_3/R + \alpha_C}\,,\; l>0 \tag{4.11}$$

whereas particle number conserving perturbations with $l{=}0$ have a growth rate of $\omega_{0,0}{=}\alpha_M{-}3\alpha_C/R$. The latter rate corresponds to spatially homogeneous perturbations where growth of the membrane concentration is accompanied by a corresponding depletion of the cytosolic pool. Hence, the homogeneous fix point M_0, C_0 is stable to particle number conserving homogeneous perturbations if

$$\alpha_M - 3\alpha_C/R < 0\,. \tag{4.12}$$

Remarkably, the linear stability of the homogeneous fix points depends on the geometry of the cell via cell radius R. In the following we assume that (4.12) holds for the fix point under consideration.

Using dispersion relation (4.11) we determine the conditions which allow pattern formation from a uniform inital state. We focus our analysis on the growth rate of the first modes $1, m$ as Eq. (4.11) is a concave function with respect to l and changes sign at $l{=}0$. This implies that unpolarized states are stable to spatial perturbations if the rate $\omega_{1,m}$ remains positive, i.d.

$$0 < -\frac{2D_2}{R^2} + \frac{\alpha_M D_3/R}{D_3/R + \alpha_C}\,. \tag{4.13}$$

For positive Jacobi coefficients we reexpress Eq. (4.13) in terms of characteristic 'diffusion' lengths [114]. The length $l_M{=}\sqrt{D_2/\alpha_M}$ can be interpreted as the average distance travelled by particles along the membrane which diffuse with diffusion constant D_2 and detach with rate α_M. The average time needed for proteins to reattach to the membrane with rate α_C after detachment is given by R/α_C [125]. Therefore, the length $l_C{=}\sqrt{D_3 R/\alpha_C}$ corresponds

to the average distance travelled by particles in the cytosol between detachment from and rebinding to the membrane.

Using these definitions we arrive at the linear instability condition

$$\frac{l_M^2}{R^2} < \frac{l_C^2/R^2}{2(l_C^2/R^2+1)}\,. \tag{4.14}$$

For the limiting cases $l_C \gg R$ and $l_C \ll R$ we get the finite size condition $l_M^2 < R^2/2$ and the Turing-like condition $l_M^2 < l_C^2/2$, respectively. Hence, the membrane diffusion length has to be smaller than the cell size and the cytosolic diffusion length. Both instability conditions depend on the geometry of the system via radius R.

To study the full polarization dynamics we exemplarily choose the reaction function

$$f(M,C)\big|_{r=R} = aM^2C\big|_{r=R} - bM\,. \tag{4.15}$$

Membrane species M enhances its own attachment from the cytosol with rate a and detaches back to the cytosol with rate b. For this specific model we find one stable homogenous fix point with $M_0=0$ and a second one with $M_0>0$ if $AM_0 \geq VC_0$. This condition obtained from Eq. (4.12) implies that pattern formation can be switched off by a decrease of the protein membrane fraction below a critical threshold. The Jacobi coefficients for this fix point are $\alpha_M=b$, $\alpha_C=aM_0^2$. Hence, the lengths $l_M=\sqrt{D_2/b}$ and $l_C=\sqrt{D_3R/aM_0^2}$ directly correspond to the average distance a particle diffuses on the membrane before it moves to the cytosol and vice versa.

To numerically obtain the full polarization dynamics we use Comsol Multiphysics 3.5a and start our simulations from the unpolarized state M_0, C_0 plus a random initial perturbation. To this end we select a random number from the interval $[-1,1]$ for each site of a spatial cubic lattice with spacing $1\mu m$ and used Comsol's interpolation routine to define a continuous function $f(x,y,z)$ from this lattice. The perturbations are then implemented by adding the term $kf(x,y,z)M_0$ to the membrane concentration M_0 where prefactor k denotes the relative perturbation amplitude.

By comparing the protein dynamics of our simulations for different parameters we identify two qualitatively different kinds of polarization dynamics. If the simulations are started with strong random initial perturbations, (k=1), we observe the transient formation of several macroscopic clusters on the membrane which then merge into a single final one (Fig. 4.1A,B). Macroscopic clusters are defined as having a peak intensity over background much larger than M_0. The formation of multiple transient clusters is found to be independent of the dispersion relation obtained from the linear analysis as the initial perturbation is too large (Fig. 4.1E). The protein dynamics in these cases enter the nonlinear regime with several local density maxima on the membrane that are determined by the random initial conditions. These clusters then start to attract proteins from their environment and subsequently compete for limited amounts of proteins till only a unique cluster remains similar to previous mass conserved polarity models [107, 72]. If instead the perturbation amplitude is chosen to a much smaller value (k=10^{-7}) we observe that the number of emerging clusters depends on the

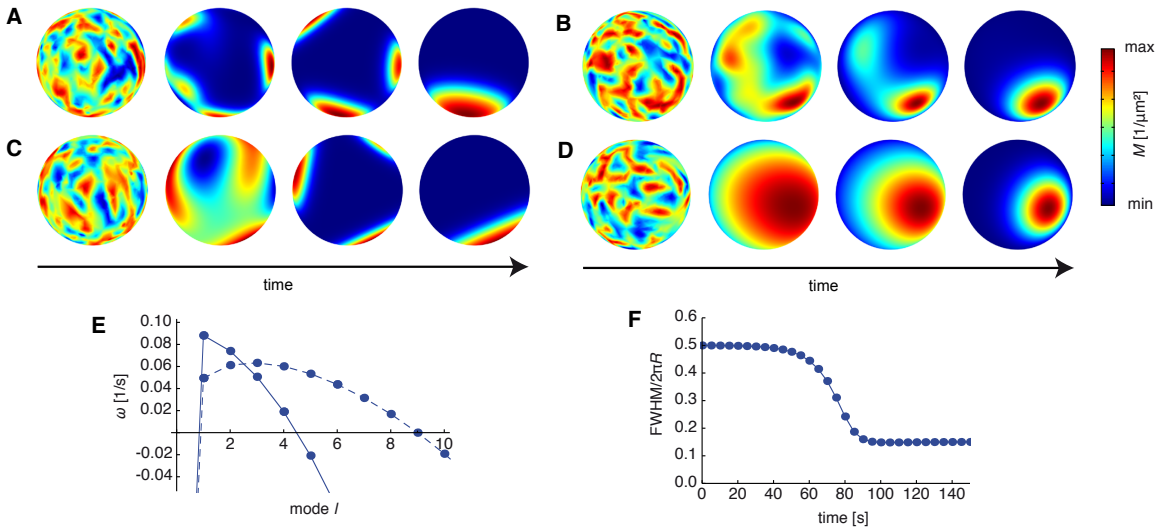

Figure 4.1: Polarization dynamics for changing parameters and initial conditions. A-D Snapshots of the time evolution of membrane species M of model (4.15) with perturbation amplitude k=1 (A,B) and k=10^{-7} (C,D). The dispersion relation for each simulation is shown in E. The first image in each time series shows the initial perturbation. **E** Dispersion relation from Eq. (4.9) for cells in (A,C) (dashed line, l_M=$R/10$, l_C=R) and in (B,D) (solid line, l_M=$R/5$, l_C=$5R$). Approximation (4.11) shows almost perfect agreement. The common model parameters used are N=10^3, R=$5\mu m$, a=$0.115\mu m^5/s$, and b=$0.1/s$. The diffusion constants are set to D_2=$0.025\mu m^2/s$, D_3=$3.99\mu m^2/s$ for the cells in (A,C) and D_2=$0.1\mu m^2/s$, D_3=$99.6\mu m^2/s$ for the cells in (B,D). **F** Numerically obtained evolution of full width at half maximum (FWHM) of an emerging polarity cluster with parameters as used in (D) but instead with a real spherical harmonics with l=1 as initial perturbation.

dispersion relation. A single cluster emerges only directly if the first mode l=1 is selected to be the fastest growing mode (Fig. 4.1D) whereas in other cases several transient macroscopic clusters still develop (Fig. 4.1C). Hence, we conclude that a single cluster can only arise directly if the initial random perturbations successfully evolve into a single cluster before reaching a macroscopic size where nonlinear effects dominate the dynamics.

The dynamics of directly emerging clusters can be divided into two parts. First, a broad faint cluster grows exponentially whose pattern is dominated by a superposition of the first real spherical harmonics. As this cluster reaches a macroscopic size it starts to narrow and finally reaches a more localized protein cluster with a shape depending on the details of the model (Fig. 4.1F). These dynamics are generic for all directly arising unique clusters as only the extent of the narrowing depends on the specific model whereas the initial shape remains unchanged.

To determine in which situations a single cluster emerges directly we compare the growth rates for different modes l. In general, the dominant mode is expected to be the mode with the largest real part as the linear stability analysis predicts that this mode exponentially outgrows all other modes. We make use of the concavity of the growth rates (4.11) with respect to l and considered the difference between the first and second modes. The first modes $1, m$ will be the fastest growing modes if $\Delta\omega$=$\omega_{2,m}$−$\omega_{1,m}$<0, i.d.

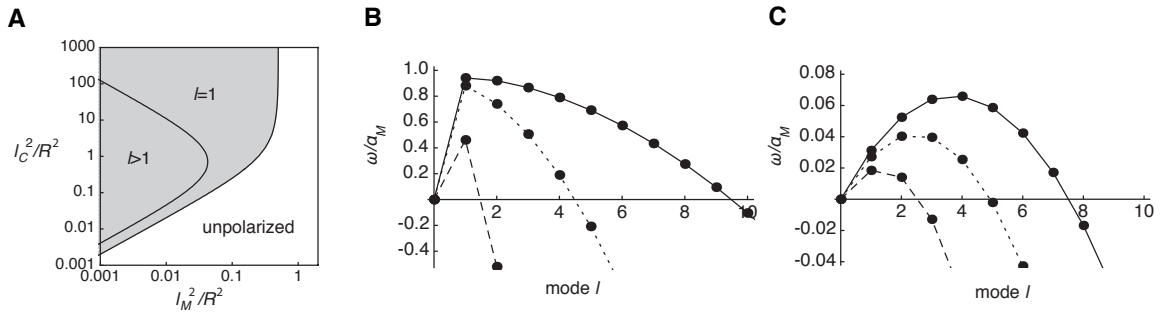

Figure 4.2: Polarization efficiency and dispersion relations. **A** Linear instability from Eq. (4.14) (gray region) and fastest growing modes l obtained from Eq. (4.16) as indicated for different diffusion lengths l_M, l_C. **B** Dispersion relation from Eq. (4.11) for l_c=5R and l_M=R/10 (solid line), l_M=R/5 (dotted line), and l_M=R/2 (dashed line). **C** As in (B) for l_c=R/5 and l_M=3R/50 (solid line), l_M=3R/40 (dotted line), and l_M=R/10 (dashed line). The growth rates $\omega_{0,0}$ in (B,C) need to be nonpositive and are chosen to zero for convenience.

$$\frac{l_M^2}{R^2} > \frac{l_C^2/R^2}{4(2l_C^2/R^2+1)(l_C^2/R^2+1)}\,. \tag{4.16}$$

By combining Eqs. (4.16) and (4.14) we get a condition for pattern formation with the first mode being the fast growing mode,

$$\frac{l_C^2/R^2}{4(2l_C^2/R^2+1)(l_C^2/R^2+1)} < \frac{l_M^2}{R^2} < \frac{l_C^2/R^2}{2(l_C^2/R^2+1)} \tag{4.17}$$

as shown in Fig. 4.2A in comparison to the instability condition (4.14).

It is instructive to consider the two limiting cases $l_C \ll R$ and $l_C \gg R$. For $l_C \ll R$ condition (4.17) reduces to

$$\frac{l_C^2}{4} < l_M^2 < \frac{l_C^2}{2}\,. \tag{4.18}$$

Only a narrow parameter regime with approximately equal diffusion lengths exists in this limit where pattern formation is possible and where the first mode grows fastest. In contrast, for $l_C \gg R$ we got

$$\frac{R^2}{8l_C^2} < \frac{l_M^2}{R^2} < \frac{1}{2}\,. \tag{4.19}$$

The membrane diffusion length l_M can take very small values as long as this change is compensated by an appropriate choice of l_C. Examples for the two different regimes $l_C \ll R$ and $l_C \gg R$ are shown in Figs. 4.2B,C. In the limit $l_C \gg R$ the maximum of the dispersion relation

remains at l=1 over a large range of different l_M (Fig. 4.2B). In contrast, for $l_C \gg R$ the dispersion relation has a parabola-like shape and its maximum is found at a higher mode l for most values of l_M (Fig. 4.2C). Hence, Eq. (4.17) provides a necessary condition for direct emergence of unique polarity cluster which is robustly satisfied for $l_C \gg R$. Our findings imply that the qualitative polarization dynamics can be switched between both alternatives by a change of the cellular protein number N as the diffusion lengths in general depend on the fix point concentrations M_0, C_0. For example, an increase of the protein number in our model of Eq. (4.15) reduces the diffusion length l_C and might therefore by virtue of Eq. (4.16) induce a change from direct unique cluster formation towards coalescence dynamics.

4.3 Discussion

In summary, we identified the following qualitative properties of our minimal model of cell polarity. Two qualitatively different polarization dynamics exist depending on the choice of diffusion lengths. Cells can either polarize via coalescence of multiple growing clusters [107, 72] or through direct formation of a single polarization site. The latter process can be robustly facilitated for cytosolic diffusion lengths much larger than the cell size and is accompanied by generic narrowing dynamics of the cluster. In addition, we found that variation of the protein number can induce a change between both kinds of polarization dynamics.

Given that our model takes into account the key features of cell polarity we expect our results to qualitatively apply to reaction-diffusion driven polarity systems in general. Consistently, narrowing dynamics have indeed been observed experimentally in polarizing yeast cells (Figs. 3.5, 3.6; [66]). In addition, the occasional occurrence of multiple transient clusters was increased artificially by overexpression of the polarity proteins Cdc42, Bem1, and Cdc24 [66, 49]. These proteins have been shown to polarize and to be involved in the generation of a positive feedback loop that enhances their accumulation on the plasma membrane [41, 42, 16, 38]. Our findings suggest that these observations may arise from a reaction-diffusion driven polarization mechanism even though the molecular details remain controversial [48].

5 Summary and Outlook

This work focuses on the mechanisms of cell polarization in the budding yeast *Saccharomyces cerevisiae* as an example of biological pattern formation in microscopic systems. Cell polarization is a fundamental cellular process that defines an orientation within cells and is a prerequisite for developmental processes such as cell proliferation or differentiation. Malfunction of polarization can result in severe or even lethal consequences for the organism and it is therefore crucial that polarization functions reliably even in the presence of particle fluctuations or changing environmental conditions.

Two independent polarization pathways have been proposed to concentrate polarity GTPase Cdc42 on the plasma membrane in yeast. One was thought to depend on directed transport of Cdc42 along actin filaments [60] whereas the second one was proposed to rely on recycling of Cdc42 through the cytosol by binding to GDP dissociation inhibitor (GDI) Rdi1 [29]. However, the details or even existence of these pathways remained controversial [48, 62]. Previous work showed that certain mutations in yeast induce formation of several stable polarization sites in contrast to wild-type cells which always form a unique polarity cluster [22, 17, 35]. The origin of this behavior remained elusive given that a deeper mechanistic understanding of the underlying processes was missing.

In this manuscript we aimed to identify the mechanisms which drive stable formation of a unique polarization site in yeast. First, we tested different previously proposed polarization mechanisms. We tested experimentally whether polarization is lost at higher Cdc42 expression as predicted by a stochastic polarization model [73]. In addition, we derived and tested a prediction for the fluorescence recovery after photobleaching (FRAP) of GFP-tagged guanine nucleotide exchange factor (GEF) Cdc24 in polarity clusters based on a proposed Turing-type model [72]. However, our experimental findings could not verify these predictions arguing against a dominant role of these models in polarity establishment.

To gain a deeper understanding of yeast cell polarity we used a combined experimental and theoretical approach to derive a minimal stochastic model of the two polarization pathways. Actin-independent polarization through cytosolic transport of Cdc42 by GDI Rdi1 is based on reaction-diffusion dynamics with two positive feedback loops of active Cdc42 enhancing membrane attachment and activation of further Cdc42. For actin-dependent polarization we used a coarse-grained description and assumed that establishment of stable actin filament bundles on the membrane occurs instantaneously. This establishment is induced by active Cdc42 and leads to directed transport of Cdc42 towards the actin bundles on the membrane.

In agreement with our experiments GDI-mediated polarization reliably forms a single stable cluster characteristic for mass conserved polarity models due to competition for a limited amount of proteins [107, 72]. The actin-dependent part of the model is prone to occasional formation of more than one stable cluster as there is always the possibility that two actin

bundles are established at distant sites on the plasma membrane. The risk of forming distant polarization sites can be increased by a higher probability for actin bundle nucleation as it provides the polarization site which is established first with less time to redistribute Cdc42 on the membrane and therefore reduces the probability to nucleate the second actin bundle in close vicinity to the first one. This model prediction is consistent with our experimental finding that ΔRdi1 cells exhibit a higher probability to form multiple stable clusters if Cdc42 activity is increased at the onset of polarization.

Combination of both polarization pathways in our model successfully results in wild-type behavior as the formation of multiple stable clusters is suppressed. The model predicted that reduced Cdc42 deactivation in wild-type cells causes reduced Cdc42 exchange between cluster and remaining cellular compartments as well as the occurrence of multiple stable clusters. These predictions were verified experimentally. Reduced Cdc42 deactivation by deletion of GTPase-activating protein (GAP) Bem2 in wild-type cells leads to slower FRAP of GFP-tagged Cdc42 in polarity clusters and occasional emergence of stable multiple clusters. Using our model these observations are explained by the lower fraction of Cdc42 which is extracted by GDI Rdi1 and the reduced or lost ability of GDI-mediated polarization to polarize active Cdc42 before the actin bundles are established.

Hence, our results provide evidence that stable actin structures can be established under control of active Cdc42 which then guide directed transport of Cdc42. Successful coordination of both polarization pathways is necessary to achieve a single polarization site as needed for unique budding and proliferation. Indeed, our experiments indicate that multiple stable polarization sites lead to cell division defects as the probability of mis-segregated nuclei increases with the number of double buds.

A previous model of GDI-mediated polarization predicted that several transient clusters arise that then merge into a single cluster due to competition for limited amounts of proteins [72]. However, multiple transient caps could only be detected in a small subpopulation of wild-type cells so far and it has not been clarified whether these caps rather rely on actin than the GDI-mediated pathway [66, 49]. In addition, the role of the cell cycle in polarity regulation remained incompletely understood.

The coexistence of the two independent polarization pathways and the unclear polarization dynamics prompted us to investigate the fundamental features of GDI-mediated polarization and to develop a more detailed mechanistic model for this polarization pathway. The model relies on deterministic reaction-diffusion dynamics and explicitly incorporates the polarity regulators Cdc42, Cdc24 and Cdc42 effector Bem1 as well as the accurate geometry of the cell.

Our model provides a unified understanding of many known mutant phenotypes and predicts further phenotypes which we verified experimentally. It robustly yields the direct emergence of a unique polarization site and predicts this feature to be accompanied by characteristic narrowing dynamics. The latter is confirmed experimentally providing further evidence for GDI-mediated polarization being driven by deterministic reaction-diffusion dynamics. Hence, the GDI-mediated polarization mechanism itself does not actively form multiple clusters but, in contrast, acts to suppress them and therefore reduces the risk of misguided Cdc42 signaling in wild-type cells. In addition, the observed narrowing dynamics argue against a previously

proposed phase separation model predicting polarization to start with small germs which expand and coalesce on the membrane [74].

Furthermore, we have shown that enhancement of the positive feedback loops of Cdc42 membrane attachment and activation is the key mechanism that initiates polarization. Its characteristic feature is a switch-like direct change from an unpolarized state to a highly localized polarization site. The mechanism of this switch lies in the success or failure of the positive feedback loops to self-enhance, and is not related to the ability to counteract lateral membrane diffusion. In addition, the switch to the polarized state is accompanied by a strong increase of activated Cdc42 levels.

Both release of the GEF Cdc24 from the nucleus and reduction of Cdc42 hydrolysis by phosphorylation of GAPs have been shown to contribute to activation of Cdc42 and subsequent polarity establishment [33, 34, 35]. Our results provide strong evidence that these changes are used for temporal control of GDI-mediated cell polarity as both parameter changes can induce polarization by enhancement of the positive feedback loops. Hence, our findings provide a mechanistic understanding of how polarity establishment in yeast is regulated by the cell cycle. Using this regulation yeast cells acquire the ability to initiate Cdc42 signaling in a controlled switch-like manner in a spatially confined region of the plasma membrane.

Our model also predicted that polarity clusters would broaden if the Cdc42 extraction or hydrolysis rates were reduced. Consistently, we found that deletion of the GAP Bem2 led to significant broader clusters in latrunculin-treated cells indicating that the GDI-mediated polarization is indeed optimized to robustly provide a narrow final cluster.

Hence, GDI-mediated polarization is accompanied by a significant fold change in active Cdc42 amounts and directly produces a single cluster and not several intermediate clusters which then coalesce into a single one. In addition, cell cycle induced changes in Cdc42 activation directly lead to the robust formation of a narrow final cluster with only very small changes in Cdc24 concentrations or hydrolysis rates. Our results indicate that all these aspects are simultaneously optimized under physiological conditions in order to provide controlled Cdc42 signaling with a minimized risk of accidentally initiating further processes downstream of Cdc42 at the wrong time or position.

To gain a more qualitative understanding of the polarization dynamics of our mechanistic model in comparison to previous models [72, 73, 74] we developed a minimal conceptual model of cell polarity including only its central features. We assumed that cell polarity is facilitated by deterministic mass conserved protein dynamics in a spherical cell consisting of a cytosolic volume surrounded by a plasma membrane. A single protein species was allowed to diffuse in both compartments and to exchange between both.

We identified two qualitatively different polarization dynamics depending on the choice of diffusion lengths. Cells can either polarize via coalescence of multiple growing clusters [107, 72] or through direct formation of a single polarization site. The latter process can robustly be facilitated for cytosolic diffusion lengths much larger than the cell size and is accompanied by generic narrowing of the emerging cluster as found for our mechanistic model of yeast polarization. In addition, we found that variation of the protein number can induce a change between both kinds of polarization dynamics. This change is consistent with experiments which found that the occasional occurrence of multiple transient clusters in polarizing yeast

cells was increased artificially by overexpression of Cdc42, Bem1, and Cdc24 [66, 49]. Our findings suggest that these observations may arise from a deterministic reaction-diffusion mechanism even though the details of yeast polarization remain incompletely understood [48].

In summary, our findings about the disturbed coordination of two polarization pathways provide a mechanistic explanation for cell division defects. Moreover, our results reveal the fundamental design principles that allow GDI-mediated cell polarization to reliably initiate developmental processes at a specific time and place.

Many important aspects of yeast cell polarity remain to be addressed. Promising advances have been made in modeling the details of actin-dependent polarization such as vesicle trafficking [75, 62]. However, these approaches do not provide polarization for measured diffusion constants [28] and make predictions which we could not confirm experimentally indicating that some molecular details are still incompletely understood. Taking into account the explicit membrane composition might help to improve these models as plasma membrane components have been shown to be polarized as well due to directed versicle transport [101]. Furthermore, it would be interesting to identify the molecular mechanisms which can stabilize actin structures to such an extend that double caps do not coalesce on the time scale of budding.

Beyond yeast one might use our findings as testable predictions to identify similar polarity mechanisms in other eukaryotes. For example, deletion of the plant GAP Ren-1 of GTPase ROP1 defocused polarization in *Arabidopsis thaliana* pollen tubes [120] similar to our characteristic finding that reduced hydrolysis of polarity GTPase Cdc42 causes broadening of polarity clusters in yeast.

Several lines of evidence suggest that cell division defects in mammalian cells might arise from an origin similar to that in yeast. A previous study showed that hyperactive Cdc42 induces formation of multiple buds in budding yeast [22] and we found that multiple buds can lead to failed cell division and multi-nucleated cells. In addition, strong overexpression of GEF Cdc24 was shown to result in giant multi-nucleated cells presumably due to cell division defects [32]. Similar to these observations in yeast, hyperactive Cdc42 was shown to cause giant multi-nucleated cells in mouse cell lines [23] suggesting that these phenotypes may arise from similar polarization defects.

Bibliography

[1] http://en.wikipedia.org/wiki/Morphogenesis. Date: 3rd December 2012.

[2] M P Scott and S B Carroll. The segmentation and homeotic gene network in early Drosophila development. *Cell*, 51(5):689–98, Dec 1987.

[3] D M Raskin and P A de Boer. Rapid pole-to-pole oscillation of a protein required for directing division to the middle of Escherichia coli. *Proc Natl Acad Sci USA*, 96(9):4971–6, Apr 1999.

[4] W Driever and C Nüsslein-Volhard. A gradient of bicoid protein in Drosophila embryos. *Cell*, 54(1):83–93, Jul 1988.

[5] W Driever and C Nüsslein-Volhard. The bicoid protein determines position in the Drosophila embryo in a concentration-dependent manner. *Cell*, 54(1):95–104, Jul 1988.

[6] Oliver Grimm, Mathieu Coppey, and Eric Wieschaus. Modelling the Bicoid gradient. *Development*, 137(14):2253–64, Jul 2010.

[7] Oliver Grimm and Eric Wieschaus. The Bicoid gradient is shaped independently of nuclei. *Development*, 137(17):2857–62, Sep 2010.

[8] G Struhl, K Struhl, and P M Macdonald. The gradient morphogen bicoid is a concentration-dependent transcriptional activator. *Cell*, 57(7):1259–73, Jun 1989.

[9] W Driever and C Nüsslein-Volhard. The bicoid protein is a positive regulator of hunchback transcription in the early Drosophila embryo. *Nature*, 337(6203):138–43, Jan 1989.

[10] K A Nasmyth. Molecular genetics of yeast mating type. *Annu Rev Genet*, 16:439–500, Jan 1982.

[11] J E Segall. Polarization of yeast cells in spatial gradients of alpha mating factor. *Proc Natl Acad Sci USA*, 90(18):8332–6, Sep 1993.

[12] A C Butty, P M Pryciak, L S Huang, I Herskowitz, and M Peter. The role of Far1p in linking the heterotrimeric G protein to polarity establishment proteins during yeast mating. *Science (New York, NY)*, 282(5393):1511–6, Nov 1998.

[13] http : //en.wikipedia.org/wiki/Mating_of_yeast. Date: 6th December 2012, Image: Artur Jan Fijałkowski / CC BY-SA 2.5.

[14] Jacob Halatek and Erwin Frey. Highly canalized MinD transfer and MinE sequestration explain the origin of robust MinCDE-protein dynamics. *Cell Rep*, 1(6):741–52, Jun 2012.

[15] J Chant and I Herskowitz. Genetic control of bud site selection in yeast by a set of gene products that constitute a morphogenetic pathway. *Cell*, 65(7):1203–12, Jun 1991.

[16] Javier E Irazoqui, Amy S Gladfelter, and Daniel J Lew. Scaffold-mediated symmetry breaking by Cdc42p. *Nat Cell Biol*, 5(12):1062–70, Dec 2003.

[17] Roland Wedlich-Soldner, Steve Altschuler, Lani Wu, and Rong Li. Spontaneous cell polarization through actomyosin-based delivery of the Cdc42 GTPase. *Science*, 299(5610):1231–5, Feb 2003.

[18] Hay-Oak Park and Erfei Bi. Central roles of small GTPases in the development of cell polarity in yeast and beyond. *Microbiol Mol Biol Rev*, 71(1):48–96, Mar 2007.

[19] D I Johnson and J R Pringle. Molecular characterization of CDC42, a Saccharomyces cerevisiae gene involved in the development of cell polarity. *J Cell Biol*, 111(1):143–52, Jul 1990.

[20] K Shinjo, J G Koland, M J Hart, V Narasimhan, D I Johnson, T Evans, and R A Cerione. Molecular cloning of the gene for the human placental GTP-binding protein Gp (G25K): identification of this GTP-binding protein as the human homolog of the yeast cell-division-cycle protein CDC42. *Proc Natl Acad Sci USA*, 87(24):9853–7, Dec 1990.

[21] The image was provided by Tina Freisinger.

[22] Juliane P Caviston, Serguei E Tcheperegine, and Erfei Bi. Singularity in budding: a role for the evolutionarily conserved small GTPase Cdc42p. *Proc Natl Acad Sci USA*, 99(19):12185–90, Sep 2002.

[23] R Lin, S Bagrodia, R Cerione, and D Manor. A novel Cdc42Hs mutant induces cellular transformation. *Curr Biol*, 7(10):794–7, Oct 1997. t.

[24] Y Zheng, R Cerione, and A Bender. Control of the yeast bud-site assembly GTPase Cdc42. Catalysis of guanine nucleotide exchange by Cdc24 and stimulation of GTPase activity by Bem3. *J Biol Chem*, 269(4):2369–72, Jan 1994.

[25] B J Stevenson, B Ferguson, C De Virgilio, E Bi, J R Pringle, G Ammerer, and G F Sprague. Mutation of RGA1, which encodes a putative GTPase-activating protein for the polarity-establishment protein Cdc42p, activates the pheromone-response pathway in the yeast Saccharomyces cerevisiae. *Genes Dev*, 9(23):2949–63, Dec 1995.

[26] Aron R Marquitz, Jacob C Harrison, Indrani Bose, Trevin R Zyla, John N McMillan, and Daniel J Lew. The Rho-GAP Bem2p plays a GAP-independent role in the morphogenesis checkpoint. *EMBO J*, 21(15):4012–25, Aug 2002.

[27] Gregory R Smith, Scott A Givan, Paul Cullen, and George F Sprague. GTPase-activating proteins for Cdc42. *Eukaryotic Cell*, 1(3):469–80, Jun 2002.

[28] Eugenio Marco, Roland Wedlich-Soldner, Rong Li, Steven J Altschuler, and Lani F Wu. Endocytosis optimizes the dynamic localization of membrane proteins that regulate cortical polarity. *Cell*, 129(2):411–22, Apr 2007.

[29] B Slaughter, A Das, J Schwartz, and B Rubinstein.... Dual modes of Cdc42 recycling fine-tune polarized morphogenesis. *Developmental cell*, Dec 2009.

[30] Jared L Johnson, Jon W Erickson, and Richard A Cerione. New insights into how the Rho guanine nucleotide dissociation inhibitor regulates the interaction of Cdc42 with membranes. *J Biol Chem*, 284(35):23860–71, Aug 2009.

[31] L H Hartwell, J Culotti, J R Pringle, and B J Reid. Genetic control of the cell division cycle in yeast. *Science (New York, NY)*, 183(4120):46–51, Jan 1974.

[32] S Sakaguchi, S Miyamoto, H Iida, T Suzuki, and Y Ohya.... Overproduction of Cdc24p (Cls4p), a guanine nucleotide-exchange factor toward Cdc42 GTPase, impairs initiation of budding inSaccharomyces cerevisiae. *Protoplasma*, Jan 1995.

[33] A Nern and R A Arkowitz. Nucleocytoplasmic shuttling of the Cdc42p exchange factor Cdc24p. *J Cell Biol*, 148(6):1115–22, Mar 2000.

[34] Y Shimada, M P Gulli, and M Peter. Nuclear sequestration of the exchange factor Cdc24 by Far1 regulates cell polarity during yeast mating. *Nat Cell Biol*, 2(2):117–24, Feb 2000.

[35] Michèle Knaus, Marie-Pierre Pelli-Gulli, Frank van Drogen, Sander Springer, Malika Jaquenoud, and Matthias Peter. Phosphorylation of Bem2p and Bem3p may contribute to local activation of Cdc42p at bud emergence. *EMBO J*, 26(21):4501–13, Oct 2007. ucle.

[36] K A Toenjes, M M Sawyer, and D I Johnson. The guanine-nucleotide-exchange factor Cdc24p is targeted to the nucleus and polarized growth sites. *Curr Biol*, 9(20):1183–6, Oct 1999.

[37] M P Gulli, M Jaquenoud, Y Shimada, G Niederhäuser, P Wiget, and M Peter. Phosphorylation of the Cdc42 exchange factor Cdc24 by the PAK-like kinase Cla4 may regulate polarized growth in yeast. *Mol Cell*, 6(5):1155–67, Nov 2000.

[38] Lukasz Kozubowski, Koji Saito, Jayme M Johnson, Audrey S Howell, Trevin R Zyla, and Daniel J Lew. Symmetry-breaking polarization driven by a Cdc42p GEF-PAK complex. *Curr Biol*, 18(22):1719–26, Nov 2008.

[39] Stephanie C Wai, Scott A Gerber, and Rong Li. Multisite phosphorylation of the guanine nucleotide exchange factor Cdc24 during yeast cell polarization. *PLoS ONE*, 4(8):e6563, Jan 2009.

[40] Yukiko Shimada, Philippe Wiget, Marie-Pierre Gulli, Efrei Bi, and Matthias Peter. The nucleotide exchange factor Cdc24p may be regulated by auto-inhibition. *EMBO J*, 23(5):1051–62, Mar 2004.

[41] I Bose, J E Irazoqui, J J Moskow, E S Bardes, T R Zyla, and D J Lew. Assembly of scaffold-mediated complexes containing Cdc42p, the exchange factor Cdc24p, and the effector Cla4p required for cell cycle-regulated phosphorylation of Cdc24p. *J Biol Chem*, 276(10):7176–86, Mar 2001.

[42] Anne-Christine Butty, Nathalie Perrinjaquet, Audrey Petit, Malika Jaquenoud, Jeffrey E Segall, Kay Hofmann, Catherine Zwahlen, and Matthias Peter. A positive feedback loop stabilizes the guanine-nucleotide exchange factor Cdc24 at sites of polarization. *EMBO J*, 21(7):1565–76, Apr 2002.

[43] A Bender and J R Pringle. Use of a screen for synthetic lethal and multicopy suppressee mutants to identify two new genes involved in morphogenesis in Saccharomyces cerevisiae. *Mol Cell Biol*, 11(3):1295–305, Mar 1991.

[44] H O Park, E Bi, J R Pringle, and I Herskowitz. Two active states of the Ras-related Bud1/Rsr1 protein bind to different effectors to determine yeast cell polarity. *Proc Natl Acad Sci USA*, 94(9):4463–8, Apr 1997.

[45] T Ago, R Takeya, H Hiroaki, F Kuribayashi, T Ito, D Kohda, and H Sumimoto. The PX domain as a novel phosphoinositide- binding module. *Biochem Biophys Res Commun*, 287(3):733–8, Sep 2001.

[46] Yoshihiro Yamaguchi, Kazuhisa Ota, and Takashi Ito. A novel Cdc42-interacting domain of the yeast polarity establishment protein Bem1. Implications for modulation of mating pheromone signaling. *J Biol Chem*, 282(1):29–38, Jan 2007.

[47] Kurt A Toenjes, David Simpson, and Douglas I Johnson. Separate membrane targeting and anchoring domains function in the localization of the S. cerevisiae Cdc24p guanine nucleotide exchange factor. *Curr Genet*, 45(5):257–64, May 2004.

[48] Rong Li and Roland Wedlich-Soldner. Bem1 complexes and the complexity of yeast cell polarization. *Curr Biol*, 19(5):R194–5; author reply R195, Mar 2009.

[49] Audrey S Howell, Meng Jin, Chi-Fang Wu, Trevin R Zyla, Timothy C Elston, and Daniel J Lew. Negative feedback enhances robustness in the yeast polarity establishment circuit. *Cell*, 149(2):322–33, Apr 2012.

[50] D Leonard, M J Hart, J V Platko, A Eva, W Henzel, T Evans, and R A Cerione. The identification and characterization of a GDP-dissociation inhibitor (GDI) for the CDC42Hs protein. *J Biol Chem*, 267(32):22860–8, Nov 1992.

[51] T Masuda, K Tanaka, H Nonaka, W Yamochi, A Maeda, and Y Takai. Molecular cloning and characterization of yeast rho GDP dissociation inhibitor. *J Biol Chem*, 269(31):19713–8, Aug 1994.

[52] G Koch, K Tanaka, T Masuda, W Yamochi, H Nonaka, and Y Takai. Association of the Rho family small GTP-binding proteins with Rho GDP dissociation inhibitor (Rho GDI) in Saccharomyces cerevisiae. *Oncogene*, 15(4):417–22, Jul 1997.

[53] Christopher Tiedje, Imme Sakwa, Ursula Just, and Thomas Höfken. The Rho GDI Rdi1 regulates Rho GTPases by distinct mechanisms. *Mol Biol Cell*, 19(7):2885–96, Jul 2008.

[54] Arupratan Das, Brian D Slaughter, Jay R Unruh, William D Bradford, Richard Alexander, Boris Rubinstein, and Rong Li. Flippase-mediated phospholipid asymmetry promotes fast Cdc42 recycling in dynamic maintenance of cell polarity. *Nat Cell Biol*, 14(3):304–10, Jan 2012.

[55] J Chant. Cell polarity in yeast. *Annu Rev Cell Dev Biol*, 15:365–91, Jan 1999.

[56] Antonio Casamayor and Michael Snyder. Bud-site selection and cell polarity in budding yeast. *Curr Opin Microbiol*, 5(2):179–86, Apr 2002.

[57] J Chant, K Corrado, J R Pringle, and I Herskowitz. Yeast BUD5, encoding a putative GDP-GTP exchange factor, is necessary for bud site selection and interacts with bud formation gene BEM1. *Cell*, 65(7):1213–24, Jun 1991.

[58] H O Park, J Chant, and I Herskowitz. BUD2 encodes a GTPase-activating protein for Bud1/Rsr1 necessary for proper bud-site selection in yeast. *Nature*, 365(6443):269–74, Sep 1993.

[59] Keith G Kozminski, Laure Beven, Elizabeth Angerman, Amy Hin Yan Tong, Charles Boone, and Hay-Oak Park. Interaction between a Ras and a Rho GTPase couples selection of a growth site to the development of cell polarity in yeast. *Mol Biol Cell*, 14(12):4958–70, Dec 2003.

[60] K R Ayscough, J Stryker, N Pokala, M Sanders, P Crews, and D G Drubin. High rates of actin filament turnover in budding yeast and roles for actin in establishment and maintenance of cell polarity revealed using the actin inhibitor latrunculin-A. *J Cell Biol*, 137(2):399–416, Apr 1997.

[61] M Evangelista, K Blundell, M S Longtine, C J Chow, N Adames, J R Pringle, M Peter, and C Boone. Bni1p, a yeast formin linking Cdc42p and the actin cytoskeleton during polarized morphogenesis. *Science (New York, NY)*, 276(5309):118–22, Apr 1997.

[62] Natasha S Savage, Anita T Layton, and Daniel J Lew. Mechanistic mathematical model of polarity in yeast. *Mol Biol Cell*, 23(10):1998–2013, May 2012.

[63] Javier E Irazoqui, Audrey S Howell, Chandra L Theesfeld, and Daniel J Lew. Opposing roles for actin in Cdc42p polarization. *Mol Biol Cell*, 16(3):1296–304, Mar 2005.

[64] Ertugrul M Ozbudak, Attila Becskei, and Alexander van Oudenaarden. A system of counteracting feedback loops regulates Cdc42p activity during spontaneous cell polarization. *Developmental Cell*, 9(4):565–71, Oct 2005.

[65] Roland Wedlich-Soldner, Stephanie C Wai, Thomas Schmidt, and Rong Li. Robust cell polarity is a dynamic state established by coupling transport and GTPase signaling. *J Cell Biol*, 166(6):889–900, Sep 2004.

[66] Audrey S Howell, Natasha S Savage, Sam A Johnson, Indrani Bose, Allison W Wagner, Trevin R Zyla, H Frederik Nijhout, Michael C Reed, Andrew B Goryachev, and Daniel J Lew. Singularity in polarization: rewiring yeast cells to make two buds. *Cell*, 139(4):731–43, Nov 2009.

[67] A. M Turing. The Chemical Basis of Morphogenesis. *Philosophical Transactions of the Royal Society of London. Series B*, 237:37, Aug 1952.

[68] A Gierer and H Meinhardt. A theory of biological pattern formation. *Kybernetik*, 12(1):30–9, Dec 1972.

[69] H Meinhardt and A Gierer. Applications of a theory of biological pattern formation based on lateral inhibition. *J Cell Sci*, 15(2):321–46, Jul 1974.

[70] Alexandra Jilkine and Leah Edelstein-Keshet. A comparison of mathematical models for polarization of single eukaryotic cells in response to guided cues. *PLoS Comput Biol*, 7(4):e1001121, Apr 2011.

[71] M. Cross and H. Greenside. *Pattern formation and dynamics in nonequilibrium systems*. Cambridge University Press, New York, 2009.

[72] A Goryachev and A Pokhilko. Dynamics of Cdc42 network embodies a Turing-type mechanism of yeast cell polarity. *FEBS Lett*, 582(10):1437–1443, Apr 2008.

[73] Steven J Altschuler, Sigurd B Angenent, Yanqin Wang, and Lani F Wu. On the spontaneous emergence of cell polarity. *Nature*, 454(7206):886–9, Aug 2008.

[74] Matteo Semplice, Andrea Veglio, Giovanni Naldi, Guido Serini, and Andrea Gamba. A bistable model of cell polarity. *PLoS ONE*, 7(2):e30977, Jan 2012.

[75] Anita T Layton, Natasha S Savage, Audrey S Howell, Susheela Y Carroll, David G Drubin, and Daniel J Lew. Modeling vesicle traffic reveals unexpected consequences for Cdc42p-mediated polarity establishment. *Curr Biol*, 21(3):184–94, Feb 2011.

[76] Tina Freisinger*, Ben Klünder*, Jared Johnson, Nikola Müller, Garwin Pichler, Gisela Beck, Michael Costanzo, Charles Boone, Richard A Cerione, Erwin Frey, and Roland Wedlich-Soldner. Establishment of a robust single axis of cell polarity by coupling of multiple positive feedback loops. Submitted for publication.

[77] Sandrine Etienne-Manneville. Cdc42–the centre of polarity. *Journal of cell science*, 117(Pt 8):1291–300, Mar 2004.

[78] D I Johnson. Cdc42: An essential Rho-type GTPase controlling eukaryotic cell polarity. *Microbiol Mol Biol Rev*, 63(1):54–105, Mar 1999.

[79] Tamara J Richman, Mathew M Sawyer, and Douglas I Johnson. Saccharomyces cerevisiae Cdc42p localizes to cellular membranes and clusters at sites of polarized growth. *Eukaryotic Cell*, 1(3):458–68, Jun 2002.

[80] M Ziman and D I Johnson. Genetic evidence for a functional interaction between Saccharomyces cerevisiae CDC24 and CDC42. *Yeast*, 10(4):463–74, Apr 1994.

[81] David Pruyne, Lina Gao, Erfei Bi, and Anthony Bretscher. Stable and dynamic axes of polarity use distinct formin isoforms in budding yeast. *Mol Biol Cell*, 15(11):4971–89, Nov 2004.

[82] Y Barral, V Mermall, M S Mooseker, and M Snyder. Compartmentalization of the cell cortex by septins is required for maintenance of cell polarity in yeast. *Mol Cell*, 5(5):841–51, May 2000.

[83] Roland Wedlich-Soldner and Rong Li. Closing the loops: new insights into the role and regulation of actin during cell polarization. *Exp Cell Res*, 301(1):8–15, Nov 2004.

[84] Jayme M Johnson, Meng Jin, and Daniel J Lew. Symmetry breaking and the establishment of cell polarity in budding yeast. *Current opinion in genetics & development*, Sep 2011.

[85] Brian D Slaughter, Sarah E Smith, and Rong Li. Symmetry breaking in the life cycle of the budding yeast. *Cold Spring Harbor Perspect Biol*, 1(3):a003384, Sep 2009.

[86] Kathryn P Harris and Ulrich Tepass. Cdc42 and vesicle trafficking in polarized cells. *Traffic*, 11(10):1272–9, Oct 2010.

[87] Naël Osmani, Florent Peglion, Philippe Chavrier, and Sandrine Etienne-Manneville. Cdc42 localization and cell polarity depend on membrane traffic. *J Cell Biol*, 191(7):1261–9, Dec 2010.

[88] Takaharu Yamamoto, Junko Mochida, Jun Kadota, Miyoko Takeda, Erfei Bi, and Kazuma Tanaka. Initial polarized bud growth by endocytic recycling in the absence of actin cable-dependent vesicle transport in yeast. *Mol Biol Cell*, 21(7):1237–52, Apr 2010.

[89] Etienne Boulter, Rafael Garcia-Mata, Christophe Guilluy, Adi Dubash, Guendalina Rossi, Patrick J Brennwald, and Keith Burridge. Regulation of Rho GTPase crosstalk, degradation and activity by RhoGDI1. *Nat Cell Biol*, 12(5):477–83, May 2010.

[90] Michael Costanzo, Anastasia Baryshnikova, Jeremy Bellay, Yungil Kim, Eric D Spear, Carolyn S Sevier, Huiming Ding, Judice L Y Koh, Kiana Toufighi, Sara Mostafavi, Jeany Prinz, Robert P St Onge, Benjamin VanderSluis, Taras Makhnevych, Franco J Vizeacoumar, Solmaz Alizadeh, Sondra Bahr, Renee L Brost, Yiqun Chen, Murat Cokol, Raamesh Deshpande, Zhijian Li, Zhen-Yuan Lin, Wendy Liang, Michaela Marback, Jadine Paw, Bryan-Joseph San Luis, Ermira Shuteriqi, Amy Hin Yan Tong, Nydia van Dyk, Iain M Wallace, Joseph A Whitney, Matthew T Weirauch, Guoqing Zhong, Hongwei Zhu, Walid A Houry, Michael Brudno, Sasan Ragibizadeh, Balázs Papp, Csaba Pál, Frederick P Roth, Guri Giaever, Corey Nislow, Olga G Troyanskaya, Howard Bussey, Gary D Bader, Anne-Claude Gingras, Quaid D Morris, Philip M Kim, Chris A Kaiser, Chad L Myers, Brenda J Andrews, and Charles Boone. The genetic landscape of a cell. *Science*, 327(5964):425–31, Jan 2010.

[91] R M Gibson and A L Wilson-Delfosse. RhoGDI-binding-defective mutant of Cdc42Hs targets to membranes and activates filopodia formation but does not cycle with the cytosol of mammalian cells. *Biochem J*, 359(Pt 2):285–94, Oct 2001.

[92] David J Katzmann, Christopher J Stefan, Markus Babst, and Scott D Emr. Vps27 recruits ESCRT machinery to endosomes during MVB sorting. *J Cell Biol*, 162(3):413–23, Aug 2003.

[93] Jared L Johnson, Jon W Erickson, and Richard A Cerione. C-terminal di-arginine motif of Cdc42 protein is essential for binding to phosphatidylinositol 4,5-bisphosphate-containing membranes and inducing cellular transformation. *J Biol Chem*, 287(8):5764–74, Feb 2012.

[94] Estelle Dransart, Birgitta Olofsson, and Jacqueline Cherfils. RhoGDIs revisited: novel roles in Rho regulation. *Traffic*, 6(11):957–66, Nov 2005.

[95] Stefan Schoebel, Lena Katharina Oesterlin, Wulf Blankenfeldt, Roger Sidney Goody, and Aymelt Itzen. RabGDI displacement by DrrA from Legionella is a consequence of its guanine nucleotide exchange activity. *Mol Cell*, 36(6):1060–72, Dec 2009.

[96] Yelena Ugolev, Yevgeny Berdichevsky, Carolyn Weinbaum, and Edgar Pick. Dissociation of Rac1(GDP).RhoGDI complexes by the cooperative action of anionic liposomes containing phosphatidylinositol 3,4,5-trisphosphate, Rac guanine nucleotide exchange factor, and GTP. *J Biol Chem*, 283(32):22257–71, Aug 2008.

[97] V Jung, W Wei, R Ballester, J Camonis, S Mi, L Van Aelst, M Wigler, and D Broek. Two types of RAS mutants that dominantly interfere with activators of RAS. *Mol Cell Biol*, 14(6):3707–18, Jun 1994.

[98] L Stowers, D Yelon, L J Berg, and J Chant. Regulation of the polarization of T cells toward antigen-presenting cells by Ras-related GTPase CDC42. *Proc Natl Acad Sci USA*, 92(11):5027–31, May 1995.

[99] Matthew D Onsum and Christopher V Rao. Calling heads from tails: the role of mathematical modeling in understanding cell polarization. *Curr Opin Cell Biol*, 21(1):74–81, Feb 2009.

[100] Yao-Wen Wu, Lena K Oesterlin, Kui-Thong Tan, Herbert Waldmann, Kirill Alexandrov, and Roger S Goody. Membrane targeting mechanism of Rab GTPases elucidated by semisynthetic protein probes. *Nat Chem Biol*, 6(7):534–40, Jul 2010.

[101] Gregory D Fairn, Martin Hermansson, Pentti Somerharju, and Sergio Grinstein. Phosphatidylserine is polarized and required for proper Cdc42 localization and for development of cell polarity. *Nat Cell Biol*, 13(12):1424–30, Dec 2011.

[102] Céline DerMardirossian and Gary M Bokoch. GDIs: central regulatory molecules in Rho GTPase activation. *Trends Cell Biol*, 15(7):356–63, Jul 2005.

[103] Alex Mogilner, Jun Allard, and Roy Wollman. Cell polarity: quantitative modeling as a tool in cell biology. *Science*, 336(6078):175–9, Apr 2012.

[104] D Gillespie.... Exact stochastic simulation of coupled chemical reactions. *The journal of physical chemistry*, Jan 1977.

[105] David Bernstein. Simulating mesoscopic reaction-diffusion systems using the Gillespie algorithm. *Physical review E, Statistical, nonlinear, and soft matter physics*, 71(4 Pt 1):041103, Apr 2005.

[106] Sina Ghaemmaghami, Won-Ki Huh, Kiowa Bower, Russell W Howson, Archana Belle, Noah Dephoure, Erin K O'Shea, and Jonathan S Weissman. Global analysis of protein expression in yeast. *Nature*, 425(6959):737–41, Oct 2003.

[107] Mikiya Otsuji, Shuji Ishihara, Carl Co, Kozo Kaibuchi, Atsushi Mochizuki, and Shinya Kuroda. A mass conserved reaction-diffusion system captures properties of cell polarity. *PLoS Comput Biol*, 3(6):e108, Jun 2007.

[108] Carsten Janke, Maria M Magiera, Nicole Rathfelder, Christof Taxis, Simone Reber, Hiromi Maekawa, Alexandra Moreno-Borchart, Georg Doenges, Etienne Schwob, Elmar Schiebel, and Michael Knop. A versatile toolbox for PCR-based tagging of yeast genes: new fluorescent proteins, more markers and promoter substitution cassettes. *Yeast*, 21(11):947–62, Aug 2004.

[109] J. Sambrook and D. W. Russel. *Molecular Cloning: A laboratory Manual, third edn.* Cold Spring Harbor Laboratory Press, New York, 2001.

[110] Bobby-Joe Breitkreutz, Chris Stark, Teresa Reguly, Lorrie Boucher, Ashton Breitkreutz, Michael Livstone, Rose Oughtred, Daniel H Lackner, Jürg Bähler, Valerie Wood, Kara Dolinski, and Mike Tyers. The BioGRID Interaction Database: 2008 update. *Nucleic Acids Res*, 36(Database issue):D637–40, Jan 2008.

[111] Lukasz Salwinski, Christopher S Miller, Adam J Smith, Frank K Pettit, James U Bowie, and David Eisenberg. The Database of Interacting Proteins: 2004 update. *Nucleic Acids Res*, 32(Database issue):D449–51, Jan 2004.

[112] H Werner Mewes, Andreas Ruepp, Fabian Theis, Thomas Rattei, Mathias Walter, Dmitrij Frishman, Karsten Suhre, Manuel Spannagl, Klaus F X Mayer, Volker Stümpflen, and Alexey Antonov. MIPS: curated databases and comprehensive secondary data resources in 2010. *Nucleic Acids Res*, 39(Database issue):D220–4, Jan 2011.

[113] Amy Hin Yan Tong and Charles Boone. Synthetic genetic array analysis in Saccharomyces cerevisiae. *Methods Mol Biol*, 313:171–92, Jan 2006.

[114] A Gierer. Generation of biological patterns and form: some physical, mathematical, and logical aspects. *Progress in Biophysics and Molecular Biology*, 37(1):1–47, Jan 1981.

[115] E Frey and K Kroy. Brownian motion: a paradigm of soft matter and biological physics. *Annalen der Physik*, Jan 2005.

[116] Herbert Levine and Wouter-Jan Rappel. Membrane-bound Turing patterns. *Physical review E, Statistical, nonlinear, and soft matter physics*, 72(6 Pt 1):061912, Dec 2005.

[117] Alexandra Jilkine, Sigurd B Angenent, Lani F Wu, and Steven J Altschuler. A density-dependent switch drives stochastic clustering and polarization of signaling molecules. *PLoS Comput Biol*, 7(11):e1002271, Nov 2011.

[118] H Meinhardt and A Gierer. Pattern formation by local self-activation and lateral inhibition. *Bioessays*, 22(8):753–60, Aug 2000.

[119] Alexandra Jilkine and Leah Edelstein-Keshet. A comparison of mathematical models for polarization of single eukaryotic cells in response to guided cues. *PLoS Comput Biol*, 7(4):e1001121, Apr 2011.

[120] Jae-Ung Hwang, Vanessa Vernoud, Amy Szumlanski, Erik Nielsen, and Zhenbiao Yang. A tip-localized RhoGAP controls cell polarity by globally inhibiting Rho GTPase at the cell apex. *Curr Biol*, 18(24):1907–16, Dec 2008.

[121] Andreas Wodarz and Inke Näthke. Cell polarity in development and cancer. *Nat Cell Biol*, 9(9):1016–24, Sep 2007.

[122] Qiong Lin, Reina N Fuji, Wannian Yang, and Richard A Cerione. RhoGDI is required for Cdc42-mediated cellular transformation. *Curr Biol*, 13(17):1469–79, Sep 2003.

[123] Maria Carolina Florian and Hartmut Geiger. Concise review: polarity in stem cells, disease, and aging. *Stem Cells*, 28(9):1623–9, Sep 2010.

[124] Jerry H Yu, Alvaro H Crevenna, Mario Bettenbühl, Tina Freisinger, and Roland Wedlich-Söldner. Cortical actin dynamics driven by formins and myosin V. *J. Cell sci.*, 124(Pt 9):1533–41, May 2011.

[125] Denis S Grebenkov. Subdiffusion in a bounded domain with a partially absorbing-reflecting boundary. *Phys Rev E Stat Nonlin Soft Matter Phys*, 81(2 Pt 1):021128, Feb 2010.

[126] Kelly Orlando, Xiaoli Sun, Jian Zhang, Tu Lu, Lauren Yokomizo, Puyue Wang, and Wei Guo. Exo-endocytic trafficking and the septin-based diffusion barrier are required for the maintenance of Cdc42p polarization during budding yeast asymmetric growth. *Mol Biol Cell*, 22(5):624–33, Mar 2011.

[127] Angela C Wild, Jong W Yu, Mark A Lemmon, and Kendall J Blumer. The p21-activated protein kinase-related kinase Cla4 is a coincidence detector of signaling by Cdc42 and phosphatidylinositol 4-phosphate. *J Biol Chem*, 279(17):17101–10, Apr 2004.

[128] Makio Tokunaga, Naoko Imamoto, and Kumiko Sakata-Sogawa. Highly inclined thin illumination enables clear single-molecule imaging in cells. *Nat Methods*, 5(2):159–61, Feb 2008.

[129] Kristy Stengel and Yi Zheng. Cdc42 in oncogenic transformation, invasion, and tumorigenesis. *Cell Signal*, 23(9):1415–23, Sep 2011.

[130] M. Abramowitz and I. A. Stegun. *Handbook of Mathematical Functions with Formulas, Graphs, and Mathematical Tables, 10th printing.* Dover, New York, 1972.

[131] G. N. Watson and E. T. Whittaker. *A Course of Modern Analysis.* Cambridge University Press, 1927.

[132] H. Triebel. *Analysis und mathematische Physik.* Carl Hauser Verlag, München, 1982.

[133] F. Sherman, G.R. Fink, and J.B. Hicks. *Methods in yeast genetics.* Cold Spring Harbor Laboratory, 1981.

[134] A J Molendijk, F Bischoff, C S Rajendrakumar, J Friml, M Braun, S Gilroy, and K Palme. Arabidopsis thaliana Rop GTPases are localized to tips of root hairs and control polar growth. *EMBO J*, 20(11):2779–88, Jun 2001.

[135] F P Finger and P Novick. Spatial regulation of exocytosis: lessons from yeast. *J Cell Biol*, 142(3):609–12, Aug 1998.

[136] Ying Gu, Vanessa Vernoud, Ying Fu, and Zhenbiao Yang. ROP GTPase regulation of pollen tube growth through the dynamics of tip-localized F-actin. *J Exp Bot*, 54(380):93–101, Jan 2003.

[137] Brian D Slaughter, Joel W Schwartz, and Rong Li. Mapping dynamic protein interactions in MAP kinase signaling using live-cell fluorescence fluctuation spectroscopy and imaging. *Proc Natl Acad Sci USA*, 104(51):20320–5, Dec 2007.

[138] Ben Klünder*, Tina Freisinger*, Roland Wedlich-Soldner, and Erwin Frey. Cell polarization in yeast optimizes spatial and temporal control of Cdc42 signaling. Submitted for publication.

*: These authors contributed equally.

Danksagung

An dieser Stelle möchte ich mich bei all den Menschen bedanken, die mich während der Anfertigung meiner Dissertation unterstützt und begleitet haben.

Zuallererst möchte ich meinem Doktorvater Prof. Dr. Erwin Frey für die Betreuung meiner Dissertation danken. Unsere Diskussionen und Gespräche waren mir eine große Hilfe und haben meine Arbeit immer wieder vorangebracht. Ohne Erwins umfangreiches Wissen, seine Erfahrung und seine Ideen wäre diese Arbeit nicht möglich gewesen.

Mein besonderer Dank geht an Dr. Roland Wedlich-Söldner und Dr. Tina Freisinger für die fruchtbare interdisziplinäre Zusammenarbeit, in der große Teile dieser Arbeit entstanden sind und durch die ich viel lernen konnte.

Sehr gefreut habe ich mich über die erfolgreiche Zusammenarbeit mit Steffen Rulands. Bedanken möchte ich mich auch bei Prof. Dr. Ulrich Gerland, Alexander Buchner und Jacob Halatek für die hilfreichen Diskussionen über meine Arbeit.

Die schöne gemeinsame Zeit mit meinem Zimmerkollegen Alexander und all meinen anderen Kollegen am Lehrstuhl werde ich nicht vergessen.

Das Internationale Doktorandenkolleg Nanobiotechnologie unterstützte meine Arbeit finanziell und stellte mir großzügig Reisemittel zur freien Verfügung.

Danken möchte ich schließlich meiner Familie und meinen Freunden für ihr Interesse und ihren Beistand und ganz besonders Melanie für das Korrekturlesen dieser Arbeit und für all ihre Unterstützung während der gesamten Zeit.